

Feasibility of a weather sensor network for agricultural purposes using low-cost sensors and materials

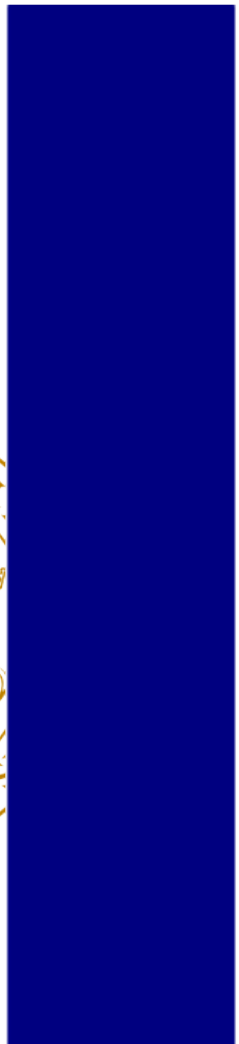
A preliminary assessment

Kees van Duijvendijk

2015

Department of
Physical Geography and Ecosystem Science
Centre for Geographical Information Systems
Lund University
Sölvegatan 12
S-223 62 Lund
Sweden

Seminar series nr XX



Kees van Duijvendijk (2015). *Feasibility of a weather sensor network for agricultural purposes using low-cost sensors and materials: A preliminary assessment.*

Master degree thesis, 30 credits in Master in Geographical Information Sciences Department of Physical Geography and Ecosystems Science, Lund University

Feasibility of a weather sensor network for agricultural purposes using low-cost sensors and materials

A preliminary assessment

Kees van Duijvendijk

*Master degree thesis, 30 credits in Master in Geographical Information Sciences
Department of Physical Geography and Ecosystems Science, Lund University*

Supervisor 1:

Dr. Jonas Ardö
Associate Professor
Department of Physical Geography and Ecosystem Services
Lund University
Lund, Sweden

Supervisor 2:

Dr. Jacob van Etten
Senior Scientist, Theme Leader, Adaptation to Climate Change
Bioversity International
Turrialba, Costa Rica

i Abstract

ii Acknowledgements

Contents

i Abstract	5
ii Acknowledgements	7
1 Introduction	13
1.1 Problem Statement	14
1.2 Research Aim	14
1.2.1 Aim of Section I: Data accuracy	15
1.2.2 Aim of Section II: Spatial aspects of the network	15
1.2.3 Aim of Section III: Interpolation strategies	15
1.3 Research Questions	15
1.4 Thesis Outline	16
1.5 Workflow	16
2 Background	17
2.1 Climate Science & Sensors	17
2.2 Sensors and Standards	18
2.3 Implementation of Sensor Networks in Agriculture	18
2.4 Sensor Networks and Citizen Science	20
2.5 Crop and Disease Thresholds	21
3 Data accuracy	22
3.1 Introduction	22
3.2 Materials and methodology	23
3.2.1 Sensors	23
3.2.2 Weather station and shield	24
3.2.3 Alternative shields for the iButton sensors	24
3.2.4 Experiment 1: Sensor and temporal resolution	25
3.2.5 Experiment 2: Shields	26
3.2.6 Experiment 3: Data calibration	28
3.3 Results	31
3.3.1 Experiment 1A: Sensor resolution	31
3.3.2 Experiment 1B: Temporal resolution	32
3.3.3 Experiment 2: Shields	34
3.3.4 Experiment 3: Data calibration	37
3.4 Discussion	41
3.5 Recommendations	44

4 Spatial aspects	45
4.1 Introduction	45
4.2 Methodology	46
4.2.1 Study area and sampling	46
4.2.2 Data correction and validation	47
4.2.3 Analysis of covariates	49
4.2.4 Selected covariates	50
4.2.5 Analyses	54
4.3 Results	55
4.3.1 Network accuracy	55
4.3.2 Correlation between covariates	56
4.3.3 Average correlation with covariates	57
4.3.4 Daily trends in correlation	58
4.4 Discussion	62
4.5 Recommendations	63
5 Data interpolation	64
5.1 Introduction	64
5.2 Methodology	65
5.2.1 Data inputs	65
5.2.2 Prediction grid	65
5.2.3 Geostatistical interpolation	66
5.2.4 Selected kriging-approaches	66
5.2.5 Analyses	68
5.3 Results	69
5.3.1 Ordinary Kriging	69
5.3.2 Universal Kriging	70
5.3.3 Dynamic universal kriging	72
5.3.4 Co-kriging approaches	73
5.3.5 Spatio-temporal kriging	74
5.4 Discussion	75
5.5 Recommendations	76
6 Conclusions & Recommendations	77
7 References	78
8 Annexes	86
8.1 Regression models	86

List of Figures

1	Steps taken in this study to reach a robust and low-cost climate network	16
2	Top-tube lay-out of the shields	24
3	CATIE Meteorological station with PVC shields	27
4	High-resolution T sensor-data	31
5	Low-resolution T sensor-data	31
6	High-resolution RH sensor-data	32
7	Low-resolution RH sensor-data	32
8	Temperature in the Stevenson (blue) vs. PVC (red) shields	34
9	Correction based on actual Ta	36
10	Correction on change of Ta in time	36
11	Observed temperature in three sensors around the eddy tower (blue = shadow sensor)	38
12	Corrected change in time (1 hour) based on a calibration model based with 55 values	40
13	Boundaries of the Aquiares estate and placement of the recovered sensors)	47
14	Boundaries of the Aquiares estate and placement of the recovered sensors)	51
15	Canopy height in the Aquiares estate based on LiDAR data)	52
16	Daily $T_{a\max}$ vs RMSE	55
17	Daily trends in average RMSE	55
18	Average RMSE of the 80 recovered sensors in Aquiares	56
19	RMSE vs. hourly correlation of Ta with elevation	57
20	Relative importance of different covariates in explaining temperature	57
21	Temperature/elevation correlation	58
22	max Ta vs Ta/alt correlation	58
23	Temperature/slope correlation	58
24	Temperature/aspect correlation	58
25	Temperature/LAI correlation	59
26	Temperature/canopy correlation	59
27	Temperature/hourly radiation cor.	60
28	Max Ta vs mean radiation cor.	60
29	Mean linear regression strength (R^2) throughout the day that explains temperature variation	60
30	Contribution of different covariates to the best model explaining temperature variation	61
31	Ordinary Kriging (80 sensors)	69
32	Ordinary Kriging (40 sensors)	69
33	Ordinary Kriging (20 sensors)	69
34	Ordinary Kriging (8 sensors)	69
35	Universal Kriging (80 sensors)	70
36	Universal Kriging (40 sensors)	70
37	Universal Kriging (20 sensors)	70

38	Universal Kriging (8 sensors)	70
39	Mean temperature for the hours 11AM-4PM based on universal kriging with 20 sensors	71
40	Mean temperature for the hours 11AM-4PM based on universal auto-kriging with 20 sensors	71
41	Predicted temperature based on dynamic kriging and 8 sensors	72
42	Hourly mean temperature during 5-10AM with Universal Kriging (top) and Co-Kriging (bottom)	73
43	Daily temperature trends in Aquiares, based on ST Ordinary Kriging with 80 sensors	74

List of Tables

1	Input of crowd-sourcing projects	20
2	Output of crowd-sourcing projects	20
3	Time covered by different sensor settings (one micro-sensors contains a Ta and RH sensor)	23
4	Characteristics of the different coatings of the PVC shields	28
5	Differences in temperature at different quantiles using a range interpolation approaches	33
6	Analysis of adjustments on 50mm PVC shields	36
7	Analysis of adjustments on 25mm PVC shields	36
8	Errors in different types of calibration (Ta) compared to data in a Stevenson shield .	37
9	Correlation between the selected (static) covariates	56
10	Summary of selected interpolation approaches	67
11	Hourly strength of regression models and relative importance of the selected covariates	86
12	Errors with Ordinary Kriging	87
13	Errors with Universal Kriging (Elevation)	87
14	Errors with automatized Universal Kriging (Elevation)	88
15	Errors with basic dynamic kriging	88
16	Errors with automatized dynamic kriging	88
17	Errors with random forest kriging	88
18	Errors with co-kriging (elevation only)	89
19	Errors of co-kriging (with elevation and radiation)	89
20	Errors with co-kriging (with elevation, radiation, slope and aspect)	89
21	Errors with spatio-temporal ordinary kriging	89
22	Errors with spatio-temporal universal kriging (elevation)	90
23	Errors with spatio-temporal dynamic kriging (elevation, radiation, slope and aspect) .	90

1 Introduction

This thesis will discuss the need for low-cost networks of climate sensors and will deal with several of the issues that have to be taken into account when implementing such networks. At the same time that advances in the developed world make weather predictions possible at a very high spatial/temporal scale, and models can recommend crop varieties based on trillions of observations (e.g. FieldScripts (Monsanto, 2014)), the costs for maintaining a basic network of weather stations still form a constraint for their use in many low-income countries (Barnett & Mahul, 2007). One of the larger efforts to create high-resolution global climate data is the WorldClim dataset (Hijmans et al., 2005), for which the current climate has been assessed (1950-2000) based on over 14,835 locations (depending on the units measured). This dataset, which also includes the projected climate for four representative concentration pathways (RCPs), is often linked with crop databases (e.g. EcoCrop (FAO, 2013)) to predict the impact of climate change on crops (Hijmans & Graham, 2006; Lane & Jarvis, 2007; Ramirez-Villegas, Jarvis, & Läderach, 2013). Except for downscaling climate data by statistical downscaling and interpolation of weather station data, an alternative approach to create the climatic data at a scale that is useful for crop models is by using stochastic weather generators (Wilks & Wilby, 1999). Downscaling of climatic data can be used for numerous purposes, including short term weather prediction (Pielke & Wilby, 2012).

A limitation of current crop models - and the role of climate data within these - is that it is difficult to include the impact of extreme temperatures on specific phenological events (Porter & Christensen, 2013); these are the important crop phases such as leaf initiation, shoot growth, and leaf growth. Another issue with linking local climate and crops in models is that climate variation at the local level is so high that models have to be validated by data from a number of years resulting in smoothed datasets (Lobell, Cassman, & Field, 2009). While this is useful in models related to current and future crop potential (possibly linked to transfer of genetic material), by focusing on climate analogues, this will not be useful for understanding the impact of local climatic extremes on crop production. Climate analogues are expected to move and cause shifts in crops at the global scale (Ramirez-Villegas et al., 2011), whereas options for adaptation will generally depend on the local context (Nhemachena & Hassan, 2007). An important gap in climate science, which will be addressed in this thesis, is the difficulty to predict the impact of local climatic changes (Schiermeier, 2010). In this study, local scale is defined as areas $<1\text{km}^2$, as data will be linked to performance of crops in field trials at farmers fields. At this level there will be many different micro-climates, which are influenced by factors such as the canopy height, the openness to wind, general topography and the vicinity of larger water bodies (Ashcroft & Gollan, 2013). While many of the relevant physical processes have already been added to models (e.g. MeteoTool), working at a very small scale with real-time data remains an important challenge. Access to weather forecasts is linked to uptake of different adaptation practices (Wood et al., 2014). Taking into account the many local factors that influence climate, and that smallholders mostly cultivate small areas in risk prone areas (Morton, 2007), low cost climate-networks can provide clear benefits to smallholders.

Site-specific information can be provided by a range of low-cost technologies and mobile applications. Mobile applications in small-scale agriculture (hereafter referred to as e-Agriculture) can assist in providing (top-down) information about market prices and recommended timing and quantity of agro-chemicals, but can also be used in more participatory approaches, such as crowd sourcing of crop improvement (Van Etten, 2011). The large number of standards that certified weather stations have to meet (e.g. World Meteorological Organization, 2008) is likely associated with higher costs. This can become a serious limitation to their creation and maintenance in rural areas in the developing world. As smallholder farmers often cultivate more complex (marginal/mountainous) terrain (Altieri, 2002), information about climatic differences at this scale will be especially relevant to them. The hypothesis of this research is that reliable networks of climate sensors can be created with very little costs, and that these fit well in the context of climate monitoring and low-cost precision agriculture.

1.1 Problem Statement

While studies on the separate subjects of climate downscaling and crop thresholds have received a lot of attention, and micro-sensors are already used in a wide range of environmental studies, there is still a lack of weather stations that provide basic climatic data (temperature and humidity) with high spatial and temporal accuracy in rural areas of developing countries. Downscaled climate data can be useful in agricultural modelling and can accurately be estimated up to hourly intervals (Cheng et al., 2008). A problem, however, remains the limited understanding of impacts at the local level (Jones & Thornton, 2013). Data at this level ($<1\text{km}^2$) can be used for variety recommendations and pest monitoring. One of the related data-gaps, discussed in the 5th Assessment Report of the IPCC (Chapter 7), is that most adaptation studies focus on the future climatic conditions, and less on the potential impacts in the current climate (IPCC, 2014). The difficulty of many poor countries to maintain weather-station networks does not only limit the options to provide smallholders with insurance to weather-related risks (Barnett & Mahul, 2007), but can also impact on other important aspects of climate adaptation, such as the uptake of more suitable crop-varieties (Wood et al., 2014).

1.2 Research Aim

The main aim of this research is to provide clear recommendations about a range of crucial issues that are faced when setting up a network for climate observations with a budget that is sufficiently low to be used in agronomic trials in developing countries, while still providing significant gains over currently available weather data. Issues include the set-up of the sensor (resolution, temporal interval), shielding of the sensor (PVC shields plus certain adjustments), data correction (different types of calibration), and interpolation of data. All these issues are linked to the initial set-up of the network and aim to reduce the number of sensors that is required for accurate data, while increasing the period of data collection. The secondary aim of the study is to provide a range of uses of the created network in addition to the initial objective of linking climate data to field trials which can make the networks interesting for other extension projects. Aims of the sub-sections include:

1.2.1 Aim of Section I: Data accuracy

Provide information about the trade-offs between costs and accuracy when working at different sensor and temporal resolution, which should be relevant to assess the short-term extremes. Evaluate approaches of temporal-data interpolation that can be used to create a regular time-series from the irregular time-series that the sensors provide, without losing crucial information. Test a range of adjustments (external coating and aeration) to PVC shields and study how the data from the sensors inside these shields relates to data to a certified (Stevenson) sensor shield.

1.2.2 Aim of Section II: Spatial aspects of the network

Quantify the data accuracy of the network; this includes verification with external temperature and humidity observations and with internal observations (based on a leave-one-out approach). Calculate the linear relationship between several static (elevation, slope, aspect, canopy height, leaf area index) and dynamic (hourly hillshade, cast shadows and maximum solar intensity) covariates and the hourly mean, minimum and maximum temperature.

1.2.3 Aim of Section III: Interpolation strategies

Assess different types of (geostatistical) methods for spatial interpolation of the data. Different types of Kriging (Ordinary, Universal, Co-Kriging, Spatial) will be compared to see how they influence the (internal and external) network accuracy. Calculation time is also compared.

1.3 Research Questions

Main research question: How can the costs of a network of micro-sensors be kept low, while maintaining a robust and accurate network that can provide plot-level weather information (100 meter resolution)?

Data accuracy research question: What is the optimal sensor and temporal resolution that allows to cover the longest period in the field, and which type of sensor shield would be most suitable to use to hold these sensors?

Spatial aspects research question: Which of the different covariates have a linear relationship with hourly temperature throughout the study area; at which moments are these strongest and can they be used in co-kriging?

Spatial interpolation question: What are the differences between different kriging strategies when it comes to accuracy of the data and time spent on calculations? What is the minimum number of sensors in each network?

1.4 Thesis Outline

The thesis is divided into five chapters. The first chapter introduces the research and the second chapter discusses the wider context of local meteorological measurement networks, including history, limitations and possible use. The third chapter covers a range of experiments focused at the sensor resolution and shielding. The fourth chapter explains the initial network accuracy and possible covariates. The fifth chapter focusses on different geostatistical approaches to data interpolation and the fifth and final section include conclusions and recommendations for practical use. Sections two, three and four all have separate sections for introduction, methodology, results, discussion and recommendations. This should make these sections - in combination with the background - understandable as stand-alone documents.

1.5 Workflow

The steps that have been taken during this thesis are provided in *figure 1*, with the main thought-processes at the sides. All scripts are provided at <https://github.com/cornelisvd/thesis>. The thought processes required with each practical step, from selection of the study area to practical implementation, form the basis of the structure of this thesis. Based on the raw data, all steps will be easy to reproduce, which make these steps relevant to other projects using the same sensors. The subsequent practical uses after creation of final field data will be discussed, but not implemented, in this study.

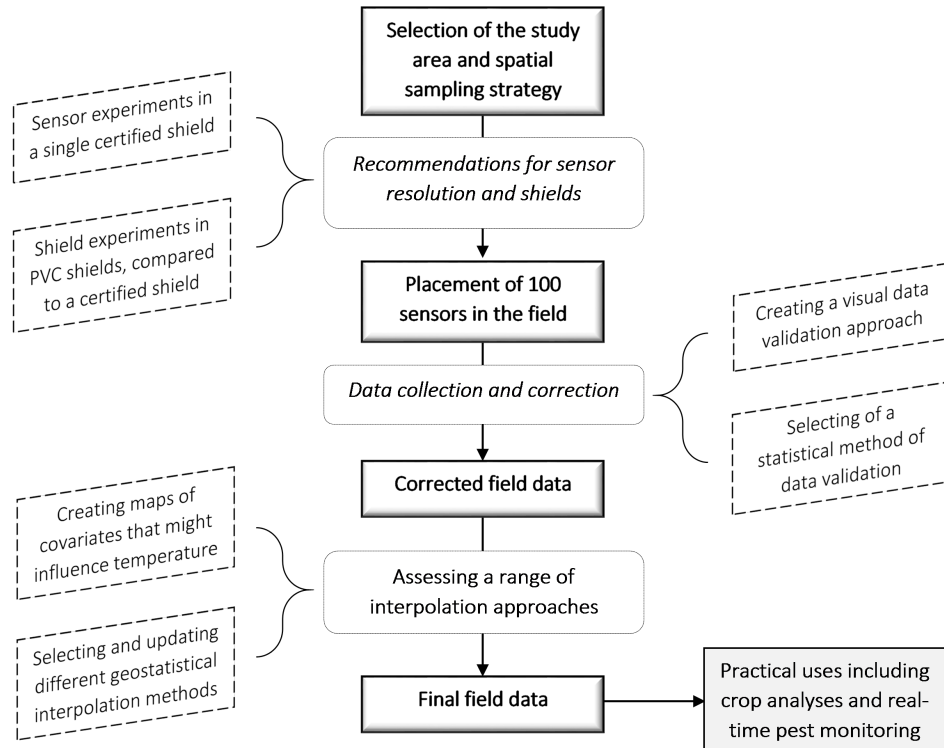


Figure 1: Steps taken in this study to reach a robust and low-cost climate network

2 Background

2.1 Climate Science & Sensors

Climate science has a long history which will not be covered in detail here, as it has already been covered in much detail in numerous papers and books. The first time a network (Reseau Mondial) was proposed for real-time data sharing (by telegram in that time) was as early as 1900 (Edwards, 2010), but only once the computer arrived, different formats could easily be merged to use in forecasting. The first weather satellites were launched in the late 1950s (Erickson, 1964), after which both weather stations and satellite data could be used in climate science. When used in agriculture science, the main difference between satellites and weather stations is that weather stations provide accurate - but sporadic - data, while for satellites it is hard to measure near-surface phenomena (e.g. precipitation), although the spatial coverage is complete (Mendelsohn et al., 2007). The difficulties with interpolating weather station-data in areas with limited coverage in combination with the critique they often receive based on their exposure (e.g. Menne, Williams, & Palecki, 2010), has created the need for additional networks of connected weather stations. Examples of weather networks to which users can attach their personal weather station (PWS) include Weather Underground (Geller, 2007) and WeatherLink (DAVIS, 2014b). Despite the fact these networks generally demand certain standards of the stations, basic shields with micro-sensors could increase spatial coverage in areas where such networks still have limited coverage.

The decreasing cost, together with the increasingly small size of sensors and advancements in technology (related to data storage & transmission) are making the use of micro-sensors interesting for a wide range of purposes in the agricultural sector (Ruiz-Garcia et al., 2009). The initial objective of many of these sensors is generally related to commercial and closed-environment observations, such as logistics (e.g. Jedermann et al., 2006), but micro-sensors have already been used in clinical studies (van Marken Lichtenbelt et al., 2006), environmental studies including habitat monitoring (Mainwaring et al., 2002) and measuring ocean acidification (Rérolle et al., 2012). Weather observations can be linked to many local-scale recommendations related to variety recommendations and pest management; this includes linkages with IPM modules (DAVIS, 2014a), and assessment of the risk of phytophtora in potato (Baggio, 2005). Another use of high-resolution temperature and humidity data is to analyze the risk of (future) pests during different phenological phases. Different pest-models are discussed in Gaur and Sharma (2014). While basic temperature and humidity data can easily be used to calculate other issues such as Vapour Pressure Deficit and radiation estimates (*section 2.5 on crop thresholds*), additional information that is needed to provide detailed pest/disease risk and variety recommendations will include soil maps (including soil type, depth, pH), and the geographic distribution of pests/diseases. The current limitations of the creation of networks and related software for precision agriculture in developed countries are expected to include several issues. This includes the costs for the physical network (shields, sensors), and costs of maintaining these. A difficulty for creation of models linked to varieties is that the diversity of cultivated crops/varieties (and thus models) is expected to be higher in developing countries than in the developed world.

2.2 Sensors and Standards

While climate-monitoring networks can work with many different sensors, important issues in making the provided data robust is not only the sensor itself, but also the shield in which the sensor is placed. The actual sensors can be very cheap¹, while the larger construction in which they are placed adds important features such as memory, connectivity and sometimes robustness to shocks and water damage. The sensor housing - in case of the cheaper sensors - does not add active ventilation or other protection from radiation. This, together with the standards that are set by the WMO (*box 1*), creates the need for a robust shield in which the sensor will be placed. Some of the recommendations are easy to address in a low-cost sensor-shield (including height, inspection, comparison, coordinates, and metadata), while others are obviously more problematic when working with a limited budget. These include the addition of adequate radiation shielding, insulating material, and protection from water. While some 'robustness' can be added to the shield at low-cost, additional correction will likely have to be done by computer models. An important note made in the WMO Guide to Meteorological Instruments and Methods of Observation is that, while it is acknowledged that it might not be economically feasible to work with sensors that directly meet the accuracy requirements, '*it is necessary to limit the size of the corrections to keep residual errors within bounds*'. Issues related to the sensor resolution, temporal interval, and shielding, are discussed in the chapter on the data accuracy; a number of experiments will be analysed regarding different shield constructions with materials that can be found in almost all areas.

2.3 Implementation of Sensor Networks in Agriculture

Real-time climate monitoring and micro-sensors can provide useful information throughout the food sector. As a separate element, micro-sensors can be used to track commodities throughout the value chain, to assure it reaches the right people; sensor networks are promoted for use in integrated supply chains to get food to the poor in India (Viswanadham, n.d.). Climate monitoring, without using micro-sensors, can be linked to climate risk management (CRM) at a larger scale (an overview of CRM in agriculture is discussed in Selvaraju (2012)), although understanding local differences requires more detailed information. Similarly, small scale yield prediction and crop insurance can be based on satellite monitoring (Seelan et al, 2003; Singh et al., 2002), since satellites can detect vegetation changes (e.g. Vegetation Health Products - NOAA/NESDIS) and provide information at a level which is interesting for crop insurers. Sensors are also not absolutely necessary to study the microclimate, as issues such as elevation (Charney, 1949), canopy height (Deardorff, 1978) and leaf area index (Goudriaan, 1977) can also be linked to differences in local climate without having information about the actual atmospheric temperature.

The expected impact of canopy on understory climate (decrease of T_{max} and increase in RH_{max}) has been confirmed by Von Arx, Dobbertin & Rebetez (2012) based on long-term meteorological data. Although the relationship between temperature and humidity is well studied, and can be converted

¹Online markets (e.g Alibaba.com and Ebay.com) have (temperature and RH) sensors available for less than US\$ 1.

based on simple formulae (Lawrence, 2005), humidity indicators are less common in crop models than indicators based on temperature. Humidity thresholds are mainly interesting for prediction of plant diseases (Wilks & Shen, 1991), and for this reason could provide a valuable extra source of information to farmers. Low-cost climate networks can be linked to varietal trials and risk assessment, but research related to biodiversity can also benefit from this, by enabling to better study the relationship between local temperature and plant diversity (Letten et al., 2013) and to locate microrefugia (Ashcroft & Gollan, 2013).

Box1: Summary of relevant recommendations for weather stations (WMO, 2008)

1. For general meteorological work, the observed air temperature should be representative of the free air conditions surrounding the station at a height of between 1.2 and 2.0m above ground level.
2. A radiation shield or screen should be designed to provide an enclosure with an internal temperature that is both uniform and the same as that of the outside air; it should completely surround the thermometers and exclude radiant heat, precipitation and other phenomena that might influence the measurement.
3. Thermally insulating plastic-based material is preferred as material for the shield over the better performing highly polished, non-oxidized metal, because of its simple maintenance requirements; thermally insulating material must be used if the system relies on natural ventilation.
4. A humidity sensor may be combined with or co-located with a temperature sensor in its radiation shield as long as the sensor thermal output (self-heating) is very low.
5. Direct contact with liquid water will seriously harm sensors using hygroscopic electrolyte as a sensor element. Great care should be taken to prevent liquid water from reaching the sensitive element sensors.
6. Desirably characteristics include reliability and stability, simplicity of design, durability and acceptable cost.
7. Agricultural meteorological stations should be inspected at interval sufficiently short to ensure the maintenance of a high standard of observations and the correct functioning of the sensor.
8. Recording instruments should be compared frequently with instruments of the direct-reading type.
9. The position of a station referred to in the World Geodetic System 1984 (WGS-84) Earth Geodetic Model 1996 (EGM96) must be accurately known and recorded (1/1000 degrees latitude & longitude).
10. It is important that records should be kept not only of the temperature data, but also of the circumstances in which the measurements are taken (metadata).

2.4 Sensor Networks and Citizen Science

The term *e*-Agriculture was first promoted at the World Summit on the Information Society (Singh, 2012) in which it was identified as a key-action line to address the Millennium Development Goals. E-Agriculture is defined as an emerging field in the intersection of agricultural informatics, agricultural development and entrepreneurship, referring to agricultural services, technology dissemination, and information delivered or enhanced through the Internet and related technologies, but is going beyond technology and has as aim to improve the communication and learning processes in the agricultural sector (e-Agriculture, 2014). Although e-agriculture applications provide an interesting prospect to generate cost-effective solutions to information delivery, it will be relatively difficult to include farmer participation and avoid the risk of being a limited top-down approach. One way to include participation in e-agriculture, linked to sensor networks, is by applying a crowd-sourcing approach. Crowdsourcing is an approach in which tasks are outsourced to (paid or unpaid) volunteers, and has a long history in ecological research (Miller-Rushing, Primack, & Bonney, 2012).

Bioversity International, an international agricultural research institute member of the CGIAR Consortium, has developed an approach in which large numbers of farmers can test different modern and traditional crop varieties. Each farmer tests a set of small seed samples of three different varieties. They compare the varieties for a number of characteristics and report back on their findings and can also order more seed. Advanced algorithms, used in market research applications, are used to extract patterns from the data which are returned to farmers in an easily interpretable form (Van Etten, 2011). Involvement of farmers in these projects is not necessarily limited to providing feedback, but could also include the creation of the sensor shields (or more advanced climate-monitoring devices) by farmers (*tables 1 & 2*). After testing whether farmers can create the sensor shielding, other - more complex - instruments could possibly also be created by them. This has the potential to provide a win-win situation by providing off-farm income to farmers and by creating a cost-effective way of increasing the possibility for researchers to make climate measurements in rural areas.

Input:

- Micro-sensors
- Shield material
- Crop varieties
- Mobile phones
- Charging station
- Mobile application
- Financial support*

* If farmers create the PVC shields/
other required constructions.

Output:

Scientific:

- Varietal trials that can be linked to climate
- High-resolution temperature and humidity data
- More climate observations in rural areas
- Potential to study issues related to microclimates

Practical:

- Weather data that can be used in forecasting
- Data that can be linked to pest/disease risk
- Participation of - and income for - smallholders

Table 1: Input of crowd-sourcing projects

Table 2: Output of crowd-sourcing projects

2.5 Crop and Disease Thresholds

Thresholds related to temperature and in lesser extent humidity are available for a large number of crops. While these are often studied in detail for specific (staple) crops, models can be used to assess the impact of several limits on a wide range of crops. One of the first models to do this was the PLANTGRO model (Hackett, 1991), while one of the best known records - based on the same concepts - is the EcoCrop database. A well-documented threshold for crops is a daytime temperature of 30°C, while warm nights are also projected to have a negative impact on most crops (IPCC, 2014). The EcoCrop database does not include humidity, while elevation - not expected to have an impact outside of its relationship to temperature - is also left-out in the dataset in the *dismo* R-package. There are, however, still absolute and optimal minimum and maximum temperatures. The impacts will vary for the different phenological phases (Menzel et al., 2006). Studies that include this level of detail have only been made for few crops, such as maize, rice and wheat (Ewert & Pleijel, 1999; Sánchez, Rasmussen, & Porter, 2014). A model that includes the impact of thresholds during specific crop phases is the DSSAT model (Jones et al., 1998), but this model currently includes only 28 crops. The difficulty to model non-linear responses of crops to climate change is expected to result in an underestimation of the overall impact (Porter & Christensen, 2013). Not only does climate change impact on crops in different ways that are hard to accurately model, climate change will also have an impact on plant pests and diseases (Chakraborty, Tiedemann, & Teng, 2000; Rosenzweig et al., 2001). While combining all the different impacts into one model will be overly complicated when also considering different crop varieties, it can be expected that - when adjusting the agronomy to minimize risks - certain basic thresholds will be valid for a wide range of crops.

The network that will be created in this project is not intended to be linked to performance of crops in different phonological phases, but aims to create (with low costs) as many different indicators of crop performance and risk of diseases, as possible. Pest and diseases can be linked to humidity and temperature data, while crop performance requires information related to additional factors, such as soil type, water availability and solar radiation. Information about the soil (including pH, depth, permeability, and water content) is a completely different aspect, which would require at least a one-time soil sampling and continuous soil moisture measurements to include in models. The other factors can - at least partly - be derived from basic temperature and humidity data. With few additional parameters, temperature and humidity data can be related to solar irradiation (R_s) (Winslow, Hunt, & Piper, 2001), net evapotranspiration (ET) (Allen et al., 1998), and vapour pressure deficit (VPD) (Wang et al., 2004). Most of these indicators only require the maximum and/or minimum temperature and humidity as input, which means observations every three hours (assumed to give values relatively close to this) can be sufficient for basic studies of crop performance. While this would also be sufficient to calculate the mean temperature (the WMO standard formula for mean air temperature is provided below), more frequent observations will provide better information of daily extremes and the period above or below a certain crop/disease related threshold.

$$T_{mean} = \frac{(T_{min} + T_{max})}{2}$$

3 Data accuracy

3.1 Introduction

The objective of this study is to create a low-cost and robust network of climate-sensors. For this reason, it will be important to find a good balance between costs (both for materials as labour for maintenance) and data accuracy. The data has to provide relatively high-resolution information regarding the local climatic differences in the area, including daily and seasonal extremes. The number of sensors that are needed for a particular network has a high influence on the total cost. The sensors used have a resolution that provides output that is better than 0.5°C and 5% RH for a large temperature range. This resolution in itself is sufficient to link to most crop and pest/disease thresholds, as explained in *section 2.5*. As sensors cannot be placed everywhere, spatial interpolation will be needed to estimate weather data for locations between the sensors. This will decrease the accuracy of the data. The spatial accuracy will need to correspond to the spatial units about which farmers make decisions and where they conduct their experiments. Fields of smallholders are a fraction of a hectare in Central America, where this study was conducted, but accurate data at one hectare (100×100 m) resolution will be considered sufficiently useful in this project. Another factor of influence on the total cost of running a sensor network is the labour required to collect and process the data. The sensors used in this study do not yet allow for remote retrieval of the data. A straightforward solution to increase the period that the sensors can be used in the field is to adjust the resolution at which the sensors make their observations. Another option that is considered is whether it will be useful to include humidity measurements, as these will have some correlation with temperature and can be derived by a few sensors and some basic formulae (Lawrence, 2005).

Shields are also a major cost factor. Sensors are placed inside shields that should ensure that the measured temperature and humidity will be comparable to that in certified sensor shields. In case this is not possible, some form of data regression can be done, although this is not preferred. Several studies that have focused on low-cost sensor shielding, and have provided interesting recommendations for this research: Thomas and Smoot (2013) have used PVC tubes, but also included an aspirator unit in the shield. Tarara and Hoheisel (2007) warned for large errors when using open-bottomed shields. Holden et al. (2013) transferred the shields that are normally used beneath a forest canopy to the field by mounting them to poles, and Clark et al. (2006) have created a passively ventilated (inverted-U shaped) shield with PVC pipe. A general conclusion from these studies is that including (low-cost) active aeration and working beneath a canopy improve the results, as this can reduce the impact of midday radiation. The ISO Standard 17714 (ISO, 2007) '*Air temperature measurements: Test methods for comparing the performance of thermometer shields/screens and defining important characteristics*', is also considered in this experiment. Another issue that will be taken into account is that certain shields have previously been recommended by Bioversity International (Mittra, Van Etten, & Franco, 2013), based on Hellström and Mark (2006). The main differences with this study is that it was conducted at higher elevation and thus measured a lower ($2\text{--}16^{\circ}\text{C}$) temperature range, and used slightly smaller PVC tubes ($\frac{3}{4}$ inch) compared to the experiments in this study (1 and 2 inch

diameter, which is 25 and 50mm). As a first approximation, this study limits itself to a comparison of shields that have been used in previous studies. Recommendations are made regarding sensor resolution and shielding, as well as calibration techniques.

3.2 Materials and methodology

3.2.1 Sensors

The sensor that has been used in this research is the iButton Hygrochron (DS1923). This sensor has been selected because it can measure both temperature and humidity at low and high resolution, which can help to assess whether high-resolution, as well as humidity, data is required. This sensor costs US\$ 60. A simpler version of this sensor that can only measure temperature at a low resolution costs US\$ 15 (Maxim Integrated, n.d.). According to the specifications, the temperature accuracy is better than 0.5°C for most of the range (-10°C to $+65^{\circ}\text{C}$), while the accuracy of the humidity measurements is 5% RH. The DS1923 can store the temperature values with 8- or 11-bit resolution (0.5°C or 0.0625°C), and humidity with 8- or 12-bit resolution (0.6% or 0.04% RH). The total memory for this sensor (current generation) is 8192 bytes. By using the lower resolution sensor for both temperature and humidity, the sensor can store double the number of observation at the same time interval (*table 3*). The three options that are most interesting are highlighted; these options can cover a period of almost one year, but either require separate sensors to measure humidity and temperature, or measure at two-hour intervals. The other option measures both temperature and humidity (low resolution) at 1-hour intervals, but only has sufficient memory to store data over a period of 171 days, which would still be sufficient for many of the important staple crops around the world (at least the modern varieties), including rice, maize and wheat.

	Observations (n)	2-Hour interval	1-Hour interval	30-Minute interval	15-Minute interval
<i>One sensor at low-resolution</i>	8,192	683 days	341 days	171 days	85 days
<i>One sensor at high-resolution / two sensors at low-resolution</i>	4,096	341 days	171 days	85 days	43 days
<i>One sensor at low-resolution & one sensor at high-resolution</i>	2,560	213 days	107 days	53 days	27 days
<i>Two sensors at high-resolution</i>	2,048	171 days	85 days	43 days	21 days

Table 3: Time covered by different sensor settings (one micro-sensors contains a Ta and RH sensor)

3.2.2 Weather station and shield

CATIE (Centro Agronomico Tropical de Investigacion y Enseanza) is an agricultural research centre with headquarters in Turrialba, Costa Rica (Latitude: $9^{\circ} 53'$, Longitude: $-83^{\circ} 38'$). The centre has a meteorological station, which has been making measurements since 1942. The station includes two Stevenson shields, one of which houses a long-term (analogue) observation instrument. Data derived from sensors in this shield has been used to compare with the data derived from sensors in PVC shields to assess the accuracy of alternative PVC-shields. Also, our data can be compared with historical measurements. Additional information - except for temperature and humidity - that this station provides, includes precipitation, solar radiation, solar intensity, evapotranspiration and wind speed. This data will especially be important to compare with field data.

3.2.3 Alternative shields for the iButton sensors

In this study, the basic shield will be based on the Bioversity International manual '*Collecting Weather Data in the Field with High Spatial and Temporal Resolution Using iButtons*' (Mittra, Van Etten, & Franco, 2013). The PVC tube that has been selected is ± 1.5 meter long to be in line with WHO recommendations for weather instruments. It is white to reflect radiation, and can include holes for additional ventilation. The sensor is placed on a wire mesh at the end of the tube with an open bottom and is thus exposed to reflecting radiation (figure 2). The study on which this has been based has been conducted at high-elevation, which means the shields were not calibrated to $>20^{\circ}\text{C}$. Bioversity International projects in other regions that have used similar shields resulted in extreme temperatures that were not in line with what would be expected in these regions, indicating that the construction needs adjustment or the data requires calibration. The selected sensor design and exterior coating has been based on the research mentioned in the introduction. Bioversity International has worked with a similar design in other projects, so adjustments to this basic shield have been prioritized in this project.

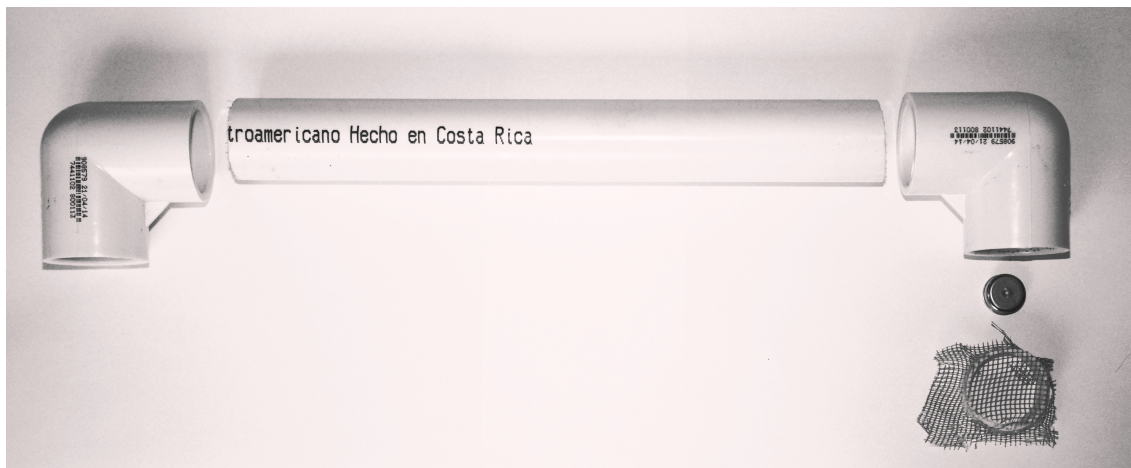


Figure 2: Top-tube lay-out of the shields

The reason to use PVC pipes is that these are to be used in field crops, where sensors cannot be hung from trees as is normally done in (agro-) forestry studies where these networks have a longer history. A self-sustained structure is needed and PVC pipes are a universally available material so that the shield can be constructed in any part of the world using exactly the same design. All tubes in the experiments were thin (25 to 50mm), white, PVC tubes existing of several parts: 1) a 1.75m main tube (25cm to anchor); 2) a PVC elbow attached to the main tube; 3) a small (20cm) second tube that will be attached horizontally to the elbow; 4) a second elbow that will be attached to the horizontal section and that will point down again; 5) a final 5cm tube that will be attached to the elbow and in which the sensor is placed. The sensor was placed on plastic mesh that will be located between the elbow and the final part. The position of the sensor and material of this mesh might influence the measurements, but alternatives were not tested. The PVC was sold per 6 meters (which might depend on the region). Three 1.75m tubes could be created of which 25cm has been used to firmly place the shield in the soil with the remainders used for the other parts.

3.2.4 Experiment 1: Sensor and temporal resolution

Objective

The aim of Experiment 1 has been to analyse the influence of temporal resolution and interval scale on the overall accuracy and fitness-for-use of information. This experiment serves to analyse the trade-off between the time the sensor can be left in the field and the accuracy of the resulting information. While a higher precision can be useful for some purposes, the data for the intended uses of this network do not have to be exact to 0.1°C ; around 0.5°C will be considered satisfactory, as most of the relevant thresholds are provided at a slightly lower resolution (1°C : *section 2.5 on thresholds*).

Set up

Experiment 1 has been done with a total of 30 sensors, making observations at 5-minute interval during one week in July 2014 at the CATIE meteorological station (observations started at noon). The sensors have been placed inside the Stevenson shield to ensure the conditions are very similar for all sensors. This shield, located at 1.5 m above the surface, provides protection against precipitation and radiation, while it still allows for sufficient (passive) ventilation inside the shield. For the first experiment, 15 sensors have been set at the highest temperature resolution (0.0625°C) and humidity resolution (0.04% RH), while 15 sensors have been set at low-res (0.5°C and 0.6% RH, respectively).

Analysis

The high- and low resolution sensors have been placed together throughout the shield to limit the possible impact of differences inside the shield, and linear interpolation has been used to attain values at 1-minute intervals. Basic statistics (mean, range, and standard deviation) have been calculated over the resulting dataset (30 *.csv files with >10.000 observations each). A second analysis that will be based on the same dataset of this first experiment focuses on the different statistics that results from working at different temporal intervals. The number of observations was reduced to

hourly or 2-hourly intervals by selecting the (a) closest observation to the full hour in the original 5-minute dataset, and (b) a random observation in the same time-window. The software that is provided with the iButtons does not enable the user to select an exact start-moment, so it has to be analysed whether this will make a difference. The user can select a certain delay before measurement starts, but when launching many buttons, this might become complicated and possibly costly when taking into account the time required. A third analysis of experiment 1 tests different interpolation techniques to transform the data to a regular time series. This includes using linear and spline interpolation approaches, which are available in the *zoo* R-package (Zeileis & Grothendieck, 2005).

Temperature differences are calculated for every day in different quantiles, and compared to the same data for the original dataset. Humidity is not analysed separately, as shielding is the same, and the relationship between temperature and humidity will be the same as in experiment 1. The average of the daily differences has been calculated and provided in a table for comparison. Differences between the temperature in the original dataset and the data that is the result from the adjusted interval and interpolated data have been categorized into different categories: $<0.1^{\circ}\text{C}$ is insignificant, $0.1\text{-}0.25^{\circ}\text{C}$ is *small*, $0.25\text{-}0.5^{\circ}\text{C}$ is *medium*, $0.5\text{-}1^{\circ}\text{C}$ differences can be considered *high*, and $>1^{\circ}\text{C}$ is *problematic*.

3.2.5 Experiment 2: Shields

Objective

The aim of the second experiment has been to test different low-cost adjustments to the control PVC tubes, to see if they result in robust outputs. Adjustments were mainly focused at improving the aeration around the sensor, and increase the reflectivity of the shield to avoid high temperature peaks during the periods with strongest solar radiation. No special tools (only tape, scissors, and a drill) were used for assembly. Comparing the data from different adjustments with the Stevenson shield has given some insight in the performance of the shields and possibilities for further calibration. The availability of several decades of climate observations was also used to place the data into context.

Set up

The second experiment (sensor shields) has been conducted during July 2014 at the meteorological station at CATIE (*figure 3*). As only one month was available, and different types of day are required to provide the most context, the sensors have been measuring for a long period and have been removed for reading after a day was found to be significantly useful to provide new information. Two diameters (25 and 50mm) have been tested. The first set of experiments on both a sunny and rainy day was conducted with the wider (50mm) tubes, after which the cheaper and lighter 25mm tubes were also tested on a sunny and cloudy/rainy day with most of the same adjustments, to analyse whether they had the same impact. While perforation was based on drilling holes, the materials for coating have been selected based on their cost and likely global availability. The materials have included reflective (red/white) tape, gutter tape, 6mm thermal insulation foil, fibre glass mosquito mesh, and different types of white paint. Galvanized metal sheets and metal mesh were also bought, but was



Figure 3: CATIE Meteorological station with PVC shields

found too difficult to cut/attach to the shields. Receipts of all purchases are provided in Annex 1. The coatings and holes were selected to provide the same functions as can be found in the certified Stevenson shield (*table 4*). As the time for this experiment was limited, and different types of day (sunny, cloudy/rainy) had to be analysed to assess the performance of the shields, some aspects could not be studied during this research. This includes placement of the sensor at different locations in the shield (now relatively exposed to reflective radiation) and the inverted-U shaped shield that has been recommended by Clark et al. (2006). As the shields were expected to provide incorrect data under periods of strong solar radiation, different approaches to data regression have also been studied.

Analysis

As, based on existing literature (*section 3.1: introduction*), shields were expected to have an exaggeration of the midday temperature in low-cost shielding, different approaches have been tested to reduce these peaks. Smoothing is expected to reduce the peaks during the midday, but these techniques (e.g. smoothing splines, LOWESS, and Turkeys running median) are symmetrical approaches and hence reduce the range of the lower temperatures as well. While settings have been adjusted to match the maximum temperatures in the Stevenson shield, the resulting minimum temperature was a lot higher as well, which gives a different picture of the local climate. For this reason, smoothing

Table 4: Characteristics of the different coatings of the PVC shields

Shielding	Description
<i>Stevenson shield</i>	The reference station is a Stevenson shield that has been used for temperature and humidity measurements at CATIE for several decades. The shield is placed at 1.5 m above the surface and contains an analogue temperature/humidity logger.
<i>White paint</i>	Paint has been applied to the top-tube of the shield, as well as the elbows. Spray paint (Bosny Blanco Brillante) was used, but this did not provide a reflective layer on the tube and could be considered a matt paint layer with limited reflectivity.
<i>Perforations</i>	Perforations have been made by an electric hand-drill and the size of the holes was different for the larger and smaller tubes. The exact size of the holes is not known, but it was assessed (visually) that approximately 30% of the top-tube was drilled out.
<i>Insulating foil</i>	The top-tube, as well as an extra 10cm on both sides of this tube, was covered by a 6mm insulating foil with a white and silver side. The foil, with the silver side facing outwards, was tightly tied to the top tube at two places with thin adhesive tape.
<i>Insulating foil + perforations</i>	This combination included the 30% holes, and the same insulating foil as above. The foil was more loosely attached to the tube, the holes at the bottom were still completely open. Holes at other locations might have had restricted air flow.
<i>Reflective tape</i>	Two types of tape have been used. The first (red/white reflective) is normally attached to trucks to increase visibility, while the other was a silver-coloured tar-based tape that can be used to close holes in roofs. This tape was very thick.

was not attempted in this study. Two approaches that were tested are polynomial and quantile regression. An important advantage of quantile regression is that it can provide more robust data with less impact of outliers (Yu, Lu, & Stander, 2003). Studying the required data-correction has not only focused on the actual temperature/humidity in the reference shield versus the temperature/humidity in the test shields, but has also analysed whether differences can be explained by looking at the rate of change over time (ΔT in Stevenson vs. PVC shield). The latter will be more difficult to correct the data, as there is a risk of cumulative errors and it will have to be done for all separate days (using an anchor-hour). An algorithm has been tested (experiment 3) to assess whether correction based on change over time provides good results. Both temperature and humidity were analysed, as shield-adjustments were expected to have an impact on both types of data that was measured, due to differences in thermal inertia.

3.2.6 Experiment 3: Data calibration

Objective

After the sensor and temporal resolution have been analysed, as well as the impact of different shields, data calibration has been done to find models that can best predict the actual (Stevenson) air temperature based on the temperature in the shield. This will only be done for temperature, after which the previously found correlation between temperature and relative humidity assessed in the Stevenson can be used to predict the relative humidity as well. The objective is to find a model

that results in the least errors for all hours in the day, which can be applied to the field data as well.

Set-up

The set-up of this experiment is the same as in experiment 2, with the five different days that have been analysed in different PVC pipes. The data that has been calibrated is the 'control' data versus the Stevenson data, as the control dataset contains the most observations for calibration and the 'control' shields have already been used for experiments in different regions as well. Both sample and control dataset contain 7,200 minute observations, and 120 hourly observations, which have been analysed. The calibration has also been validated with field data, which are introduced in the next chapter.

Analysis

Two main approaches have been tested in this experiments: calibration based on the measured temperature in the PVC shields versus the Stevenson and calibration based on the hourly change in temperature in the different shields. The first approach has applied a polynomial model (1st to 3rd order) to fit the PVC data to the Stevenson data during the five days of experiments at the CATIE meteorological station. This calibration used the temperature at the minute (full days), which means all (2 times) 7,200 observations have been used to create the polynomial model. For each day the errors at every hour have been squared and subsequently the mean of the square root of these errors has been calculated. The mean of these hourly square-root errors has been compared between the different polynomial and change-in-time calibration models to find the model with the lowest errors.

In order to create the model based on change in time, first two anchor points have been created based on the five days with observations every 5-minutes. The smallest absolute difference in temperature between the PVC tube and the Stevenson has been calculated within two hours from the time of sunrise in the month of July (5.20 AM). This is expected to be the moment from which differences between the PVC and Stevenson can become problematic due to the impact of solar radiation. The median of the moments with lowest difference has been selected as the anchor point, and this moment (at a given minute) has been rounded to the closest hour. The same has been done for the evening: the lowest difference after the morning has been calculated and rounded to the closest hour. This has created a certain time-window that could be calibrated, while the rest can remain the same. For all five days, the calibrated data has been created by creating a vector with the morning, after which several hours of calibrated data were calculated, followed by the data for the evening. Data for the morning and evening has also been calibrated by testing the impact of different adjustments ($\pm 0\text{--}1^{\circ}\text{C}$) of the hourly temperature. The main calibration has been based on the change in time, for which a linear model has been created.

The linear model for the change in time has been based on hourly observations during the period that has to be calibrated (five times 12 hours). The differences over time during this period could be calculated for the 12-1 hours in between these hours. The difference in time in the PVC shields were fitted to a linear model, creating different values, which were cumulatively added to the anchor

point. New values are thus created for a number of hours every day, based on a linear model of the change in time. Several parameters in this calibration have been tested. The first is a certain multiplication of the change in time that have resulted from the prediction model. Values between 0 and 2 (steps of 0.01) have been tested to see which value provides the lowest errors with the control (Stevenson) data. The other two parameters that have been tested are the addition/subtraction of a certain temperature in both the morning as during the day (after the multiplication of change in time has been tested). Values between -1 and 1 have been tested in steps of 0.01 to find the closest match to the control data. This tuning has resulted in three parameters that were added to the calibration model. The root-mean-square errors against which data is compared has a value of 0.66°C during the five days, although the errors are significantly larger during the day (7am - 5pm: 1.21°C), compared to the night (0.27°C). Model validation has been done by leave-one-out cross-validation, in which the model and parameters has been calibrated based on $n-1$ days, after which the RMSE for the left-out day was measured. The results have been used to create a preliminary model based on the physical properties of the PVC shields.

As this analysis provides the root-mean-square-errors for the two types of calibration based on five days of testing in fully sunny positions at a meteorological station, but the field-testing will be done in an area with more shading and a more complex terrain, different polynomial models and calibration based on change in time will also be tested for the field data, to see which provides better data. Of the hundred sensors that have been placed at the Aquiares farm (discussed in more detail in the next chapter), three have been placed close to a weather station, which contains a Campbell sensor placed at 26 meters above the surface. Data for the same period is available at 30-min interval, and the hourly values will be compared with the calibrated hourly values of the three closest sensors, to see which adjustment fits best with the data at this weather station. The air temperature derived from this sensor has a range of $16.0\text{-}25.3^{\circ}\text{C}$ and a mean temperature of 19.8°C during the period that has been studied. Relative humidity is also available and has a range of 55.1- 99.9% and mean of 87.7%. As the sensor is placed high above the surface, the calibrated data will also be compared to data at CATIE (taking into account the standard/wet adiabatic lapse rate) and data for August in the WorldClim dataset.

The absolute minimum and maximum temperature (average 2003-2013) at CATIE in August are 17.3 and 30.5°C . Taking into the ± 400 meter elevation difference between both locations and a adiabatic lapse rate of $6.4^{\circ}\text{C}/\text{km}$, the range at the location in Aquiares can be expected to be around $14.8\text{-}27.9^{\circ}\text{C}$. This is a significantly larger range than was provided by the temperature logger in Aquiares. The WorldClim dataset (Hijmans et al., 2005) contains current, past and future conditions at 30 arc-second resolution, based on 24,542 locations that measured temperature (60% of which also included minimum and maximum temperature observations). In the study area, the maximum temperature is on average 4.8°C higher than the mean temperature, while the minimum temperature is 4.8°C lower in August. This range (9.6°C) is comparable to the range provided by the weather station in Aquiares (9.3°C) and is smaller than the range at the CATIE station (13.1°C).

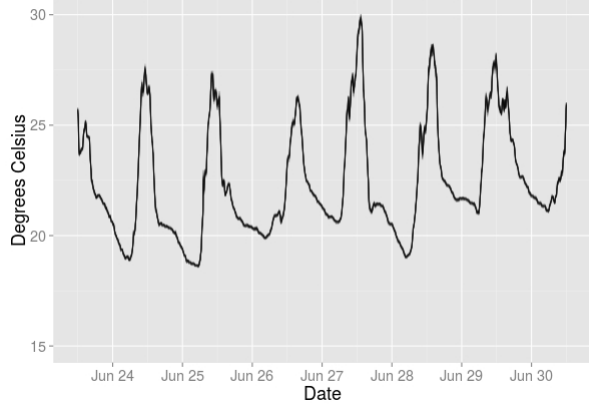


Figure 4: High-resolution T sensor-data

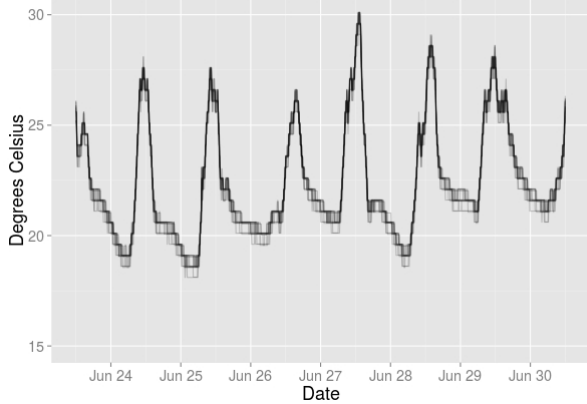


Figure 5: Low-resolution T sensor-data

3.3 Results

3.3.1 Experiment 1A: Sensor resolution

Based on a one-week experiment with 15 high- and low-resolution sensors, the (uncorrected) differences for the resulting temperature and humidity data has been studied. The temperature and humidity of the separate (15) sensors for each resolution are plotted in *figure 4 and 5*. The temperature graphs show that the lower resolution has an impact on the maximum difference and standard error at any moment: the maximum difference between any two sensors is 1.02°C for the low-res and 0.65°C for the high-res sensors and the standard error is 0.26°C for the low-res and 0.05°C for the high-resolution sensors. The errors for the low-resolution sensors are highest during the period without sun (which rises around 5.20 AM local time during August). The minimum temperature also shows the largest difference between the low- and high-resolution sensors (0.43°C), compared to 0.02°C for the mean and 0.10°C for the maximum.

The graphs of the humidity data (*figure 6 and 7*) do not show the same clear differences between the low- and high-resolution sensors as the temperature graphs. Part of this can be explained by the still relatively high resolution (0.6% on a 40% range compared to 0.5°C on a 15°C temperature range), but also by the micro changes in humidity that occur close to 100% RH. The large fluctuations at high humidity - which shows no relation with the different sensor resolution - results in fudging of the data to a $\pm 5\%$ RH window. The relative humidity range of the low-resolution sensor is 63.9-99.9%, which is 64.3-100.2% for the high-res sensors (>100% values can occur when the sensors are in contact with water). The mean is within 0.5%, with 90.4 for the low-res and 90.9 for the high-resolution sensors. The standard deviation is comparable, with 1.1% for the low-resolution sensors, and 1.2% for the sensors at high resolution. It has to be noted here that high-resolution humidity is stored in 12-bits, while high-resolution temperature data is stored in 11-bits. This could reduce the difference between low-and high-res data for both units.

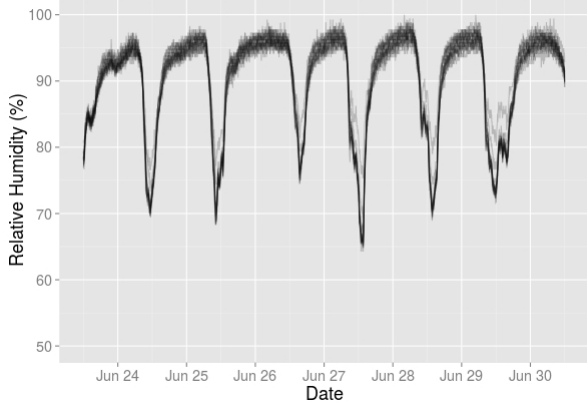


Figure 6: High-resolution RH sensor-data

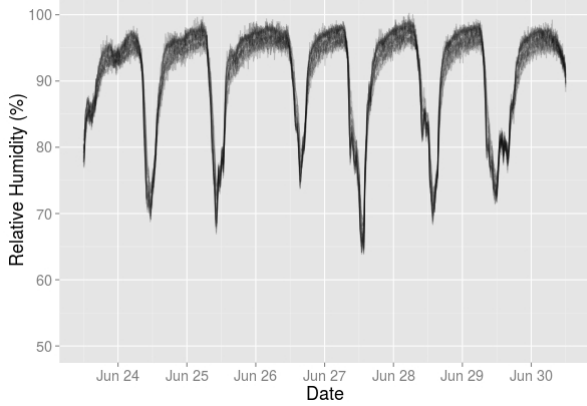


Figure 7: Low-resolution RH sensor-data

Correlation between the temperature and humidity measurements, which could be used to reduce the number of the more costly sensors that can measure both temperature and humidity in similar studies, is strong for both the low- and high resolution sensors. The mean correlation over the seven-day period is -0.91 for the low resolution sensors (never weaker than 0.86) and -0.92 for the high resolution sensors (always stronger than -0.89). This results in linear models with an R-squared of 0.84 (low-res) and 0.86 (high-res), which are strong models that can be used to reduce the number of sensors that measure humidity. The errors of using different resolutions for temperature and humidity observations has been calculated with different methods for both individual sensors and the mean data, and is consequently larger between the different temperature resolutions than the low- and high humidity resolution. The average of the maximum absolute difference at any hour is 0.27°C (max: 1.3°C) for the low-res and 0.05°C (max: 0.8°C) for the high-res sensor, while for humidity the average maximum absolute difference is 1.2% (max: 11.8%) for the low-res and 1.4% (max: 9.4%) for the high-res observations. While the high-resolution sensors provide better information in all cases, the difference is less significant for humidity than for temperature data.

3.3.2 Experiment 1B: Temporal resolution

The assessment of the impact of changing the temporal resolution has been based on the same (low- and high-resolution) dataset as the previous experiment, but with a reduced number of observations and with different moments the sensors were launched. The temperature range for any of the low-res sensors during the week of experiments has been $18.11 - 30.12^{\circ}\text{C}$, which was slightly lower ($18.54 - 30.02^{\circ}\text{C}$) for the sensors at high-resolution. Over the week of observations, the mean temperature (averages of the 15 sensors) was 22.37°C for the low-resolution sensors and 22.35°C for the high-resolution sensors. The average minimum temperature was 19.44°C for the low-resolution sensors and 19.81°C for the high-resolution sensors. Average maximum temperature was higher for the low-resolution sensors, with 28.34°C , while this was 28.10°C for the low-resolution sensors. This shows that the range for the low-resolution sensors is around 0.5°C larger, while the mean temperature is similar for both sensor types. *Table 5* shows the impact of different temporal intervals,

interpolation approaches and launching moments on the resulting temperature in different quantiles. It is clear that from the minimum temperature up to the median/mean temperature, differences are very small, and longer intervals generally result in slightly higher minimum temperatures. Differences become larger in the 3rd quantile (0.75), although in most cases still remain small.

The first medium ($>0.25^{\circ}\text{C}$) differences can be seen for some of the 2-hour data that have been created with the high-resolution sensor. At the 0.9 quantile, all values have at least a small difference, and in this case the low-resolution sensors show more medium differences as well, which can be found more for the 1-hour than for the 2-hour intervals. At the 0.95 quantile, the differences become smaller again, with the four 1-hour/low-resolution datasets providing insignificant differences. This is the case for the splined 1-hour high-resolution datasets as well. Only the closest observation datasets at 2-hour (both sensor types, both interpolation approaches) provide medium differences with the original dataset. The differences with the maximum temperature during the seven days of measurements is in almost all cases medium to large. The only small difference is found for the high-resolution sensors with random start moment and 1-hour interval. Differences are large for all - except for one (high-resolution sensor with random start moment) - of the 2-hour interval datasets. The standard deviation is small (although in line with the original dataset) for the low-resolution sensors, while this is insignificant for the high-res sensors (closest), and small for the high-res sensor (random). The maximum differences at any moment are especially problematic for the data with random start-moment, where they are in all cases larger than in the *closest* dataset.

Table 5: Differences in temperature at different quantiles using a range interpolation approaches

	Min	0.05	0.1	0.25	0.5	Mean	0.75	0.9	0.95	Max	St.dev	Diff
Low-resolution	19.44	19.94	20.04	20.54	21.60	22.37	23.97	25.84	26.84	28.34	0.26	1.07
<i>Closest</i>												
1-hour linear	+0.01	0.00	-0.02	0.00	-0.01	+0.01	-0.16	+0.27	+0.06	-0.37	0.26	0.93
1-hour spline	0.00	-0.01	-0.02	0.00	0.00	+0.01	-0.16	+0.27	+0.06	-0.32	0.27	1.01
2-hour linear	+0.01	0.00	-0.04	0.00	+0.03	+0.03	-0.13	+0.18	+0.40	-0.63	0.26	0.92
2-hour spline	0.00	0.00	-0.05	0.00	+0.03	+0.03	-0.12	+0.18	+0.40	-0.59	0.26	0.96
<i>Random</i>												
1-hour linear	+0.07	+0.01	+0.08	+0.04	0.00	0.00	-0.11	+0.15	-0.02	-0.31	0.27	1.18
1-hour spline	-0.02	-0.01	+0.05	+0.01	-0.01	0.00	-0.09	+0.25	+0.06	-0.23	0.28	1.36
2-hour linear	+0.16	+0.07	+0.16	+0.12	+0.02	+0.01	-0.23	+0.11	-0.10	-0.90	0.32	1.44
2-hour spline	+0.03	-0.02	+0.04	+0.03	-0.02	+0.01	-0.18	+0.25	+0.21	-0.62	0.33	1.58
High-resolution	19.81	19.98	20.10	20.59	21.60	22.35	23.95	25.80	26.87	28.10	0.05	0.46
<i>Closest</i>												
1-hour linear	+0.06	-0.01	-0.01	-0.01	-0.04	+0.01	-0.20	+0.23	-0.10	-0.33	0.04	0.32
1-hour spline	+0.06	-0.01	-0.01	-0.01	-0.04	+0.01	-0.20	+0.23	-0.09	-0.32	0.05	0.32
2-hour linear	+0.09	-0.01	-0.02	+0.04	-0.04	+0.03	-0.25	+0.10	+0.46	-0.63	0.04	0.31
2-hour spline	+0.09	-0.01	-0.02	+0.04	-0.04	+0.03	-0.25	+0.11	+0.47	-0.62	0.05	0.31
<i>Random</i>												
1-hour linear	+0.07	+0.02	0.00	0.00	-0.02	+0.01	-0.15	+0.22	-0.12	-0.31	0.10	0.64
1-hour spline	+0.05	0.00	0.00	0.00	-0.02	0.00	-0.13	+0.21	-0.06	-0.13	0.10	0.94
2-hour linear	+0.12	+0.08	+0.04	0.00	-0.01	0.00	-0.20	+0.15	-0.10	-0.61	0.19	1.03
2-hour spline	-0.02	+0.01	0.00	+0.06	-0.06	+0.01	-0.27	+0.29	+0.18	-0.46	0.19	1.41

3.3.3 Experiment 2: Shields

An initial test to compare the temperature in the control group (tubes with the least external coating) with the temperature in the Stevenson shield (*figure 7*) clearly shows much higher peaks in temperature in the PVC shields during the midday period. This can be seen for all days, except the fourth day (which runs from 3PM to 3PM) where temperature does not surpass 23°C , which has been a completely cloudy day. Whereas the temperature rises faster (and peaks are higher) in the PVC tubes, it also drops faster, resulting in lower temperatures in the tubes than in the Stevenson shield when the temperature is lowest (after the sun has set). This results in both a higher maximum temperature and a lower minimum temperature in the PVC tubes, although the difference is smaller and not problematic for the minimum temperatures.

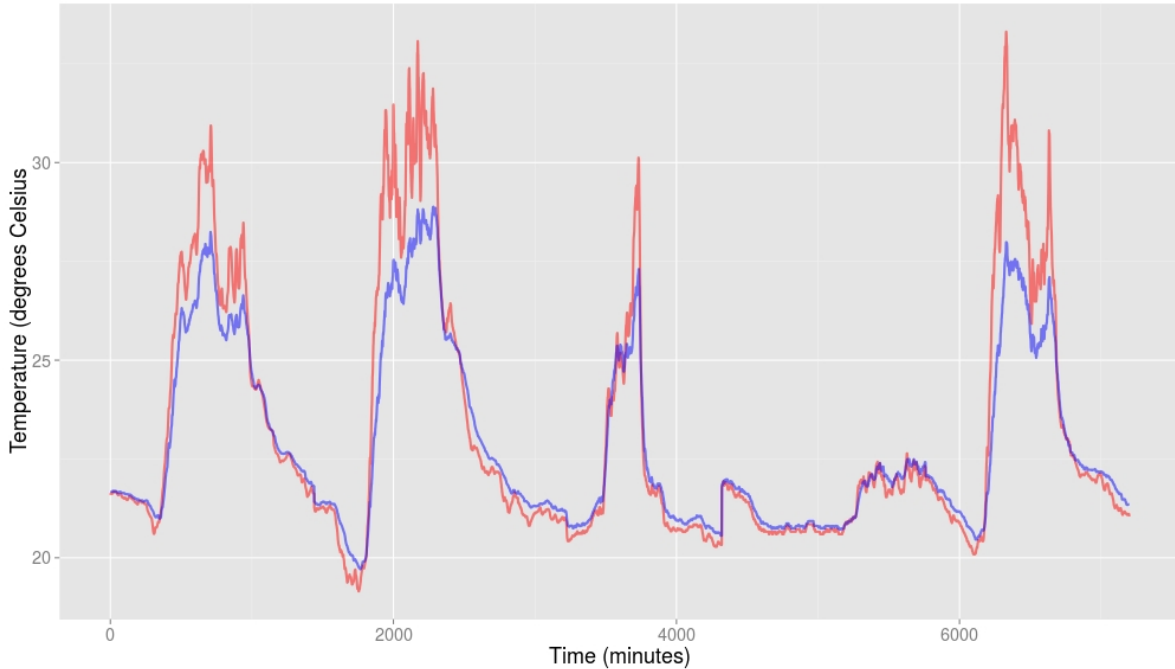


Figure 8: Temperature in the Stevenson (blue) vs. PVC (red) shields

A visual analysis of the graph (*figure 8*) shows that temperature in the Stevenson shield and the control PVC shields is similar in the early morning, which relates to a temperature around 22.5°C . The maximum temperature is several degrees higher in the PVC shield, while the minimum temperature is a bit lower. After the point where temperature in the Stevenson and PVC shields is relatively similar in the morning, a more curvilinear pattern is present. Under higher temperatures, more (short) sunny periods occurred, which warm up the PVC shields quicker than the Stevenson shield. The change in time in the Stevenson versus the control tubes is shown in *figure 9*. The linear models to predict change over 15 and 30 minutes, as well as 1 and 2 hours, are provided on the next page. The linear models of the change in temperature over time in the Stevenson versus the change in the different PVC shield adjustment is provided in Annex X.

$$15 \text{ mins} : T_{PVC} = 1.83 \times T_{station} \quad (R^2 = 0.75)$$

$$30 \text{ mins} : T_{PVC} = 1.65 \times T_{station} \quad (R^2 = 0.81)$$

$$1 \text{ hour} : T_{PVC} = 1.52 \times T_{station} \quad (R^2 = 0.87)$$

$$2 \text{ hour} : T_{PVC} = 1.46 \times T_{station} \quad (R^2 = 0.90)$$

The models with the lowest slope and the highest R-squared can be expected to provide the best results, but it has to be taken into account that there will be trade-offs with costs as well. The best adjustment to the shields on which temperature-calibration can be based is adding insulating foil, which has an R^2 that is 0.05 higher than the control tube, and a slope that is 0.09 lower (Annex X). A problem that occurred with the later experiments (smaller tubes) is that during the experiments the fence around the meteorological station was cleaned by a high-pressure hose, which caused problems to the measurements. On the fifth day of experiments, the relative humidity in the Stevenson shield was above 100% for over 40% of the day, which is likely the result of cleaning of the Stevenson. On the fourth day of experiments, humidity also showed a different trend from the other days, but in this case a similar trend (limited fluctuation over the day, but large over a short period) is also seen in the PVC tube, with 32% of the day having a relative humidity >100%. This could be the result of a fully rainy day. The table for the humidity models is provided below. The day with incorrect measurements in the Stevenson is removed, the other four days are used.

The linear models and coefficients of determination (Annex X) only provides part of the impact of the different coatings in dealing with different circumstances; *tables 6 and 7* provide the temperature statistics on different types of day and in PVC tubes with the smaller (25mm) and larger (50mm) diameter. The same analysis for temperature is provided in Annex X. The insulating foil provides the closest match for the maximum temperature on sunny days, although this difference is still $>3^\circ\text{C}$ in both types of tubes. Insulating foil also provides the closest match to minimum temperature on the sunny days, and is $<0.2^\circ\text{C}$. On the cloudy days, the overall differences are smaller, and only the shield with holes clearly provides worse results than the other adjustments (larger standard deviation and difference with maximum temperature). The standard deviation, which is based on the different shields - each with 2 sensors - with the same coating, is in the same range for most coatings on a sunny day (except for reflective tape, which shows more deviation). Holes show both the highest and lowest deviation on the two cloudy days, indicating that - while the benefits can be significant of increased aeration - there is a risk of sensor contact with water.

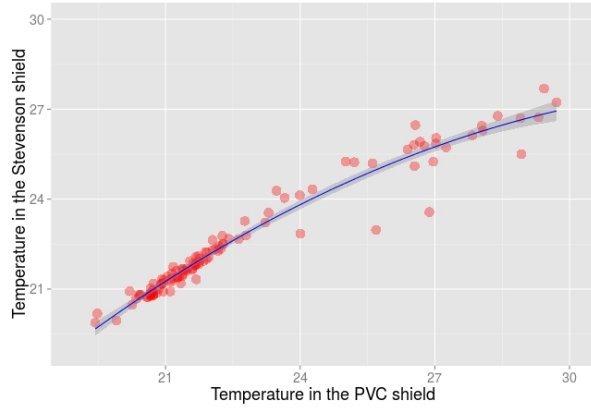


Figure 9: Correction based on actual Ta

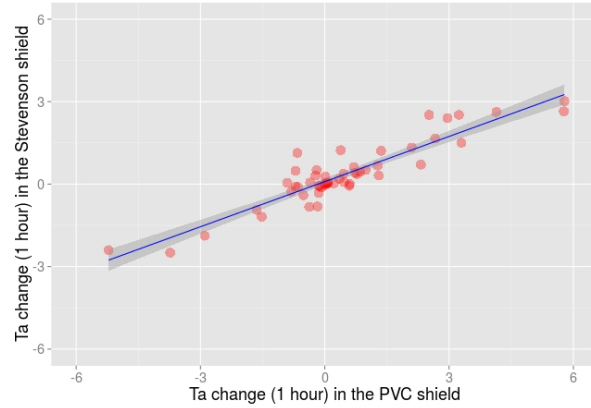


Figure 10: Correction on change of Ta in time

The humidity data in the different shields (Annex X) shows that the maximum relative humidity in the shield surpasses 100% on every day, while this is normally not the case in the Stevenson shields. The cloudy day on which the 25mm tubes were tested, however, shows a very high humidity (114% in the Stevenson). This was the day that the border around the meteorological station was cleaned, and water has infiltrated the Stevenson (where water could not escape as easily as in the PVC shields). The mean humidity that is provided by the shields is relatively similar, while insulating foil seems to increase the maximum humidity (and standard deviation) on sunny days and holes (in combination with foil) has provided clear incorrect data on the cloudy day when the 50mm was tested.

Table 6: Analysis of adjustments on 50mm PVC shields

	Sunny day				Cloudy day			
	Mean	Min	Max	Dev	Mean	Min	Max	Dec
Stevenson	23.92	19.68	28.94	0.04	21.92	20.48	27.40	0.05
White paint	24.61	19.08	33.78	0.25	21.81	20.23	30.87	0.10
Holes (+- 30%)	24.38	19.16	32.47	0.21	21.68	20.20	31.82	0.24
Insulating foil	24.61	19.48	32.17	0.22	21.92	20.27	30.20	0.08
Holes + Foil	24.76	19.36	33.24	0.24	21.80	20.23	30.31	0.12
Reflective tape	24.70	19.20	34.43	0.42	21.77	20.27	30.17	0.20

Table 7: Analysis of adjustments on 25mm PVC shields

	Sunny day				Cloudy day			
	Mean	Min	Max	Dev	Mean	Min	Max	Dec
Stevenson	23.23	20.42	28.12	0.04	21.40	20.68	22.53	0.04
No adjustment	23.94	20.05	34.07	0.17	21.29	20.55	22.70	0.05
Holes (+- 30%)	23.80	19.95	33.14	0.13	21.24	20.52	22.59	0.02
Insulating foil	23.72	20.24	32.27	0.10	21.31	20.55	22.89	0.09
Holes + foil	23.82	20.12	33.30	0.12	21.30	20.56	22.62	0.20

3.3.4 Experiment 3: Data calibration

The median moment with the smallest difference between the (control) PVC shields and the Stevenson shield - within a 2-hour window from the sunrise (5.20 am) during the five days of experiments - was 5.55AM, which is rounded to 6am in further calculations. The moment in the evening with the lowest difference during the experiments was 4.56 pm, rounded to 5PM in the model. The number of hours that has to be calibrated every day, in the case of calibration on the change in temperature over time, is 10 hours: the first calibrated hour is 7 am and the last is 4 pm. The hours between midnight and 6AM, as well as 5PM to midnight, will not be calibrated. The temperature outside the calibrated range is slightly lower in the PVC shields than in the Stevenson, (*figure 8*), which means a certain fixed temperature will be added to the PVC-temperature to get a closer match to the control temperature. Addition of a temperature of 0.22°C in this 'night' period showed the best match to the Stevenson temperature, and has reduced the RMSE during this period to 0.16°C .

The performance of the different models, compared to no calibration, are provided in *table 8*. The polynomial models perform clearly better when moving from 1st (linear) to 2nd (exponential) order, while performance of the 3rd order polynomial model is comparable to that of the 2nd order polynomial model. The fourth order polynomial model has an average RMSE of 0.25, which is a very small improvement compared to the extra order that is used in the model. The polynomial model is a clear improvement over the data without calibration, especially for the day-time temperature, maximum difference and also the overall RMSE. Calibration based on change in time, which has a linear model - calibrated based on 55 hourly observations - with an R^2 of 0.88, is done for 10 hours. No additional parameters (adjustment of night-time temperature and fitted change in time) provide only a small improvement over the non-calibrated data, and has the same RMSE during the night, and limited improvement during the day and maximum difference between the data. The best-calibrated model multiplies the fitted change in time by a factor of 1.35 (after which 0.11°C) is added), while the night-time temperature in the PVC is increased by 0.22 during the other 14 hours. The result of this model has a RMSE similar to 2nd order (and higher) polynomial models, and performs well during both the day and night. The main difference with the polynomial model is that the maximum difference at any moment remains slightly higher.

Table 8: Errors in different types of calibration (Ta) compared to data in a Stevenson shield

	No calibration	1st order polynomial	2nd order polynomial	3rd order polynomial	Delta-T, no parameters	Delta-T + parameters
RMSE overall	0.66	0.33	0.26	0.26	0.57	0.26
RMSE night	0.27	0.22	0.15	0.16	0.27	0.16
RMSE day	1.21	0.48	0.42	0.40	1.00	0.39
Max error	4.83	2.12	2.13	2.06	3.01	2.41

Calibrating has been done under homogeneous conditions, with all sensors at the same elevation and with similar exposure to sun and wind. The 2nd order polynomial has been selected as the best polynomial model, with overall good statistics with a relatively low-order. Calibration of the change in time, with the previously provided parameters, is selected as the best model to predict temperature based on change over time. This model has been validated with a leave-one-out approach, which has resulted in similar model parameters and also a low ($<0.5^{\circ}\text{C}$) RMSE for the day that was left out. This indicates that the model can explain the warming in the shields (thermal inertia) during the studied period (Annex X). This is a preliminary model that will have to be tested in other regions and in periods. Both calibration model will be tested on field-data (discussed in detail in the next chapter), which is derived from sensors placed close to a weather station for comparison. Three sensors are placed at close distance to a certified weather station (sensors 31, 41 and 57). The uncorrected data of these sensors is plotted in *figure 11*, and shows a range of $14.1 - 34.8^{\circ}\text{C}$. The problem that becomes clear from this figure is that sensors in comparable shields and at a similar location can still have very different temperature ranges. In this case, two sensors have clear extreme temperature during the period around noon - in line with the previous experiments at the CATIE weather station, while the other sector has a much more stable temperature - either caused by permanent shading or contact with water.

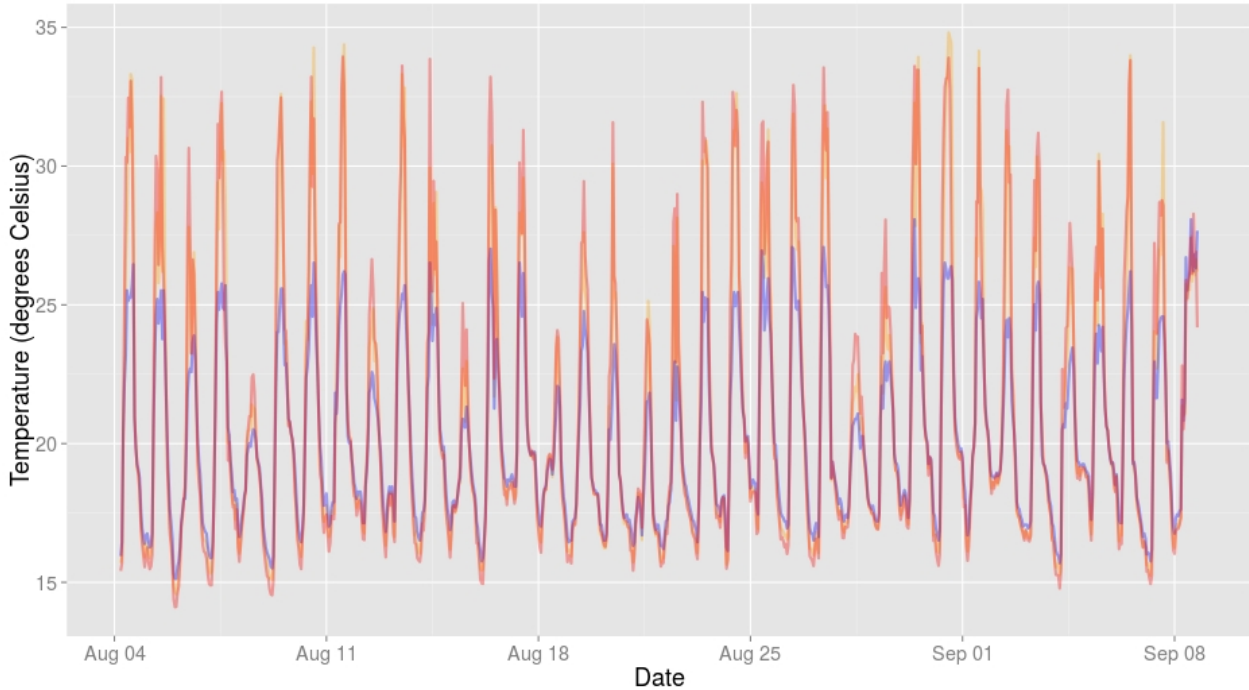


Figure 11: Observed temperature in three sensors around the eddy tower (blue = shadow sensor)

The trend of this *cool* sensor has not been encountered during any of the previous experiments, and does not show any indication of contact with water or other errors. The mean is also quite different between these sensors; the sensors with high peaks have a mean temperature of 21°C , while this is a low 20°C (20.2°C) for the *cool* sensor, which means they are still within 1°C . This figure also shows that extremes are caused by the moment of day, as even on relatively cool days the temperature around noon can differ several degrees between sensors. Based on the visual analysis and earlier experiments, it seems that most of the sensors have performed similar to the two sensors that showed the $>30^{\circ}\text{C}$ temperatures, which means correction will mainly focus on these sensors and aim to limit the impact of data-correction on the *cool* sensors. Based on the temperature range of the shaded sensor in *figure 11* ($15.1 - 28.1^{\circ}\text{C}$), it can be expected that this will be in line with the temperature range as measured by certified stations. The results of different calibrations (Annex X) generally provides a minimum temperature below 15°C during the studied period, which is 1°C lower than the eddy tower.

The linear calibration, however, provides a $>16^{\circ}\text{C}$ minimum, which could be considered closer to the temperature measured at the eddy tower. The minimum of the three other calibration approaches is generally still close to that of non-calibrated data (which has performed well in the CATIE-experiments), and also closer to the temperature (14.8°C) that can be expected based on a standard adiabatic lapse rate. The median temperature in the different calibrations ranges between 18.9 and 20.2°C . The maximum temperature fluctuates even more, which a lowest value of 23.7°C for the *cool* sensor when calibration on delta T (without calibration parameters), and a highest value of 31°C for a sensor in the calibration based on a linear relationship of the temperature in the PVC shield and in the Stevenson. The two best approaches for CATIE data-calibration (exponential and change in time with parameters) provide very different outputs when using them for the actual field data, which becomes especially clear for the higher values. While the maximum of the change-in-time (with additional parameters) provides a maximum that can be considered impossible for the study area - which is not the case for the exponentially corrected data - only from the 0.97 quantile, the data for the deltaT method becomes higher than the polynomial corrected data. At the 0.9 quantile, polynomial corrected data is still over 1°C higher than data derived from deltaT correction. This means only a small part of the data that is corrected by the latter method can be considered to be incorrect. One option to avoid these extreme values would be to set a certain quantile as the maximum temperature. Assuming change-in-time correction faces problems for 2% of the data, it could be decided to reset data above the 0.98 quantile to the 0.97 quantile. This is an easy way to avoid outliers in the dataset, although it also smooths the data.

A final test will assess whether the calibrated values still show the expected adiabatic lapse rate over the study area, and whether they show similarity to the minimum, mean and maximum temperature as assessed in the WorldClim dataset. The difference in mean, minimum and maximum in the WorldClim data for August (current climate) over the study area is around 20°C (± 600 m). This is similar for the four tested calibrations (linear, exponential, delta T with/without parameters), with a range between $1.75-2.25^{\circ}\text{C}$ (Annex X). The maximum value for the different mean temperatures (at

the lowest elevation), differs by up to 1.5°C (linear vs delta T without parameters). The trend for the minimum temperature in all cases shows a lower minimum in the higher regions. The differences are very small for the delta T calibrations (which do not adjust the minimum temperature), with values around 0.8°C . While this is a very small difference, this is the minimum that has been assessed is the absolute minimum during one month of observations under very wet conditions (especially during the night when the minimum is normally found). There might also be more local differences caused by mountain flows (McNider & Pielke, 1981); different factors can influence the collection of cooler air in the valleys(Barr & Orgill, 1989). Measurements of the minimum were quite accurate during the earlier experiments at CATIE. A low difference for the minimum is thus not a significant problem.

For the maximum temperature, the differences between the low and high areas of the study area are lowest for the exponential calibration (1.80°C) and delta T method without parameters (3.0°C), while the other two calibration approaches provide differences of 4.2°C (linear model) an 4.7°C (delta T with parameters). The calibration approach which provided the lowest RMSE during the test at the CATIE station (delta T with parameters), provides maximum temperatures that can be considered unrealistic. Not including parameters, however, provides a good match to the data at the eddy tower, while it also continues to show clear trends for the maximum temperature and does not change the minimum. This correction, however, performed worst during the experiments at CATIE.

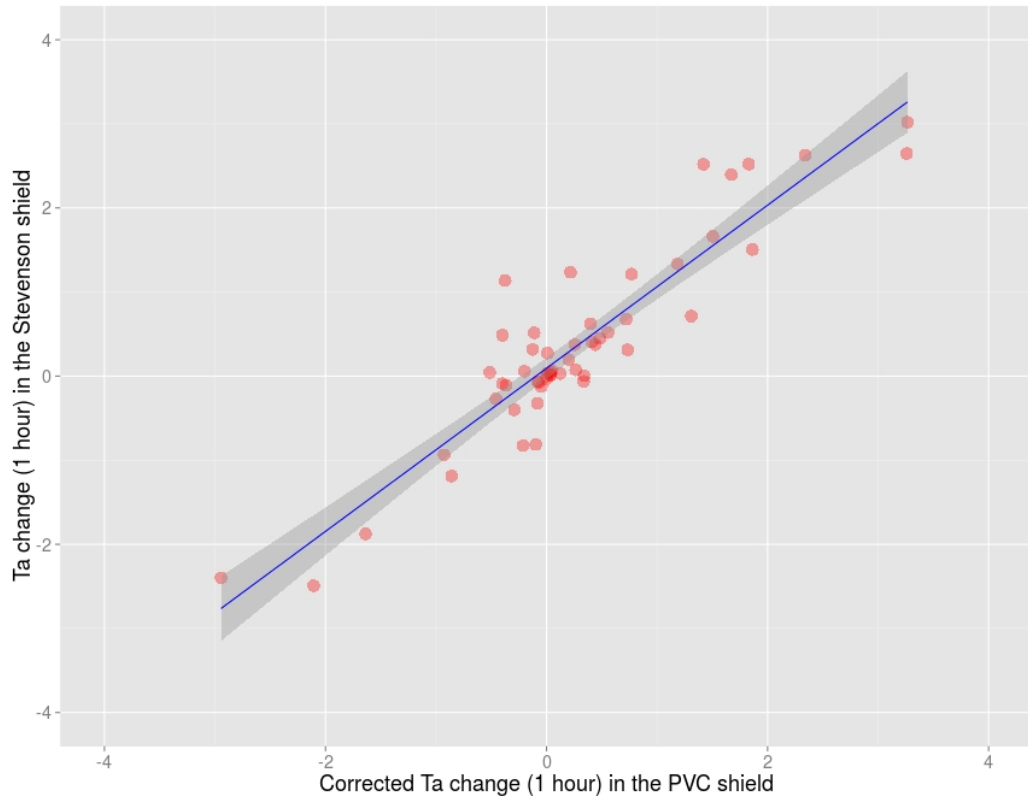


Figure 12: Corrected change in time (1 hour) based on a calibration model based with 55 values

3.4 Discussion

Experiment 1: Sensor resolution

The high-resolution sensors show a smoother temperature curve, resulting in a lower standard deviation and a lower maximum difference between any two sensors in the Stevenson shield at any moment. The humidity, however, shows similar graphs for the low- and high- resolution, which together with similar mean and standard deviations - indicates that high-resolution data is not necessary for measuring the relative humidity. The strong correlation between temperature and relative humidity (R^2 of 0.84) will make it possible to use only few sensors with both temperature and humidity sensors, as several sensors that can measure both units will enable estimation of the relative humidity curves at locations where only temperature will be measured. Changing the temporal resolution and applying different corrections shows that a shorter (1-hour) interval generally provides better results than a longer (2-hour) interval. While this could still be acceptable in some cases, the long interval will make it very difficult to calibrate data based on the change in time, which could be a good way to correct data.

Another result of the first set of experiments is that using the closest measurement to the actual hour provides much better results (at the hour) than when estimating this value at the hour based on (linear / spline) correction of measurements taken at random moments in the hour. Linear interpolation of measurements performs well in most cases even better than splines - when working with hourly measurements. When measuring only once every 2-hours, splines have the potential to provide a better match to maximum temperature, although it can also result in a lower minimum compared to results derived by using linear interpolation. The methods that provide relatively large ($>0.5^0\text{C}$) - and possibly problematic - mainly occur at the 2-hour intervals, while a random start moment generally increases the maximum difference at any moment. All 1-hour intervals are acceptable, whereas it will depend on the use of the network whether longer intervals can be used as well. Long-term studies that assess basic indicators can be done with 2-hour intervals, while calibration of the data is limited with this interval. Although differences in the maximum differ by up to 0.9^0C , the differences at the 0.9 quantile are always less than 0.5^0C compared to the temperature in the original dataset, making this data more reliable.

Experiment 2: Sensor shields

The experiments with different adjustment to the PVC shield has shown that none of the tested alternatives provides an acceptable temperature that is in line with the temperature in a certified shield. This is especially a problem on sunny days and is similar in structures of different (25 and 50mm) diameter. Differences in temperature can be close to 6^0C , while maximum humidity surpasses 100% in all experiments - reaching up to 106% RH. Whereas none of the adjustment perform sufficient for direct use (without calibration) in the field, the best coating to reduce the maximum temperature in the experiments has been insulating foil. This has provided the closest match to the temperature in the Stevenson shield in most cases. The second-best performing adjustment has been the addition

of holes, while a combination of holes and insulating foil has provided surprisingly bad results in the tests. The best adjustment to provide accurate humidity data is not very clear from the experiments. The best match differs on most days, with both the best and worst match for insulating foil in different experiments.

While the tested PVC shields are not good enough to provide data that can be used without calibration, the different coatings show a clear linear relationship when it comes to the change of temperature over time. This ranges from a 43 to 52% faster increase in temperature in the shields versus the Stevenson, with the strongest models for shields with holes and with insulating foil. The strongest model (R^2 of 0.92) is found for insulating foil, which means calibration based on a change of time could be feasible. The insulating foil - which is available in most regions - is normally used to insulate houses, and has been used by different research organizations in similar structures in the study area. The smooth surface of the foil, together with the silver colour, can be expected to reflect a significant part of the radiation heat. While the reflection of the coating plays an important role, the possible impact of surface radiation has not been well studied in the experiments. In all experiments, the sensor has been placed above the surface on a glass fibre mesh, which does not prevent a possible impact of reflecting radiation on the sensor. The small diameter of the PVC tube and the different absorptivity and thermal conductivity compared to the Stevenson shield (which these have been optimized for this use) can result in a different impact due to thermal inertia, which is '*the degree of slowness with which temperature of a body approaches that of its surroundings and which is dependent upon its absorptivity*' (Merriam-Webster dictionary).

Based on the four days of experiments, insulating foil can be considered the best performing coating. Ventilation by holes, however, only provides slightly better results than no adjustment/white paint, which indicates the type and location of holes has to be improved. This is also clear from the results of the holes + foil adjustment, which does not show the cumulative benefits of the separate adjustments. The main problem for humidity observations is derived from its link to temperature, which is often exaggerated. Another problem is the danger of water intrusion, which is especially a risk for shields with holes.

Experiment 3: Data calibration

Calibration of the PVC shields in the experiments at the CATIE meteorological station showed that a low error during both night and day can be achieved by different types of models. A calibration that changes the PVC temperature at any moment to the average Stevenson temperature that can be associated to this, is an easy approach that can quickly be done for complete datasets. The disadvantage is that this linear relationship is calibrated on a certain set of days at a different location and thus is not well suited to correcting temperature and humidity outside of the calibrated range. Another limitation is that this approach is not influenced by the physical properties of the tube. A temperature above 30°C can be an error due to the thermal inertia differences in the PVC tube on one day, while it could be the actual temperature on other days. A 2nd order polynomial

model can reduce the overall RMSE to 0.26, with values of 0.15 during the night and 0.42 during the day. The advantage of this model is that it is easy to understand and implement, and - while errors may occur when using the model outside of the calibrated range by changing the studied region or period of observation - the errors can be expected to be relatively low, as each temperature is adjusted without building up errors along the way.

Calibration based on the change in time is an approach that is based on a strong and significant linear model between the changes in the PVC tubes and the Stevenson shield, which is caused by the different dimensions, absorptivity, and resulting thermal inertia inside the PVC shields. Calibration can be done by creating an anchor point on every day, which is a moment around sunrise/sunset when differences between the Stevenson and PVC shield are still relatively low. The values at the night do not have to be calibrated, although a small adjustment could be done if the temperature has a small, constant offset. Applying this calibration, based on a linear prediction model without additional parameters, by building up the temperature for every day starting at an anchor point, shows only a small improvement over the non-calibrated data. Adding additional correction in the model (three basic parameters) can reduce the RMSE to a lower level than that of the polynomial model. Validation based on a leave-one-out cross-validation shows that the model is very accurate in prediction the temperature in the day that has been left out. The disadvantage is that this model has been tested in a location without any shelter, which could change the performance of the shielding. The corrected change in time is provided in *figure 12*.

Applying the different calibration approaches to field data indicate additional differences. The *control* temperature data against which the shield-temperature is compared shows a small range, which is different than would be expected based on data at the CATIE meteorological station - taking into account a standard adiabatic lapse rate. Testing the performance of shields around the weather station in Aquiares show that different calibration approaches can provide very different output. While the polynomial model and change-over-time model provide similar results at the CATIE weather station, the results from applying these corrections to data from the field show larger differences. The mean remains similar between these approaches, but the minimum that results from polynomial correction is exaggerated, as this lower range has not occurred during the calibration period. The maximum temperature is also lower in the dataset that has been corrected with the polynomial model. This is mainly a result of the low maximum temperature that has been measured in the Stevenson, which means temperature is always corrected to $<29^{\circ}\text{C}$. While the 2nd order polynomial correction provides data that is best in line with data from the local temperature logger, the lack of calibration in the study area, as well as the lack of relationship to the physical properties of the PVC tubes that cause the faster warming, are an important limitation to this approach. The preferred approach is the calibration based on change in time. This does not correct nocturnal data and is based on the thermal inertia (faster heating) of the PVC shields. The main constraint is the higher deviation on separate days, due to possible cumulative errors.

3.5 Recommendations

Based on the experiments that have been conducted - and taking into account the accuracy at which most crop and disease thresholds are provided - a low-resolution of the tested sensors, for both temperature and humidity, will be sufficient for most agricultural studies. The strong correlation between temperature and humidity also makes it possible to reduce the number of sensors that measure both temperature and humidity, although the ratio of T to T+RH sensors will depend on the available budget and the use that humidity data has in the project (mainly important for disease thresholds). The interval that has to be used can either be 1 or 2 hours, which will mainly be influenced by the type of calibration and crops that will be studied. With annual crops (most cereals) that are only in the field for half a year, a 1-hour resolution will be sufficient to cover the full growing season, while for perennial crops, a 2-hour resolution can cover a period of almost one year and would thus be favoured in these cases (periods are based on sensors that measure both units at low-resolution). Creating a script that can launch all sensors at the same time is expected to be a relatively small exercise for someone who is experienced with this, and can be expected to be worth the investment by improving the accuracy of the data and enabling longer intervals.

The current adjustments to the shields cannot adequately reduce the impact of radiation during the midday period and shows large differences with the control (Stevenson) shield on sunny days. This exaggerated temperature is linked to a very low humidity, which together indicate a situation of crop-stress which is not actually present. While insulating foil shows the best results, more study has to be done with combinations of aeration (holes) that reduce the impact of thermal inertia in the relatively small structure. Regarding the structure, a recommendation is to place the sensor in a position where it cannot be reached by reflecting radiation, which has been the case in the experiments. Placing the sensor inside an inverted U-shape tube (attached to a main structure) could increase aeration while still being able to cover the full structure with insulating foil. These shields can be constructed with the same costs, although not all problems might be fully solved. Calibration based on a polynomial model is relatively easy and can correct the data at any moment without building errors along the way. The limitation is the difficulty to apply this approach in different areas than were calibration has originally taken place. Calibration based on change over time (1-hour) can result in larger differences on certain days, but is based on the physical properties of the PVC shield and is thus expected to provide more accurate data.

It is recommended that future studies will mainly focus on improved shielding of the sensors, as this will reduce the need of calibration and hence of expected errors. Priority should thus be given to robust shielding, especially reducing the impact of radiation through ventilation and reflection, and reducing the risk of humidity intrusion through appropriate sealing of the area around the sensor. As shields might not function the same in all cases, it is also recommended to always have a set of sensors nearby a certified weather station for the period of study. Having access to a certified shield can be used to assess the relationship between temperature and humidity, which can be used to create a temperature-humidity model to predict humidity and thereby reduce need for RH-sensors.

4 Spatial aspects

4.1 Introduction

The objective of this chapter is to assess the relationship of the temperature and humidity data derived from a sensor-network with a number of variables in a complex terrain. Understanding the correlation between a number of these variables and temperature/humidity, can help to reduce the number of required sensors in a certain study area, by enabling interpolation approaches that can use this relationship to predict values in areas where sensors have not been placed. The main objective is thus to find a scientific basis - based on the accuracy and correlation of the data derived from point-based data - on which interpolation can be based that covers the full geospatial network. The variables that will be included in this analysis include topography (elevation, aspect, slope), land-use (leaf area index, canopy height), and factors related to the position of the sun (hill shade, cast shadow and irradiation). The influence of topography on climate especially rainfall and temperature is well studied and the relevant literature has been used to understand what strength of correlation can be expected to be useful in co-kriging/universal kriging (*next chapter*). Maps that cover canopy height and LAI are not as easily available as DEMs, but are expected to play an important role in climatic differences at the scale that is studied in this thesis. Factors related to the sun can be derived from some basic solar calculations and - based on the clear peaks in temperature that the (uncorrected) sensors provide during the period of solar noon - is expected to explain some of the variation in temperature in a terrain where cast shadows play a role during certain periods of the day.

In this chapter the data that has been collected in a coffee plantation during a period of over one month will be studied. The sampling strategy, as well as a detailed background of the topological/vegetation-related conditions on the study area, are explained. The data has been analysed in several ways to assess the accuracy of the data. A basic interpolation approaches have been applied (Inverse Distance Weighted) to assess the accuracy of the network, based on a leaving-one-out (LOO) cross-validation approach. This will be compared to geostatistical interpolation approaches that include additional variables, automatic variogram fitting, and inclusion of the time-dimension in *section 5*. After an analysis of the initial network accuracy, the correlation of temperature (humidity is not analysed due to the strong correlation with temperature) with six static covariates, and two dynamic covariates will be assessed. This will be done by analysing the correlation at every hour during the one-month of observations and subsequently providing the average hourly correlation. The relationship between errors and strength of correlation of temperature with covariates is assessed, to understand the types of days on which the accuracy is highest/lowest. It is also assessed which variables play the largest role and which (maximum three) covariates have to be included at different hours in order to create the strongest linear model that can explain temperature differences.

4.2 Methodology

4.2.1 Study area and sampling

Study area

The Aquiares coffee estate in the Turrialba region in Costa Rica. The Aquiares coffee estate is one of the largest coffee plantations in Costa Rica, located at a latitude of 9.95°N , and longitude of 83.72°W . The estate covers around 924 hectares, of which 673 are cultivated with (shade-grown) Arabica coffee. The farm is located between the Pacific (± 70 km) and Atlantic Ocean (± 55 km). The plantation is close to the Turrialba Volcano, which is $\pm 3,340$ meters high and located around 7km from the upper parts of the farm (close to 12 km from the lower parts). The farm starts just above 800m and continues to close to 1,400m. The coffee with the best quality is considered to be located $>1,100$ meter. This is around 45% of the area, but estimated to only supply 31% of the crop (Cornell University n.d.); this is likely the result of the natural areas that can also be found at the higher regions, where the inclination of the terrain is generally also steeper. The presence of natural areas can be seen in a map of the Leaf Area Index (LAI) of the farm (*figure 14*), in which areas in the upper regions often have values that can be associated with that of forest (e.g. McWilliam et al. 1993). During the period between 4 August 2014 and 8 September 2014, one hundred iButton Hygrochron (DS1923) temperature/humidity loggers have been placed in Aquiares. The lowest sensors in this study has been placed at 832 meters and the highest at 1399 meters (*figure 13*), giving a more than 500 meter elevation range to study. After 8 September, 86 sensors could be recovered; the remaining sensors were either missing from shields or the complete shields could not be found.

Sampling strategy

Sampling was based on a hexagonal grid inside one of the watersheds in the farm ($n = 50$), while the placing of the remaining 50 samples was calculated by adding two points to 25 strata's (equal areas) in the study area. This has been based on the *spcosa* R-package (Walvoort et al. 2013). Using strata's of equal area - the methodology is described in (Walvoort et al. 2010) - with two samples each, has been selected to reduce the impact of lost or broken sensors. It was estimated that around 20% of sensors would be lost (stolen or in other ways irretrievable), based on similar projects in the region. During placement of the sensors, the bad weather made it difficult to reach all selected points, which led to an assessment (together with local farmers) of other suitable locations in the vicinity of the original point. The number of points at different levels (50 in the watershed and 50 in the farm) has remained the same. A GPS has been used to store the location of all points, resulting in the coverage shown in *figure 13*. When collecting the data (which was done by a local farmer), it was discovered that 7 were removed from the shield, while 5 could not be found and 2 other were not found in time for further analysis. Of the returned 86 sensors, 6 were removed from further analysis based on visual analysis. This was mainly the result of contact with water, which resulted in a very stable temperature and high humidity. The data analysis was done with 80 sensors.

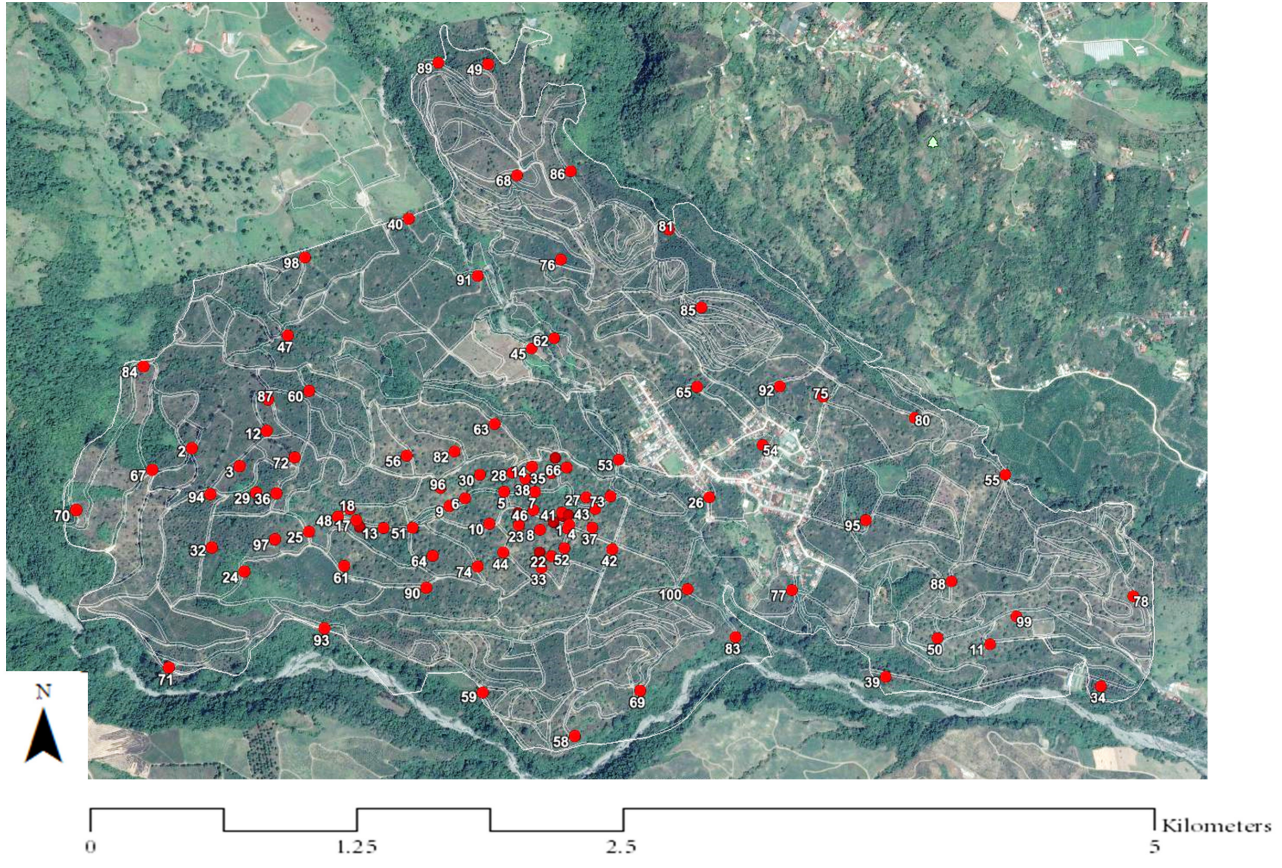


Figure 13: Boundaries of the Aquiares estate and placement of the recovered sensors)

4.2.2 Data correction and validation

Data correction

The raw data that was provided by the sensors has been calibrated based on the delta-T model (with parameters) explained in the previous chapter. This means that on every day, ten hours have been adjusted based on an anchor-point (around sunrise), expecting that the change in the PVC tube could be divided by a certain amount to get the change in temperature that could be expected at an official weather station. As the range of this calibration was still higher than would be expected in the study area, the values above the 0.98 quantile (27.9°C) were reset to this value. The values in the 0.99 quantile (28.84°C) and the maximum (32.90°C) were assessed to be too high and likely the result of limitations of the method of data correction. The resulting range after this correction is $13.4 - 27.9^{\circ}\text{C}$, with a mean of 19.9°C . The mean elevation of the sensors in the study has been 1,110 meters, which is within 50 meters of the altitude of the weather station in the study area (1,040m + 26m tower-height). The mean temperature at this weather station is very similar (19.8°C) to the average temperature across the study area derived from the sensors. Relative humidity has not been analysed in detail in this chapter. Based on a weather station in the study area, a linear model has been created to predict humidity based on temperature. The data that is derived from this correction has a range of 59.7 - 100% RH, and a mean of 87.3% RH. This is very close to the range measured at

the weather station, which has provided a range of 55.1 - 99.9% and mean of 87.7%. This shows that the strong correlation between temperature and relative humidity can be used to quite accurately predict the humidity. This strong correlation will also result in similar trends (although the opposite) of temperature and humidity with the studied covariates. For this reason, a humidity analysis has been excluded from this chapter

Data validation

In order to assess the accuracy of the network and how this is influenced by factors such as the distance to its neighbours and elevation, the data first has to be interpolated. As explaining different forms of interpolation is the aim of the next chapter, the accuracy assessment in this chapter will focus on one of the most basic spatial interpolation approaches: Inverse Distance Weighting (IDW). IDW is covered in the *gstat* R-package and does not require any variogram or model as input. The inverse distance weighting power (IDP) is set to 2.0, which is the default value. The formula for IDW is:

$$\hat{v} = \frac{\sum_{i=1}^n \frac{1}{d_i^p} v_i}{\sum_{i=1}^n \frac{1}{d_i^p}}$$

In this formula, \hat{v} is the value that will be estimated, v_i is a known value, d is the distance from the data point n to the point that is estimated, and p is the IDP, which - by default - is set to 2. Low values for the IDP will result in smoother estimates between different points, as the distance has a relatively low importance in the calculation. To quantify the prediction error in this method of interpolation, we used RMSE and a leave-one-out cross-validation (cf. Kilibarda et al., 2014). The RMSE has been calculated for the one-month dataset and included all hourly measurements. The RMSE is the square root of the mean of the squared residuals (see formula). Residuals are the differences between the predicted and known values and hence has the same unit (degrees Celsius). In each round of cross-validation, we left one sensor out, predicting temperature through an interpolation of the remaining 79 sensors, after which the original temperature at the excluded sensor has been compared with the predicted value based on the 79 sensors. The *gstat* R-package has a built-in IDW function, as well as a function to assess the residuals through a cross-validation that includes a certain number (*nfold*) of validation rounds, which in this study will be set as equal to the total number of sensors. In the formula to calculate the RMSE, which is provided below, n is the number of points (sensors), \hat{y}_t is the predicted value of the point, and y is the actual measured value of this point. The RMSE calculated in this chapter will provide the baseline for more advanced interpolation approaches in the next chapter.

$$RMSE = \sqrt{\frac{1}{n} \sum_{i=1}^n (\hat{y}_t - y)^2}$$

4.2.3 Analysis of covariates

Geostatistical concept

Interpolation of measured points to cover a wider geo-network can be done by two main approaches: *deterministic* and *geospatial*. Deterministic approaches - which include IDW and Radial Basis Functions - predict values based on the similarity between points, or other methods that do not require analysis of the statistical properties. Geostatistical approaches, which include a wide range of Kriging functions, base their predictions on the statistical properties of the original dataset and possible other variables about which information is known. Geostatistical analysis can be based on a wide range of models, from basic models that only include the original data, to models that include both space and time dimension, as well as related variables (covariates) that can strengthen the predictive potential of the interpolation. As costs are expected to be an important limitation in setting up sensor-networks for agricultural purposes in developing countries, covariates are considered an important factor that can improve the predictions of models and hence reduce the number of required sensors in a certain study area. This chapter does not yet focus on the different geostatistical functions, but is mainly focused on the covariates and the correlation they have with the temperature data derived from the network. Geostatistical approaches that use a covariate to improve estimations, which include co-kriging, make use of the correlation and generally more frequent (or cheaper) observations of these variables. Strong correlations provide a good basis for geostatistical interpolation, and will be analyzed with the Pearson's r . There is a general trend that more covariates result in better predictions, although the gains become negligible after a certain number; this was five variables for the minimum and six variables for the maximum in a study by Jarvis & Stuart (2001).

Correlation

The correlation between temperature and a set of covariates has been calculated with the Pearson product-moment correlation coefficient (Pearson's r). This coefficient provides a value that explains the degree of (linear) correlation between different variables, ranging from -1 (total negative correlation), through 0 (no correlation), to 1 (total positive correlation). A strong relationship between certain variables in this study is especially relevant to select covariates that can be used in co-kriging of temperature data. While it can be assumed that a stronger correlation with a covariate will improve the predictions based on the same number of sensors, there is no universally applicable 'minimum correlation' from which kriging approaches that use covariates start performing better than ordinary kriging. In this study, the strength of (absolute) correlation is classified as 0-0.25 (*insignificant*), 0.25-0.5 (*small*), 0.5-0.75 (*medium*) and 0.75-1 (*strong*). Theoretically, with the addition of covariates in co-kriging, it is not possible to do worse than in ordinary kriging, as lack of cross-correlation will result in a fall-back on autocorrelation for the principle variable (ESRI, web). Other approaches, such as universal kriging (based on a linear regression) can perform worse than ordinary kriging when basing it on a covariate that has a limited correlation with the principle variable (cf. Goovaerts, 1999). In addition to the correlation of the selected covariates with temperature at different times, the correlation of these variables with the other predictors is also provided.

4.2.4 Selected covariates

Covariates

Covariates are variables that can be used to predict another variable: the dependent variable. The best known covariates that can be used to predict temperature is elevation, by taking into account the adiabatic lapse rate. The adiabatic lapse rate is '*the rate at which atmospheric temperature decreases with increasing altitude in conditions of thermal equilibrium*' (Oxford, web). While studies on the impact of certain factors on temperature have covered a wide range of potential covariates, an important issue will remain the cost to obtain recent geospatial data for this covariate. Many of the more basic covariates are freely available and show an increasingly better accuracy and resolution. A basic raster Digital Elevation Model can be used to create a wide range of covariates. Static covariates that can be derived from a DEM include elevation, slope and aspect. With some additional calculations, such as the position of the sun at a given moment, dynamic covariates can also be created without any costs. These covariates include the hourly changes in hill-shading and cast shadows, which together with an hourly solar constant, can be converted to hourly (direct and total) radiation, as well as total daily radiation estimates. Other covariates that are generally more difficult to obtain, but which are used in this study, are rasters of the leaf area index (LAI) and canopy height. Both can be expected to have some influence on temperature at a very small scale and are thus useful to include in studies that focus on collecting data for agricultural purposes in developing countries. Compared to information about canopy height (created from LiDAR images), information about the LAI is both more difficult to create and subject to faster (seasonal) changes.

Elevation

Information about the elevation of the sensors in this research is available from the GPS units used to store the coordinates of sensors, and extraction of the sensor-coordinates in a DEM. A comparison between these approaches has resulted in very small differences, which means that the data from the DEM has been used in further analyses, as this is easier to implement in future models. The DEM has been derived from the SRTM 90m Digital Elevation Database, and has been cropped to the study area and disaggregated by a factor of 10. Incorporation of elevation in temperature interpolation is very common in GIS. Dodson and Marks (1997), for example, have tested three different lapse rates in a large mountainous region, while the WorldClim dataset has used a single lapse rate ($6^{\circ}\text{C}/\text{km}$) as variable in the interpolation of weather station data (Seguinot et al., 2014). Based on the existing scientific understanding of the adiabatic lapse rate, together with the fact that the measurements have taken place during the rainy season (the wet lapse rate is lower than the average lapse rate) over a height difference of 500 meters, it can be expected that the temperature in at the lower area of the farm is between 2.7 and 3.2°C higher than in the higher areas. This is based on both the average adiabatic lapse rate ($6.4^{\circ}\text{C}/\text{km}$) and wet lapse rate (for 100% RH: $5.5^{\circ}\text{C}/\text{km}$). Two factors that might have a smoothing impact on this difference include the relationship between elevation and solar UV radiation (Blumthaler et al. 1997) and the expected denser (more natural) vegetation at higher regions of the study area, which could increase shading and protection from wind.

Leaf Area Index

The Leaf Area Index (LAI) is a variable that provides information about the total area of one-sided photosynthetic tissue per unit of ground surface over which it is measured (Watson 1947); this index is dynamic and changes depending on season and age/management practices of the crops (Welles & Cohen 1996). For coffee in the study area, the LAI has been measured at 4.0 (± 2.9) in 1982 (Ewel et al. 1982), although parts of the farm are replanted at a frequent interval. More recent studies on the LAI in Aquiares have found that the LAI varies from 2.4 - 4.4 depending on the season (Taugourdeau et al. 2014); this study also mentions that inter-annual variations can be caused by pruning and plot renovation. The currently grown variety *Caturra* is characterized by relatively limited vertical growth (<2m) and planted in rows that are 2 meters apart; other trees are also planted in the farm (Dauzat et al. 2001). Above and inside canopy climate and its relationship to the LAI has been extensively studied in Goudriaan (1977), and includes impacts of canopy geometry, incoming radiation, and optical properties. The map of LAI that has been used is based on High Resolution Multi-spectral Images (MODIS) together with field verification. As sensors have been placed adjacent to coffee trees at 1.5 meters (limiting shading), the main impact on temperature would come from larger trees. It is expected that a high LAI in the study area is correlated to canopy height and is negatively correlated to temperature, as it can provide shelter from wind and can reflect incoming radiation (Sellers 1985).

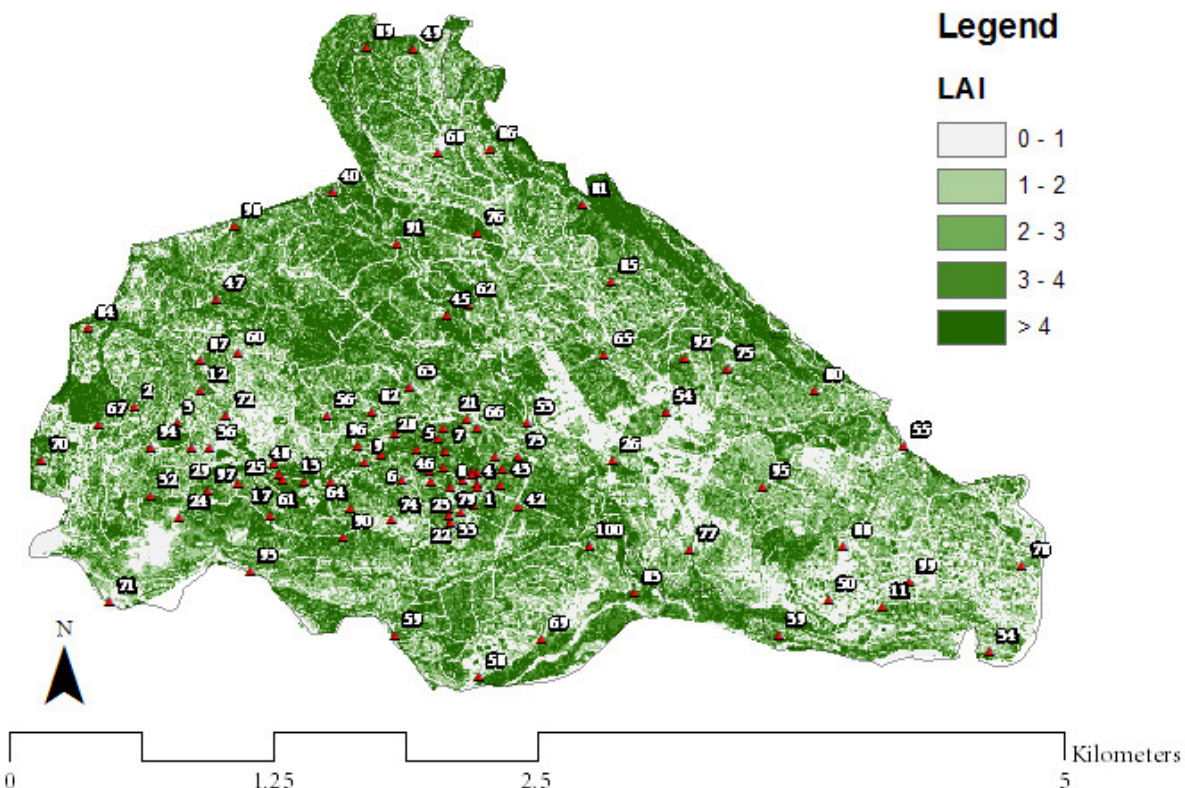


Figure 14: Boundaries of the Aquiares estate and placement of the recovered sensors)

Canopy height

The height of vegetation is another factor that can have an impact on the climate in an area, which might partly overlap with the leaf area index, as more natural areas will likely have both a high LAI and canopy height. Trees are often grown together with coffee crops in shade-grown coffee systems. Benefits include protection from wind, an improved microclimate and the addition of organic matter to the soil (Budowski 1980). In addition to this, shading can reduce the temperature stress (Butler 1977), reduce pest outbreaks (Staver et al. 2001), and overall provide a refuge to biodiversity (Perfecto et al. 1996). The data in this study is derived from the Laser Vegetation and Ice Sensors (LVIS) (Blair et al. 1999), which is a scanning laser altimeter instrument. As this data includes the absolute minimum and maximum in different cells, the values can exaggerate the canopy height, but still show a similar trend that would be the case if the median height would be taken. The used dataset is a 2005 Costa Rica dataset (Blair et al. 2006) that covers the area around the Turrialba volcano.

The resulting raster is shown in *figure 15*, and shows that vegetation is highest in areas around rivers (borders) and the highlands. This is likely caused by the difficulty of the terrain for growing coffee in these areas and additional environmental policy that might be in place; 150 hectares of the farm are covered by a protected natural forest (Anon 2008). The average height in the farm is 10.9 meters with a maximum of 76.5 meters. The vegetation is generally higher close to boundaries of the farm, which could be caused by the steepness of the terrain in these areas, or management strategy. This can create a natural farm limit, with an additional benefit that is can be considered protected area for certifications (e.g. Rainforest Alliance). It has to be noted that measurement errors can play a large role, as the map does not only show the canopy height, but also the complexity of the terrain - as the height difference within the collection size (10 to 25m) is included in the calculated canopy height. It is expected that canopy height is negatively correlated with temperature during periods of sun, although the actual shadows that the canopy will provide is not accurately modelled.

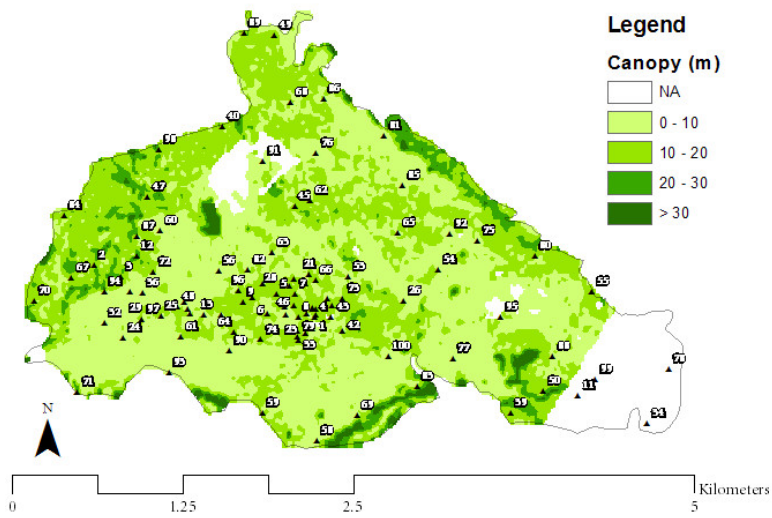


Figure 15: Canopy height in the Aquiares estate based on LiDAR data)

Sun-related covariates

The sun can have an influence on the temperature in different ways; the position of the sun during the day can result in areas that have more shading than others, while the solar radiation during different times of day will also result in different rates of heating. The time of highest insolation (amount of solar radiation on a given surface) is the solar noon; the moment when the sun crosses the meridian at the selected site. For the studied day (August 22nd 2014), the solar noon was at 11.38AM local time (NOAA n.d.). Solar radiation can be related to daily minimum and maximum temperature (Bristow & Campbell 1984) and to productivity in tropical ecosystems (Monteith 1972). Modelling the relationship between solar radiation and temperature range requires different empirical coefficients and for that reason is different to implement in general models. Calculations of the solar radiation at a certain moment at a given latitude is relatively straightforward and could be combined with DEMs to model the insolation and shadow during different times of day. Calculating the hill-shade is a well-known functionality in most GIS software, but is generally used for aesthetic improvements of the maps. The actual meaning of the values is not often discussed, but will have significant implications for the amount of insolation at a given location. The output of the algorithm generally provides values in the range from 0 to 255, but are often converted to an easier to interpret range, such as -1 to 1. Values of 0 (or -1 in a non-normalized calculation) relate to shadow areas, while values of 255 (or +1) can be found in areas with complete illumination. HillShade can be calculated with the formula below, in which s is the slope, z the zenith angle, az the azimuth angle, and as the aspect (all in radians). In a normalized calculation, values <0 are reset to 0, and all other values are multiplied by 255. Normalizing is not required in this study.

$$HillShade = (\cos(s) \times \cos(z)) + (\sin(s) \times \sin(z) \times \cos(az - as))$$

Except for the impact of the local relief on the insolation, there will also be an impact of cast shadows (sky view factor). Due to the relatively small size of the study area and its orientation, this is not expected to be a significant issue at this level, but even at this scale there will be places where the cast shadows will cause some differences throughout the day. These places can be expected to be close to larger objects (e.g. mountain tops) or in areas with steep slopes (e.g. rivers). The output of a layer of cast shadows provides values ranging from 0 (full shadow) to 1 (no cast shadow), and for this reason can easily be multiplied by a *HillShade* raster when calculating the insolation at a certain moment. Cast shadows have been calculated at 10-minute intervals throughout a day, taking into account objects within a ten kilometer buffer of the study area to include all the larger mountains and volcanos in the region. The insolation at a given moment can be calculated with the formula below, in which R_{dir} is the direct radiation, R_{dif} is the diffuse radiation (both kW/m^2), HS is the non-normalized hill-shade value, CS is the cast-shadow value (in both 0 is shadow, 1 is full sun), and ΔT is the covered time in minutes. The calculation requires input from a complex algorithm that calculates the solar position. A R-script, provided online by Josh O'Brien, has been used.

$$Insolation = ((R_{dir} \times HS \times CS) + R_{dif}) \times 60 \times \Delta t$$

4.2.5 Analyses

Analysis 1: Network accuracy

The first analysis will assess the initial network accuracy during the one month of observations. Inverse Distance Weighted interpolation will be used to interpolate the data at all 744 hours and the mean RMSE will be calculated. This will show how accurate the network can predict values in a complex terrain, and how errors change between the night and day. The RMSE is analysed in its trends in space and time. The variation over time will focus on intra- and inter-day variation of errors, and includes differences between day vs. night and hot vs. cool days. The variation of the accuracy in space will focus at the relationship of the RMSE with issues, such as the distance to neighbouring sensors, and distance to the border of the study area.

Analysis 2: Correlation between covariates

A second analysis in this chapter will focus on the correlation between the different dependent covariates. The correlation between elevation, slope, aspect, leaf area index, canopy height and total daily insolation will be provided in a table. This shows how certain of the predicting variables might be correlated, which is important to understand before applying geostatistical analyses.

Analyses 3: Average trends with covariates

The correlation of the six covariates with temperature at all 744 hours will be calculated, and the average Pearson's r will be discussed. Attention will be given to the variation between days to see how the average daily correlation fluctuates in the rainy season. As the daily insolation can be expected to only play some sort of role on days with sun, the average daily correlation might give an indication of the different types of days during the studied period. The output of this analysis will be a table of the mean and range of the Pearson's r for the different covariates. Based on the static covariates, a linear model will be created to explain the variation in temperature. The relative importance of the different covariates will be assessed with the LMG method (R^2 partitioned by averaging over orders). This function is part of the *relaimpo* R-package (Groemping. 2013)

Analyses 4: Daily trends in correlation

The final analysis of this chapter will include both the static covariates and the three dynamic covariates (hourly radiation, hillshade and cast shadow). The daily trends (mean and 1st/3rd quantiles) in correlation between temperature and the covariates will be provided as graphs to show the daily trends. The hourly values are derived after calculating the correlation at all 744 hours and subsequently aggregating this in hourly values. A final output of this chapter will create regression models at each hour and provide the average strength of these hourly models, as well as the relative importance of different covariates in these models. The trends in model strength and covariate importance will be provided in figures, and will form the basis of the next chapter on geostatistical interpolation.

4.3 Results

4.3.1 Network accuracy

The mean RMSE, based on all 80 sensors and 31 days of hourly observations (IDW-interpolation) is 0.65°C with a range of $0.18\text{--}2.62^{\circ}\text{C}$. The RMSE remains within the same range during the month of observations and does not show any change that could indicate that the network requires a period to 'stabilize'. There is a clear relationship between the daily (min, mean and maximum) temperature and the RMSE. The minimum temperature has a r of -0.12 , the mean temperature has a r of 0.67 , while the maximum temperature has a r of 0.74 with the RMSE. The daily maximum temperature (based on the mean of all 80 sensors at any hour) and RMSE are plotted in *figure 16*. Errors show clear trends during the day (*figure 17*), and show a RMSE >1.0 between 8AM and 2PM. The largest errors can be found between 11AM and noon, and can reach 1.2°C .

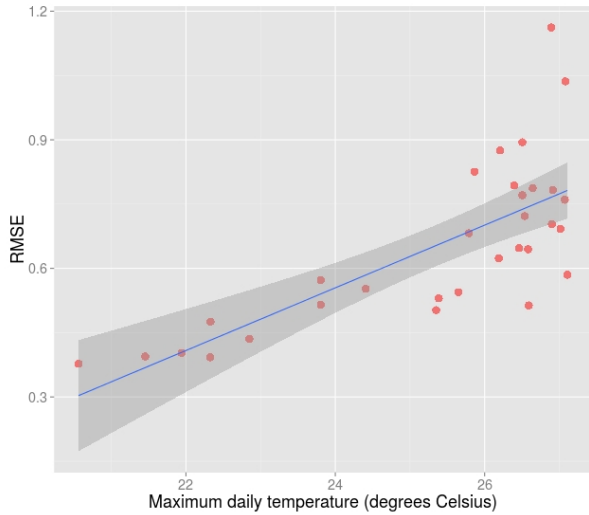


Figure 16: Daily Ta_{\max} vs RMSE

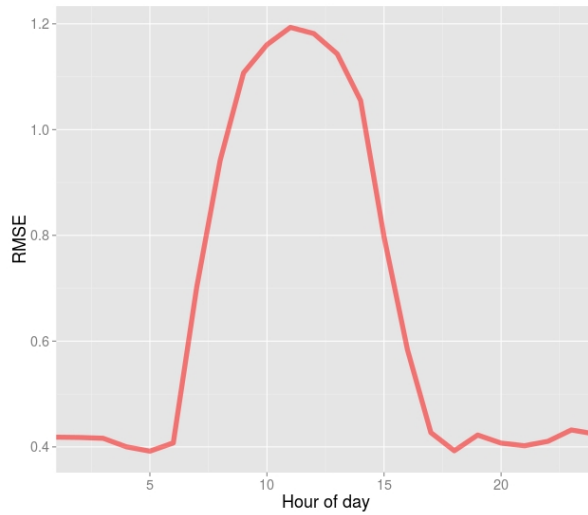


Figure 17: Daily trends in average RMSE

While the mean errors of all 80 sensors at a certain point shows a clear relation to the type and time of day, differences between sensors show limited trends. Correlation of the errors for each sensor shows the strongest correlation with elevation ($r = -0.19$) and vegetation ($r = 0.21$). The RMSE in the micro-watershed, where 50 sensors were placed (35 were recovered and used) relatively close to each-other is 0.50°C , which is very similar to the error for the entire farm (45 were recovered). The average error for sensors placed outside the watershed was 0.52°C . The RMSE shows an insignificant (negative) trend with the distance of each sensor to their closest three neighbours. The distance to the border of the area is also an insignificant factor for the RMSE of each sensor, which shows a small positive trend (further from the border is larger error). The average RMSE for each sensor during the month of observations is shown in *figure 18*. This map shows that the RMSE has no clear trends based on their location in the area and distance to each-other. The reason for the errors is unclear, and can include human activities as sensors placed close to the village show large errors.

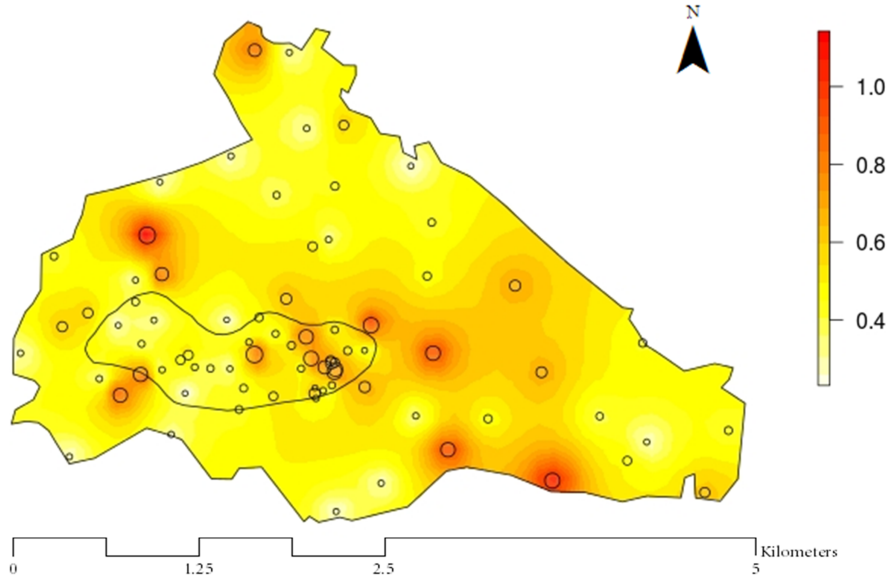


Figure 18: Average RMSE of the 80 recovered sensors in Aquiares

4.3.2 Correlation between covariates

The correlation between the different covariates is provided in *table 9*. The mean temperature for each sensor is also included for a preliminary analysis. The correlation of the mean temperature with the other covariates shows that there is a strong negative correlation with the elevation, while there is a small negative correlation with canopy height. All other covariates have an insignificant ($r < 0.25$) correlation with the mean temperature. Elevation, from which the covariates *slope*, *aspect*, and *daily radiation* are derived, shows a low positive correlation with slope and canopy height. Correlation of the slope is strong (negative) with daily radiation, which can be explained by the fact that these surfaces are tilted and receive less insolation during the periods with the highest sun-position (altitude). The aspect also shows a negative correlation with the daily radiation, which can be a result of both datasets being based on the same original data-source (DEM). The leaf area index has no significant correlation with the other covariates; the strongest correlation is -0.2 and is with the elevation. The only two covariates, out of the four that are based on the DEM, which are strongly correlation, are the daily radiation and slope.

Table 9: Correlation between the selected (static) covariates

	<i>Mean temperature</i>	<i>Elevation (meter)</i>	<i>Slope (radians)</i>	<i>Aspect (radians)</i>	<i>Leaf area index</i>	<i>Canopy height</i>	<i>Daily radiation</i>
<i>Mean temperature</i>	1.00	-0.81	-0.09	-0.03	0.07	-0.29	0.06
<i>Elevation (meter)</i>	-0.81	1.00	0.25	0.00	-0.20	0.30	-0.15
<i>Slope (radians)</i>	-0.09	0.25	1.00	0.09	0.01	0.00	-0.84
<i>Aspect (radians)</i>	-0.03	0.00	0.09	1.00	0.01	-0.12	-0.53
<i>Leaf area index</i>	0.07	-0.20	0.01	0.01	1.00	0.01	-0.04
<i>Canopy height</i>	-0.29	0.30	0.00	-0.12	0.01	1.00	0.00
<i>Daily radiation</i>	0.06	-0.15	-0.84	-0.53	-0.04	0.00	1.00

4.3.3 Average correlation with covariates

The correlation of *elevation* with temperature, when taking the mean of all 744 hours, is reduced to $r = -0.64$ (-0.98 to 0.45). The daily trends differ a lot over the days, but there is a clear correlation between the hourly RMSE and the correlation of elevation with temperature at that hour ($r = 0.73$). This shows that hours during which correlation of temperature with elevation is strong (generally periods with less sun), have smaller errors (figure 19). The mean correlation of slope and aspect with temperature is insignificant (*slope*: -0.02 (-0.32 to 0.47) and *aspect*: 0.04 (-0.38 to 0.46), and at no point reaches a medium ($r > 0.5$) strength. *Leaf area index* shows a mean correlation of -0.03 with temperature, which stays in a -0.28 to 0.19 range. The strength of the correlation with the *canopy height* is much stronger, with a mean r of -0.18 (-0.38 to 0.29), but there is quite some overlap with elevation (higher areas have more natural area). Total (potential) *daily radiation* shows a mean r of -0.05 with temperature and has a range of -0.32 to 0.19. Correlation with radiation can only be expected to be relevant during hours with sun, and is covered in section 4.3.4.

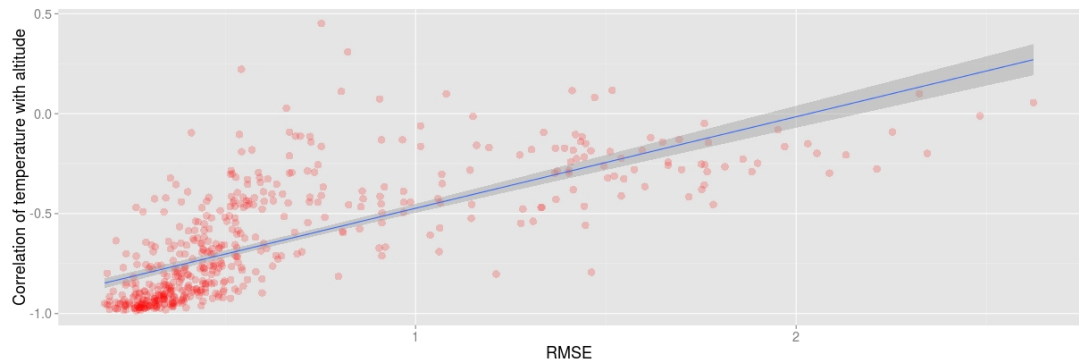


Figure 19: RMSE vs. hourly correlation of Ta with elevation

Adding all static covariates in a linear model to explain temperature at each hour result in models with a mean R^2 of 0.52 (0.03 - 0.97), in which elevation is the most important variable (figure 20).

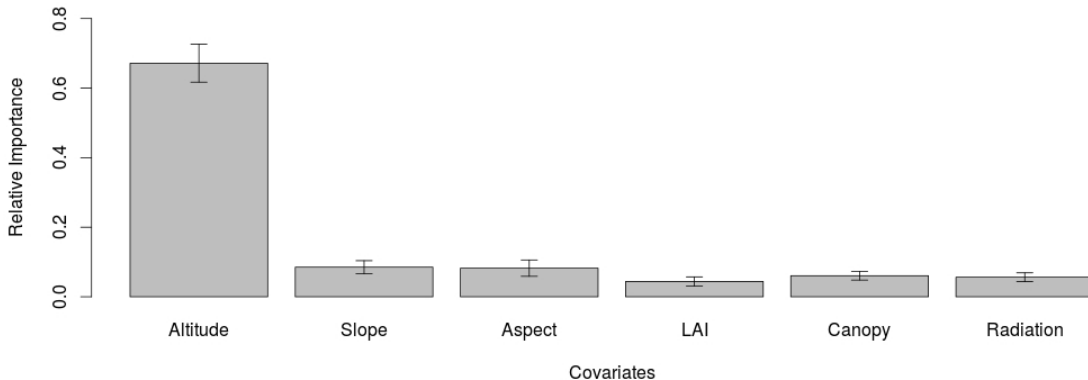


Figure 20: Relative importance of different covariates in explaining temperature

4.3.4 Daily trends in correlation

Based on the earlier explained results, errors are largest during the day - and especially during the period around solar noon. There is also a clear relationship between the errors and the strength of correlation of elevation with temperature, which indicates that correlation varies over the day. The daily trends of correlation (mean and 1st/3rd quantiles) of *elevation* with temperature are shown in *figure 21*. This shows that the mean correlation is only strong during part of the day, while it is medium for most of the hours without sun. The period with sun, plotted between the dashed lines, shows a low correlation during the period around noon. The lines of the 1st and 3rd quantile show that similar trends can be found on most days. The mean daily correlation of elevation with temperature between days is linearly related to the maximum temperature ($R^2 = 0.46$) - *figure 22*.

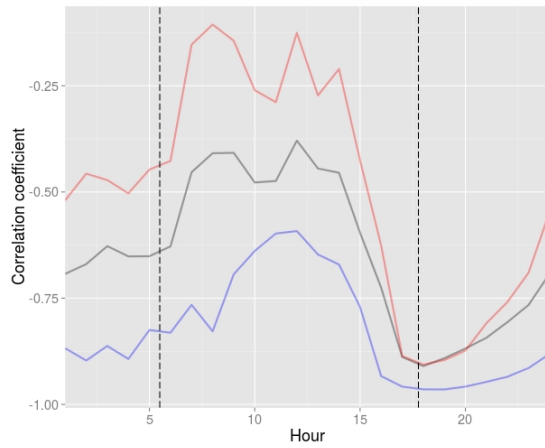


Figure 21: Temperature/elevation correlation

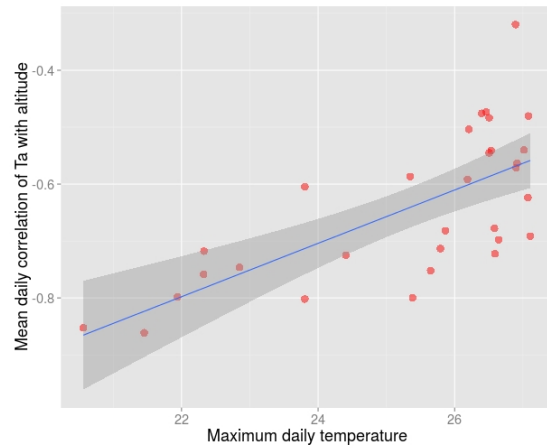


Figure 22: max Ta vs Ta/alt correlation

The correlation of the other static covariates that are derived from the same DEM, *slope* and *aspect*, is plotted in *figures 23* and *24*. There are clear trends in correlation, but the mean strength is never stronger than 0.2. Mean correlation around noon is very weak (± 0.1) for both variables.

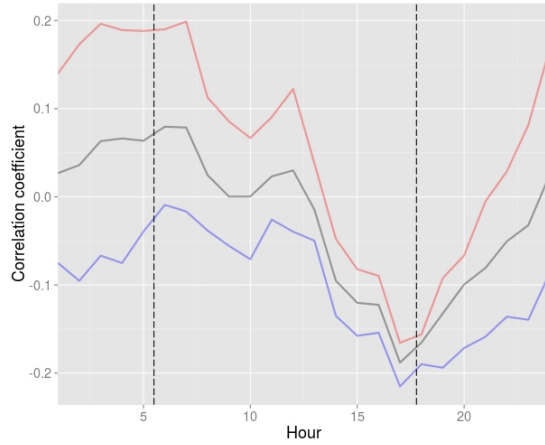


Figure 23: Temperature/slope correlation

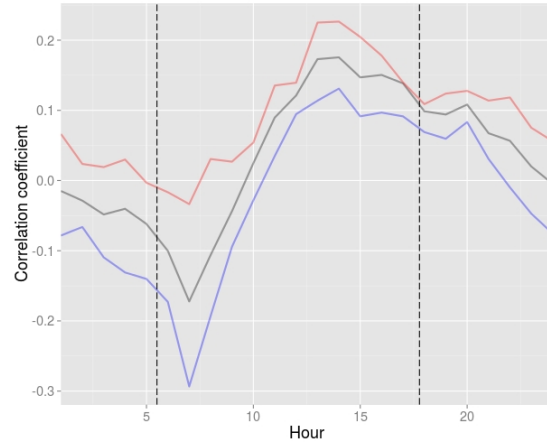


Figure 24: Temperature/aspect correlation

The correlation of two vegetation-related covariates - *leaf area index* and *canopy height* - with temperature are plotted in *figures 25* and *26*. The strength of the correlation of LAI with temperature is low, but clearly shows that there is a trend towards solar noon. Around solar noon, a high leaf area index has a (low) negative impact on the temperature, while the correlation is close to zero during hours without sun. The strength of the correlation of canopy height with temperature is stronger than that of LAI with temperature. The r is <0 for most situations, and becomes stronger (negative) from sunrise to sunset. The strongest value is found around sunset and has a r of -0.28. Similar to LAI, the correlation is stronger during the period with sun than during the period without sun.

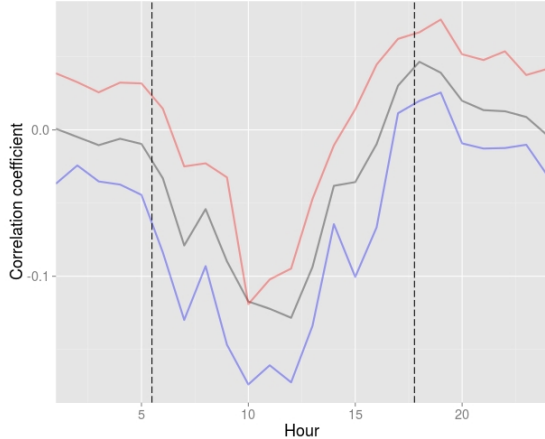


Figure 25: Temperature/LAI correlation

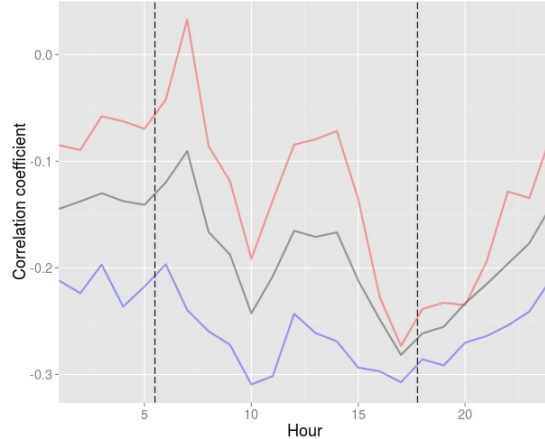


Figure 26: Temperature/canopy correlation

Correlation of temperature with the variables that can be derived from the position of the sun can be done for all hours with sun, and takes into account the changing position of the sun. These calculations can be done for the hill-shading, cast shadows, and combined (total) radiation. Correlation with *cast-shadows* is only relevant for two hours (just after sunrise and before sunset), as these are the only moments with sufficient variation between the data to assess correlation. At all other moments the value for the sensors - not necessarily for the entire area - is either 0 (no sun) or 1 (full sun). Correlation during these two hours is -0.05 (-0.09 to -0.03) in the morning and 0.18 (0.15-0.22) in the afternoon. This indicates that cast-shadows alone do not explain a lot of variation in this area. *Hill-shading*, without adjustment for radiation and cast-shadows, shows a correlation with temperature of 0.25 at 7AM, after which it reduces to -0.10 at 11AM. After this, it becomes positive again for most of the afternoon, with a mean correlation of 0.26 between 2 and 5PM.

Calculating *hourly radiation* is done by multiplying hill-shade by cast-shadows and subsequently multiplying this by a radiation value. As the radiation value depends on time and is the same for all sensors at a certain moment, this multiplication will not change the hourly correlation. The correlation of hourly radiation with temperature shows a similar trend as that of hill-shade with temperature. The difference is that the trend starts one hour later (6AM), as the sun is not yet up at 5AM. A benefit that the hourly radiation calculation has over hill-shade alone is a stronger correlation between 4-5PM ($r = 0.28$), which is marginally stronger than for hill-shade ($r = 0.25$).

The daily variation in correlation of hourly radiation with temperature is provided in *figure 27*. The mean daily correlation ranges between -0.03 and 0.28 (mean $r = 0.14$) and shows a clear linear relation ($R^2 = 0.64$) with daily maximum temperature (*figure 28*). Based on trends in *figures 22* and *28*, the decreased correlation of temperature with elevation can partly be compensated by the increased correlation of temperature with radiation on days with high temperatures. The mean daily temperature/elevation correlation has a r of 0.77 with the temperature/hourly radiation correlation².

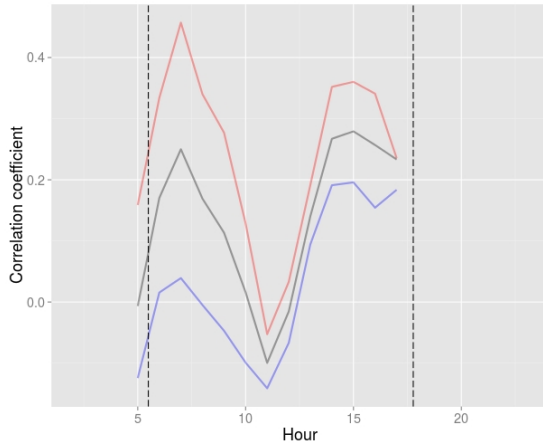


Figure 27: Temperature/hourly radiation cor.

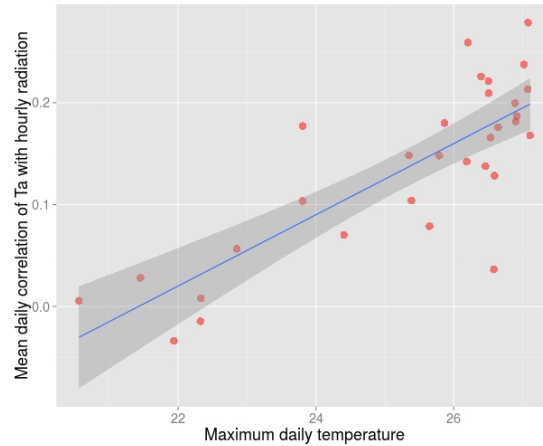


Figure 28: Max Ta vs mean radiation cor.

Creating a linear model at each hour, with the covariates discussed in this chapter (only including hourly radiation and not hill/cast shading), results in different strength of models depending on the time of day. The average strength of the regression model has an R^2 of 0.53, which means just over half the total daily variance (dashed line) in temperature can be explained with the considered covariates. The trends in mean model strength throughout the day is plotted in *figure 29*.

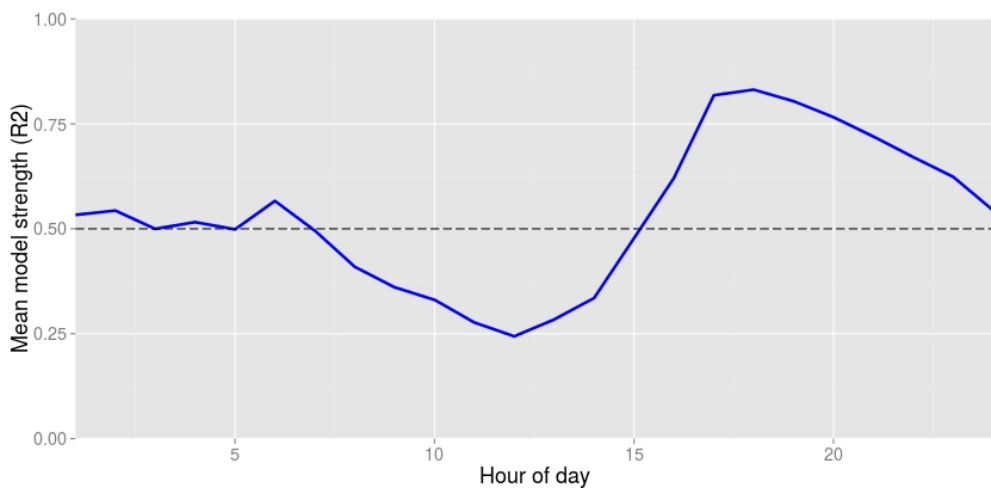


Figure 29: Mean linear regression strength (R^2) throughout the day that explains temperature variation

²The temperature/elevation correlation is negative, but is weaker when temperature/radiation correlation is stronger.

The relative importance of the different covariates during the day is plotted in *figure 30*, which includes the mean strength of the resulting model for comparison (dashed line). This figure shows that *elevation* is the most important factor in explaining temperature throughout the day. During hours with sun, the regression model is strongest, and except for elevation, the *slope* and *aspect* play a relatively large role. The exact contribution and model strength at different hours is provided in Annex X. After the sun is up, the relative importance of *hourly radiation* increases rapidly and contributes more than 30% to the regression model between 7 and 9AM. The contribution of radiation reduces to 5-10% between 11AM and noon, when the position of the sun is highest. The mean strength of the regression model is below 50% between 8AM and 3PM. During this period, the relatively contribution of other covariate than elevation plays an important role. *Canopy height* adds more than 10% to the model between 9 and 11AM, while the *leaf area index* contributes to 16% at noon. The mean model-strength is also lowest at that moment and can only explain 24% of the temperature variance. The strongest model that has been created at every hour has an $R^2 > 0.9$ for most hours, except for 12-2PM. Especially the models at 1 and 2 PM are weak (max $R^2 = 0.67$).

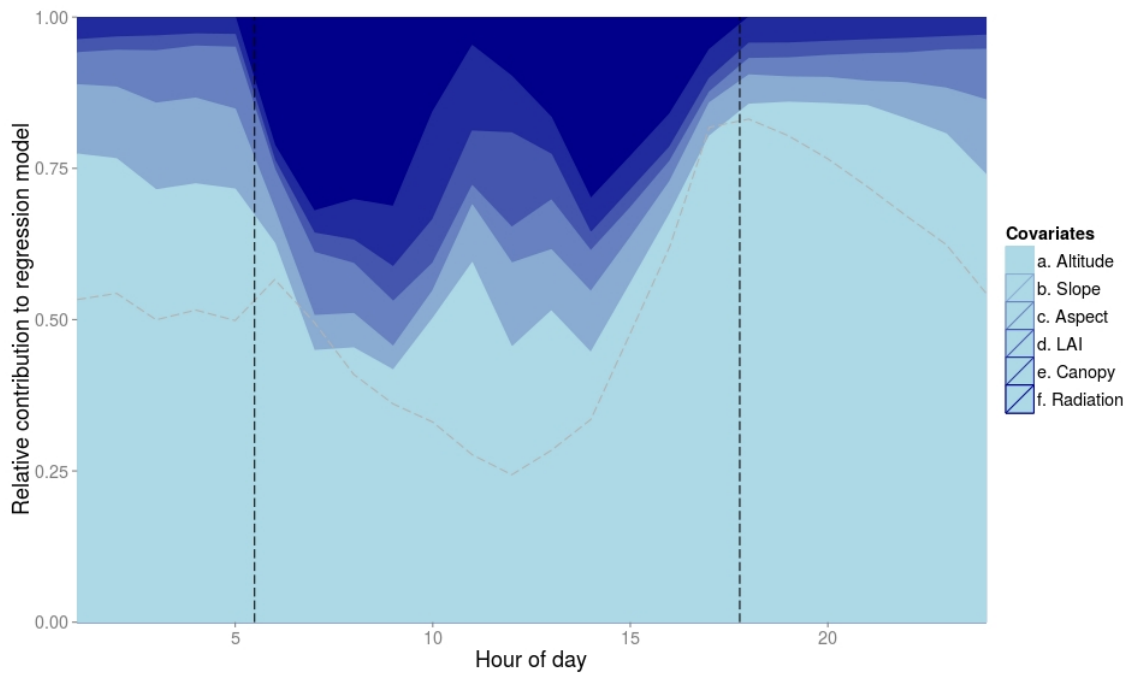


Figure 30: Contribution of different covariates to the best model explaining temperature variation

The most important covariates, on average, are elevation (67%), hourly radiation (10%) and slope (8%). During the hours with sun, hourly radiation even contributes an average of 20%, although the average model strength only has a R^2 of 0.54 during this period. The three most important covariates at every hour always include elevation. During the period without sun, the second and third most important covariates are slope and aspect, while during the day, radiation is the second most important covariate during ten of the twelve hours. Canopy height is included with the three most important covariates during three hours, and leaf area index at only one hour.

4.4 Discussion

Retrieving and loading the hundred sensors that had initially been placed in this research showed that approximately 20% of the sensors could not be used in further analysis - either due to inability to find them (in some cases they were removed from the PVC shield) or due to incorrect data. The main reason for obvious incorrect data seems to have been contact of the sensors with water. High humidity or water intrusion (which is likely with PVC tubes to which no additional tape has been added), results in very high ($>100\%$) relative humidity and very stable temperature throughout the day. In some cases this happened throughout the studied period, while in other cases this only occurred at a later stage and for a shorter period. Faulty data throughout the growing season can result from the timing of sensor-placement. The first one-third of sensors has been placed on a very rainy day, which means the sensors were wet when entered in the shields, and in some cases mud or other material might have stuck to the sensors. Data correction of the remaining sensors, based on the experiments in *chapter 3*, resulted in data that could be used for further analysis.

The accuracy of the network, calculates with a leaving-one-out cross validation in IDW interpolation, shows clear trends during the day. The mean RMSE during the month of observations was 0.65°C , which can reach 1.2°C around noon. The RMSE is higher during days which have a high maximum temperature, which are also the days when correlation of temperature with elevation is limited. The spatial distribution of the RMSE per sensor does not show any clear trends. The RMSE in the micro-watershed (high sensor density) and total farm (lower sensor density) is similar, and factors such as average distance to the closest three sensors or the farm-boundary play no role.

Correlation between the six static covariates and the temperature shows that elevation is the most important factor. Models on average, can explain 52% of temperature variation during the studied period. The strength of correlation between elevation and temperature, which is related to the type of day (maximum temperature), is correlated to the mean RMSE on these days. This indicates that it is more difficult to accurately monitor the temperature on hot/sunny days. As the study has been conducted during the rainy season, it is expected that the accuracy can change in other season.

The hourly correlation between *elevation* and temperature is strongest around sunset and weakest around noon. The correlation of the *slope* and *aspect* shows clear trend, but remains relatively weak for most of the day. The correlation of *LAI* with temperature is strongest around noon, which is what was expected based on the position of the sun and shading the denser canopy can provide. The correlation with *canopy height* is not as strong during the period of solar noon, but is strongest around sunset - which can be a result of the correlation the canopy height has with elevation. Adding *cast shadow* to the calculations of *hourly radiation* causes a slight increase in correlation strength around sunset, but does not impact the period around sunrise. Correlation of *hourly radiation* is strongest in the early morning and the hours before sunset. This correlation is linked to maximum temperature, and thus negatively correlated with the temperature/elevation correlation. All hourly covariates combined can explain 53% of the variance in temperature, which is a minor ($\pm 1\%$) improvement over only using static covariates. Radiation contributes 20% to models during the day.

4.5 Recommendations

A range of recommendations can be made based on this chapter that analyses the field data. Based on the number of useful sensors, it can be recommended that future projects take into account a loss of 20%. Part of this loss of useful data is caused by problems with the shield, which can be reduced by ensuring no water can reach the sensor. Tape could be added at places where PVC are attached to each other (e.g. the PVC elbows), and placing of the sensor could reduce potential impacts of splash water from surfaces such as leafs. Sampling can be done in different ways, but it has to be taken into account that there is a risk of losing sensors, which means that creating a number of equal area strata - each with two sensors - would be a way to ensure that the full area can be covered while reducing the problems when losing a sensor. A second recommendation is that soil and humidity sensors could be placed in vicinity of the temperature sensor at certain strategic location in order to establish the relationship between these variables and also be able to create maps of soil temperature and humidity in the area - if required. In case a local weather station is not available close to the study, it would be very useful to have one certified weather station at a protected location, in order to understand what the *certified* temperature and humidity would be in the study area, in order to correct and calculate (soil) temperature and humidity.

The accuracy assessment provides a lot of information, but the selected approach takes a long time (>24 hours) on a personal computer, which means that selection of a shorter period (e.g. 1 week instead of 1 month) could be a better alternative. A better understanding of the errors, both spatial and temporal, can increase performance of similar networks in the future. The current analysis shows no relation of error to the density of sensors or the border of the study area, which indicates differences are either caused by local climatic changes (which could explain larger errors around the village), incorrect functioning of sensors, or the inadequate correction of the resulting data. Understanding the relation between errors and the type of day can be used to improve interpolation. If the change in temperature during the day can be used to understand whether the day is sunny or cloudy (or possible other classifications), the relative importance of covariates can be adjusted in co-kriging or other kriging approaches. It is also recommended to consider use of the humidity sensor for the possible classification of days, as well as the use of satellite imagery that provides information about cloudiness. Improving understanding of the type (rainy, sunny, cloudy) day is thus recommended.

Hourly models that explain temperature and include dynamic covariates are at this moment only marginally better than models that only include static covariates, which could be improved by more studies of dynamic covariates. The linear models during the day are significantly weaker than the models during the night, which means other (combinations of) covariates have to be selected and studied. Several factors that influence local climate have not been added (e.g. distance to water bodies), as this was not relevant in this study. If a model would be created to cover a wider diversity of areas, including these factors is recommended. The relationship between the elevation/temperature and radiation/temperature can be better studied, to understand how this can be used in interpolation of the data. This would require combination of more studies from different regions/seasons.

5 Data interpolation

5.1 Introduction

The previous chapters have provided information about the resolution and shielding of the sensors that still provide sufficiently accurate results, and have also provided the correlation that temperature has with a range of covariates during the study area. The next step will be to create an accurate map of the temperature and humidity in the area, while determining how costs can be reduced in future studies. Whereas maps that provide average temperature and humidity data are relatively easy to create and show a strong correlation with factors such as altitude, the hourly data is more complex to assess based on few sensors, as correlation with covariates is weaker (*previous chapter*). In the original study, 80 sensors have been used in 8.7 km^2 , which is around one sensor per 0.1 km^2 . This density will be reduced in future studies, and especially in projects where the trials are conducted in relatively flat terrain with limited local variation. The predictive ability of interpolation models with covariates has the potential to increase the accuracy of the network, which can result in less sensors providing the same level of output. The effectiveness of applying different kriging approaches to assess climatic data (e.g. temperature, precipitation, evotranspiration) in areas with complex terrain has been well studied (Goovaerts, 2000; Martínez-Cob, 1996) and has resulted in some basic recommendations. Whether these recommendations are valid for the smaller scale, as studied in this research, will be assessed. One of the results, based on similar methodology, but a different scale, is that ordinary kriging outperforms advanced kriging (based on the relationship between rainfall and elevation) when the correlation is lower than 0.75. This is a strength that is only attained by the temperature-elevation correlation (depending on time/type of day) in this research.

The limitation of most traditional approaches to temperature downscaling, is that they ignore the topographic variation at the very local scale (Benestad, 2001), which will be important for the variation in complex terrain. Models that interpolate weather station data and cover a relatively small scale, include - except for elevation - complex topographic indexes (Daly, Conklin and Unsworth, 2007) and geographic position (Hijmans et al., 2005). The study that - in methodology - is most similar to this study is the study by Parmentier et al. (2014), which included elevation, aspect, canopy height, percentage forest cover (expected to be comparable to LAI) and land surface temperature (derived from MODIS) to predict daily maximum temperature. Holden et al. (2011) - working at a similar scale as this study, have included - outside elevation - humidity and solar radiation as covariates to explain time-space variations in temperature at the local level. An interpolation study by Morales et al. (2007) used distance to water bodies, slope, aspect, elevation, geographic position (latitude and longitude) as well as an indicator of land condition (NOAA mean NDVI). Different covariates have been found to be strongly related to micro-climates (and diurnal climate variation); this includes LAI (Hardwick et al., 2015), solar radiation (Bennie et al., 2008) and distance to streams (Eskelson, 2011). This chapter will combine different covariates - the relative importance and model strength of which is shown in *figure 30* - in a range of geostatistical interpolation methods to assess how accurate the network remains when a certain number of sensors is removed from the full dataset.

5.2 Methodology

5.2.1 Data inputs

The data that will be analysed in this chapter is the same dataset that was used in *chapter 4*. Data is derived from 80 sensors during a period of over one month (5-August to 8-September 2014) in Costa Rica. The data has been corrected during the hours with sun, due to the faster heating in the used PVC shields compared to certified sensor shields. The data above the 0.98 quantile has subsequently been corrected and reset to the value at the 0.98 quantile to have data that is in line with what can be expected in the area based on a local weather station. In this analysis 31 days are selected to calculate the accuracy, and one day for visualization to avoid the smoothing impact of taking the mean of several days. The impact of different kriging approaches will be tested on all 24 hours, which means a total of 744 layers with 80 sensor each are interpolated. The first day has been selected for the visualization. An important issue that has to be taken into account with different forms of interpolation is that missing values (*NA*) are not accepted. This means all missing values in the time-series had to be removed prior to this analysis, as otherwise the steps discussed in this chapter will not work. Removing missing values is straightforward and can be done with different forms of interpolation (covered in *chapter 3*). During the data correction that takes place after this step (e.g. removing extreme values), it is important to reset these values to other value and not to missing values. The loading and correction of data is mainly done with the R *zoo* package.

5.2.2 Prediction grid

Based on literature (*section 5.1*) and the results in *section 4.3.4*, it is expected that elevation will be the most important covariate in this study. It has also been discussed earlier in this thesis that the desired resolution of the outputs in this study is at ± 1 hectare, linked to the level at which farmers are expected to make decision regarding varieties and other inputs. The DEM that is used in this study, and is open-access (STRM 4.1), is created at 90m resolution. As all other covariates - except for LAI and canopy height - are derived from this map, the DEM will form the basis of the prediction grid in this study. The resolution is sufficiently high for this study (and could be disaggregated at a later stage), and this would require few adjustment and thus additional calculations. For different types of interpolation, different prediction grids will be required. For ordinary kriging, the DEM can be converted to a '*SpatialPixels*' object (R *sp* package), which is a blank grid with the same cell-size. In order to be able to interpolate in time, different forms of data transformation have been done. The main steps has been from *raster*, to '*SpatialPixels*' and to an object of class '*STF*', which is an object that can handle spatio-temporal data. This object does not only include a data-slot for the area, but also contains a data-slot that contains the measurements for a certain period. The prediction grid for universal kriging is also based on a '*SpatialPixels*' object, but will be filled by a selection of covariates to create a '*SpatialPixelsDataFrame*'. The values for the pixels can also be adjusted during calculations, which means hourly radiation values can be included. This prediction grid contains 1,768 cells, which is a rectangular grid that covers the entire study area.

5.2.3 Geostatistical interpolation

A short introduction to interpolation has been provided in the previous section (methodology), as spatio-temporal interpolation was already attempted for a basic assessment of network accuracy. Different interpolation have been assessed in this study, but it has been decided that kriging provides the best range of options , as it has been successfully applied in similar studies (section 5.1) . Kriging is an important geo-statistical technique that calculates values of a variable over a larger area, based on a certain sampling of this variable. The basic technique has been introduced by Matheron (1963) and has evolved from Ordinary Kriging to a wide number of more complex methods that take into account covariates and trends in both space and time dimensions. In its most basic form, kriging is very similar to IDW, as they both weigh the nearby known points to predict at an unknown location (*formula below*). In this formula, $Z(s_i)$ is the known value at location i , λ is a certain unknown weight at this location, s_0 is the location of prediction, and n the total measured values. The main difference is that kriging adds more information to the selected *weight* (λ_i) than only the distance (ESRI, web). In ordinary kriging, this weight is also dependent on the spatial relationship of the known point and a fitted model of these points (variogram). Due to the complexity of the different selected kriging algorithms, the differences will be discussed - but not provided as algorithms.

$$\hat{Z}(s_0) = \sum_{i=1}^n \lambda_i Z(s_i)$$

Except for the main R packages that deal with spatial objects (*raster*, *rgdal*, *rgeos* and *sp*), a number of specialized geostastical packages has been used in the analyses. These are *gstat* (Pebesma, 2004), and *spacetime* (Pebesma, 2012). For automatic fitting of variograms, three additional packages have been used: *automap* (Hiemstra, 2013) *randomForest* (Liaw & Wiener, 2002) and *GSIF* (Hengl, 2015). In order to use the different kriging approaches without errors, the projection of the spatial objects has been set to the WGS4 Web Mercator (Auxiliary Sphere) reference system (EPSG:3857), as this will transform the map units from degrees to meters, which is required for some calculations.

5.2.4 Selected kriging-approaches

Based on existing studies and the results provided earlier in this study, a small selection of kriging approaches has been analysed. Ordinary kriging (OK), which is relatively similar to IDW in that they both only look at the temperature data and distance (although OK includes spatial dependence), is taken as the control method. Universal kriging (UK), also known as regression kriging, combines a regression model (with a selection of covariates) with the basic kriging of residuals of the regression. UK will be analyses with one covariate (elevation) and a combination of covariates, based on *section 4.3.4*; this has included different covariates depending on the time of day (radiation cannot be included when it shows no variation). Two automatized approaches of UK were tested. This includes automatic fitting of the variogram (included in the *automap* R package), and a machine-learning method to improve regression: Random Forest (RF) kriging. Co-kriging (CK) and spatio-temporal (ST) kriging were analysed with different covariates. More details are provided in *table 11*.

Table 10: Summary of selected interpolation approaches

Kriging approach	Section
<i>Ordinary kriging</i> is considered as anchor algorithm in the field of geostatistics, as it provides robust output under a wide range of conditions (Deutch and Journel in Atkinson & Lloyd, 1998). In this study, the variogram is fitted automatically - after an initial user estimation. No covariates are included in this control method. The only requirement is a spatial object that includes the location of sensors with the data (<i>SpatialPixelsDataFrame</i>), and a prediction grid (<i>SpatialGrid</i>) that covers the full geospatial network for which data will be predicted.	5.3.1
<i>Universal kriging</i> is largely similar to OK, but will include covariates that will be included in creation of the regression model. The covariates will be log-transformed as this will make the distribution more symmetric (normal distribution) and can help to create a better fitting semi-variogram model (Armstrong & Boufassa, 1988). In the first UK approach, only elevation is included - as this shows the strongest correlation and has resulted in good result in similar studies. A second approach will include the results of section 4.3.3 and includes different covariates throughout the day. Radiation is included during the day, slope and aspect during the night.	5.3.2
<i>Automatized UK</i> is mathematically similar to UK, but includes aspects that make this approach easier to implement by reducing user input. One aspect that can cause difficulties for inexperienced users is variogram fitting; this will be done by the <i>automap</i> R package, to assess how this influences both the accuracy of the data and the time required (although time is not considered a serious restriction due to possibilities for cloud computing). Random-Forest kriging is UK in which the regression model (relation of covariates) is estimated by the computer. The advantage of this approach is that it fits all the variograms automatically based on a set of covariates, and it not sensitive to noise or overfitting of the data (Grimm et al., 2008). This approach to kriging is used in several studies (Bradter et al., 2013; Peters et al., 2007; Wiesmeier et al., 2011).	5.3.3
<i>Co-kriging</i> is an interpolation approach that is recommended in cases where sampling of the variable of interest is too costly and measurements of a correlated variable is cheaper or readily available. Compared to other methods, in which a single variogram is created, in co-kriging, different models are created for different quantiles. In co-kriging, both autocorrelation for a certain variable of interest, as well as cross-correlation between this variable and covariates are used to improve prediction accuracy. Co-kriging in R is discussed in the Technical Note on Co-kriging (Rossiter, 2007), which is taken as the basis for this analysis.	5.3.4
<i>Spatio-temporal kriging</i> can be done with most of the previously discussed forms of kriging, and can thus include covariates. Adding a temporal dimension to kriging is based on the assumption that temporally close observations have a stronger correlation than observations further apart in time. Different types of models exists, which are explained in detail in Pebesma (2012). Practical implementation is relatively similar to that of the other kriging approaches, and functions are mostly based in the <i>gstat</i> and <i>spacetime</i> packages. Autofitting of the variograms is also possible, although only one fitted variogram is used in the spatio-temporal kriging. In this study, spatio-temporal interpolation will be done with ordinary kriging and with elevation as covariate.	5.3.5

5.2.5 Analyses

The analyses in this chapter mainly focuses at the overall accuracy of the different interpolation approaches, but will also cover some other relevant issues. The RMSE will be analysed both in the spatial and temporal domain to indicate how this changes with different sets of sensors. Maps will also be provided in situations where the errors show unexpected trends. Special attention is given to the period around solar noon where, based on section 4.3.3, the covariates cannot explain more than half of the variance in temperature. All analyses include the full 80-sensor network, as well as subset of half (40), one-quarter (20) and one-tenth (8) of the sensors. At the original density, one sensor is placed per 0.1 km^2 , which reduces - in different steps - to one sensor per 1km^2 . The errors that will be included in the analyses are the (mean, spatial and temporal) root mean square error (RMSE), as well as the mean absolute error (MAE) and the mean absolute percentage error (MAPE).

RMSE - earlier explained in *section 4.2.2* - is the most used measure of accuracy. This approach provides errors in the same units as the original data and can easily be compared between similar studies. The RMSE is more sensitive to outliers than the other measures due to the squaring of residuals. As this study includes diurnal differences, and especially the errors for the extreme temperatures are relevant for the use of this network in crop-models, the RMSE is the preferred measure of accuracy in this study. This error is also best compared with other relevant studies.

MAE - the mean absolute error - is another measure of interpolation accuracy that is measured in the same unit as the original data. The difference between the MAE is that it does not include a squaring process, which will reduce the impact of outliers. Using MAE is often included in the output of forecasting based on time-series (Duke, web), and is relatively easy to calculate - although not commonly part of standard accuracy assessment functions.

MAPE - the mean absolute percentage error, is a measure of accuracy that is provided as percentage and not in the same units as the original data. This measure is easy to understand and compare between methods and works well with the used data (temperature in a $15\text{-}30^{\circ}\text{C}$ range). Using percentages also gives an indication about the relative size of errors. As this approach will give a lot of information the RMSE cannot give, it will be added in the analyses.

The analyses will include all 13,440 ($7 \times 24 \times 80$) residuals, in order to be able to provide spatial and temporal trends. The overall RMSE will be provided, based on all residuals, but attention is also given to differences in space and time. The spatial RMSE is based on the residuals at all hours, and provides the mean of the hourly RMSE for the 168 hours. The temporal RMSE is based on the errors for each sensor, and calculates the mean of the RMSE for all (80, 40, 20 or 8) sensors. Discussion of the size of errors acknowledges the level of sensor accuracy ($\pm 0.5^{\circ}\text{C}$) and possible errors that result from the interpolation of data from the original 20-minute resolution to regular one-hour interval. Errors $<0.5^{\circ}\text{C}$ will be considered *low*, errors ranging from 0.5 to 1°C are *medium*, and errors $>1^{\circ}\text{C}$ are *large*. Accuracy assessment does not only focus at the daily mean error, but gives special attention to the range during the day - which will be important for the extremes.

5.3 Results

5.3.1 Ordinary Kriging

The overall RMSE for ordinary kriging with 80 sensors is 0.83, which becomes 0.88 with 40 sensors, 0.85 with 20 sensors and 0.98 with 8 sensors. In the spatial domain the RMSE is 0.69 (*Annex X-I*), while in the temporal domain the RMSE is 0.83. The mean RMSE in the temporal domain does not change a lot when working with different numbers of sensors - as the number of hours remains the same. In the spatial domain, the trends in RMSE increases from 0.69 with 80 sensors to 0.95 with 8 sensors, although the range of the errors decreases when working with less sensors. The mean absolute percentage error increases from 2.5 to 3.3% when reducing the number of sensors from 80 to 8 sensors in both space and time dimension. The MAPE is always similar in both dimensions, and thus gives a good indication of the change in accuracy. While an increase of 0.8% in error does not seem to be a lot, this is an average value and can be larger for different times of day. The visual impact of a reduction in sensors, without adding a covariate to improve prediction, is shown in *figures 31-34*; there is a clear decrease in complexity when reducing the number of sensors. With 8 sensors, the range remains similar, but the trends over the area become very smooth.

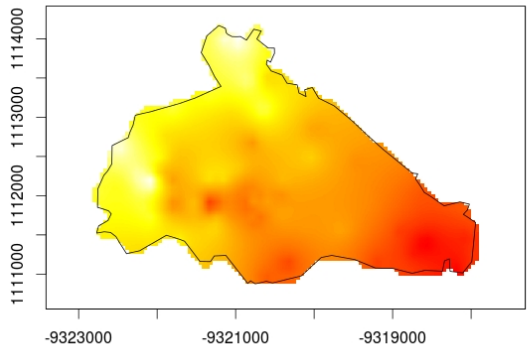


Figure 31: Ordinary Kriging (80 sensors)

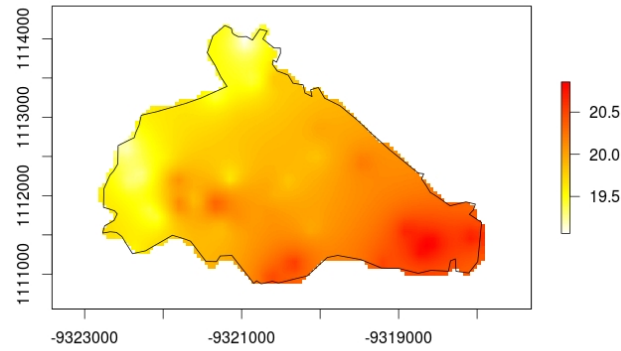


Figure 32: Ordinary Kriging (40 sensors)

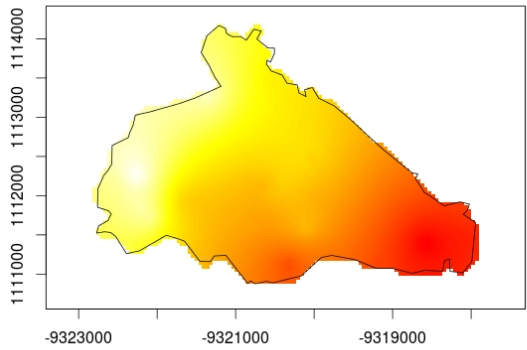


Figure 33: Ordinary Kriging (20 sensors)

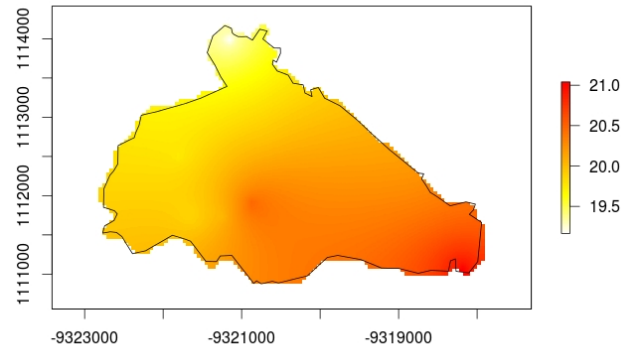


Figure 34: Ordinary Kriging (8 sensors)

5.3.2 Universal Kriging

Two variations of universal kriging have been applied with elevation as covariate; the first was fully based on the basic functionality in the *gstat* package while the second method also used automatic fitting of the variogram - without providing a sample (based on the *automap* package). Statistics of the basic universal kriging approach are provided in Annex X-II, and of automatized universal kriging in Annex X-III. Both approaches have a lower RMSE than ordinary kriging in the original dataset (0.79 vs 0.83), and in with 80 sensors, automatized fitting provides slightly lower errors overall. When reducing sensors, basic universal kriging starts performing better than automatized universal kriging, although differences remain very small. Universal kriging has a RMSE of 0.79 at 40 sensors, 0.80 at 20 sensors and 0.88 with 8 sensors. Automatic kriging takes about twice as long for calculations than universal kriging with a single sample variogram. For automatic kriging, the RMSE is 0.83 with 40 sensors, 0.81 with 20 sensors, and 0.90 with 8 sensors. Errors with UK are always lower than without inclusion of covariates (OK). Universal kriging - including elevation - shows less smoothing when reducing the number of sensors (*figures 35-38*). This can help in reducing the number of sensors (hence costs) while still having clear local variation in temperature.

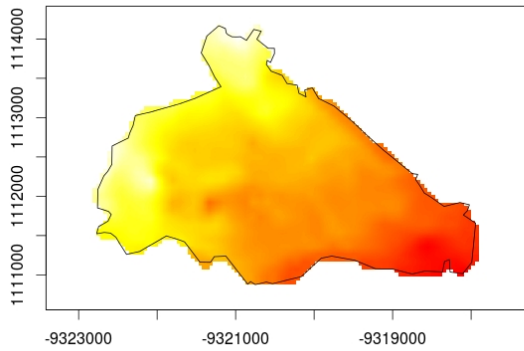


Figure 35: Universal Kriging (80 sensors)

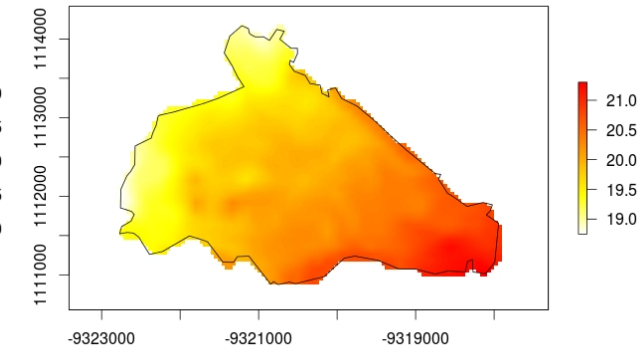


Figure 36: Universal Kriging (40 sensors)

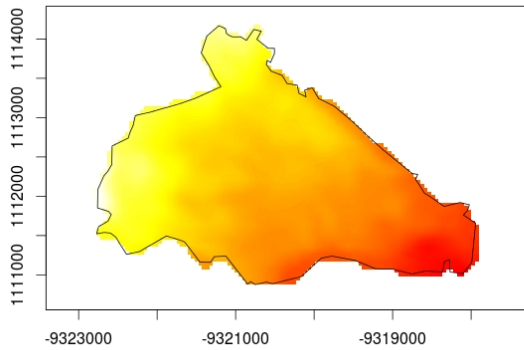


Figure 37: Universal Kriging (20 sensors)

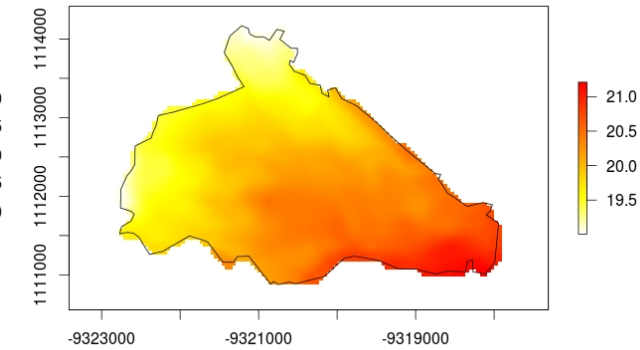


Figure 38: Universal Kriging (8 sensors)

Although the differences are very small, automatic universal kriging does provide clear different trends at hours with sun (*figures 39 and 40*). These plots, which show the most problematic hours (11AM-4PM), indicate that there are different trends in predicted mean temperature during periods when the overall differences are small. This is only the case at a small part of the study area (with a low density of sensors) and thus does not have a significant influence on the errors. These differences are the result of automatic fitting of the variogram; providing a single variogram for all hours can result in problems that result from lack of spatial dependence. In these cases - which happen frequently during periods of sun - the differences can become relatively large between universal kriging and automatic universal kriging. Universal kriging provides a smoother estimate, while automatic kriging continues to emphasize local differences. Whether this is a positive or negative characteristic in the interpolation depends on the reliability of sensors; this can possibly provide more detailed information about micro-climates, while it can also increase the impact of incorrect functioning sensors in the network. The main advantage of automatic kriging is the ease of implementation (limited user-input).

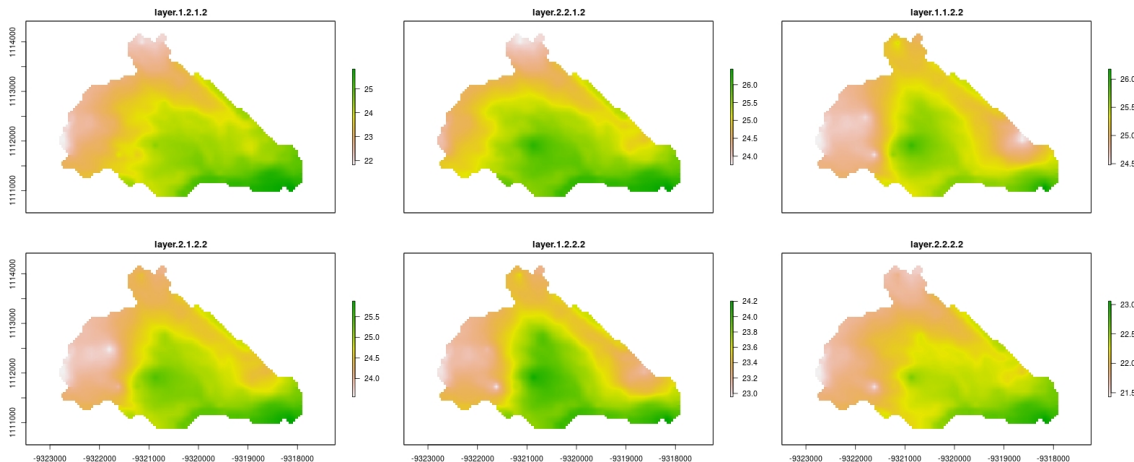


Figure 39: Mean temperature for the hours 11AM-4PM based on universal kriging with 20 sensors

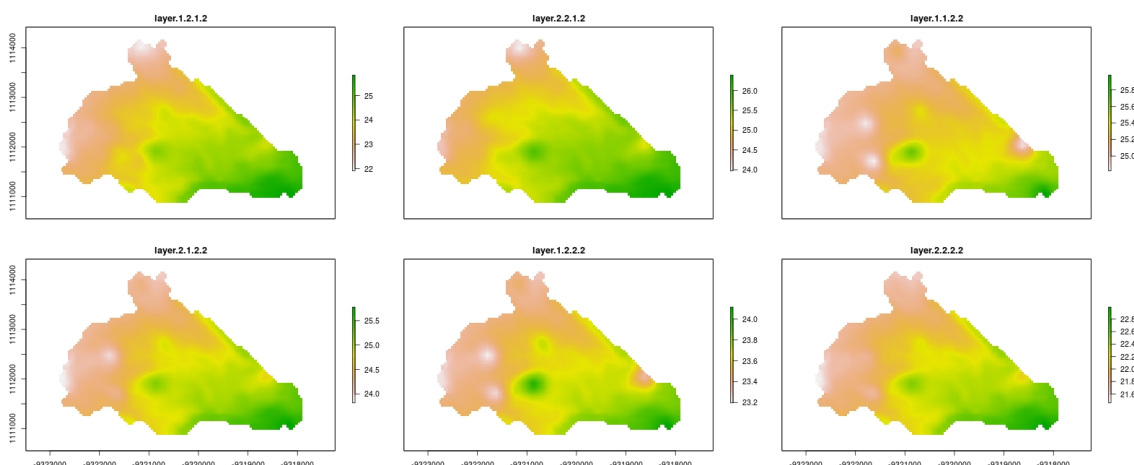


Figure 40: Mean temperature for the hours 11AM-4PM based on universal auto-kriging with 20 sensors

5.3.3 Dynamic universal kriging

Dynamic kriging, which changes the set of covariates during the day (based on *section 4.3.3*) has been done with three different approaches. The approaches used in the previous section (basic universal kriging and auto-kriging) have been applied, as well as RandomForest kriging. The limitation of RandomForest kriging is that it requires at least 50 points for validation and does not continue with predicting once a certain hour cannot be predicted based on the covariates. The statistics that resulted from the different approaches are provided in Annex X 1:III. Basic dynamic kriging has the following RMSE for the different sensor-sets: 0.77 (80), 0.81 (40), 0.88 (20), and 1.44 (8). For automatized dynamic kriging the errors are: 0.78 (80), 0.83 (40), 0.81 (20) and 0.90 (8). For random forest kriging, the RMSE for all 80 sensors is 0.78. With the full 80-sensor dataset, errors are lowest with the basic dynamic kriging approach. With a reduction in sensors, the errors become much larger, and especially with 8 sensors, the errors are problematic. With automatic dynamic kriging, the errors are almost the same as with elevation only. The errors, however, are significantly lower than for non-automatized dynamic kriging at 20 and 8 sensors. Random Forest kriging only works with the 80-sensor dataset and, while the RMSE at the full sensor-set is quite good, this method will be difficult to implement in smaller sensor-networks. The main difference between dynamic kriging - including hourly radiation - and universal kriging with elevation only, is the lower estimate of temperature at areas where cast shadow plays a role - especially with few sensors (left part and the areas close to borders in *figure 41*). The overall errors remain similar at locations of sensors, but at areas where sensors are not found, prediction results in temperatures that cannot be validated, and might be unrealistic and a result of over-estimation of the impact of hourly radiation.

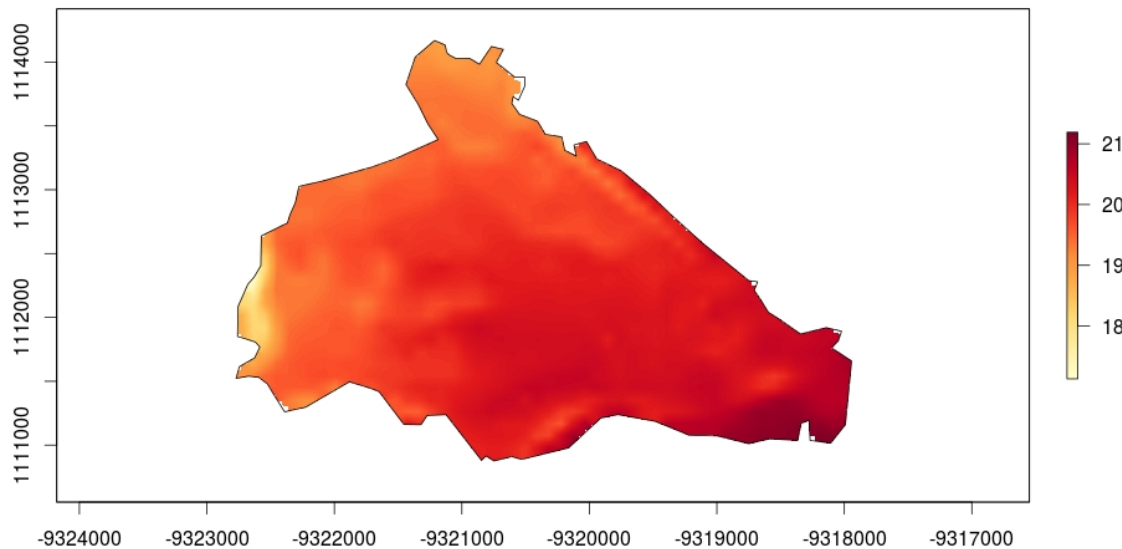


Figure 41: Predicted temperature based on dynamic kriging and 8 sensors

5.3.4 Co-kriging approaches

Co-kriging has been done with (1) elevation, (2) elevation and radiation, and (3) elevation, radiation slope and aspect. The RMSE for co-kriging with elevation with different sets of sensors is 0.86 (80), 0.90 (40), 0.91 (20) and 1.21 (8). Including radiation results in RMSE's of 0.83 (80), 0.87 (40), 0.88 (20) and 1.21 (8). Adding slope and aspect does not further reduce the errors. This shows that adding covariates improves the accuracy at 80, 40 and 20 sensors, while errors increase with 8 sensors. The benefit of using co-kriging is limited, as the errors are in all cases larger than for ordinary kriging. Co-kriging could be improved with more advanced adjustment, as in this study the same (limited) parameters are used for the different interpolation approaches. While the overall temperature trends show the same daily fluctuation, there is no clear gradient and the sensors that provide outliers are emphasized. The differences throughout the network (based on 80 sensor) between co-kriging and universal kriging (elevation only) during the hours 5-10AM are provided in *figure 42*. The difference between the two approaches increases during the periods with high temperatures.

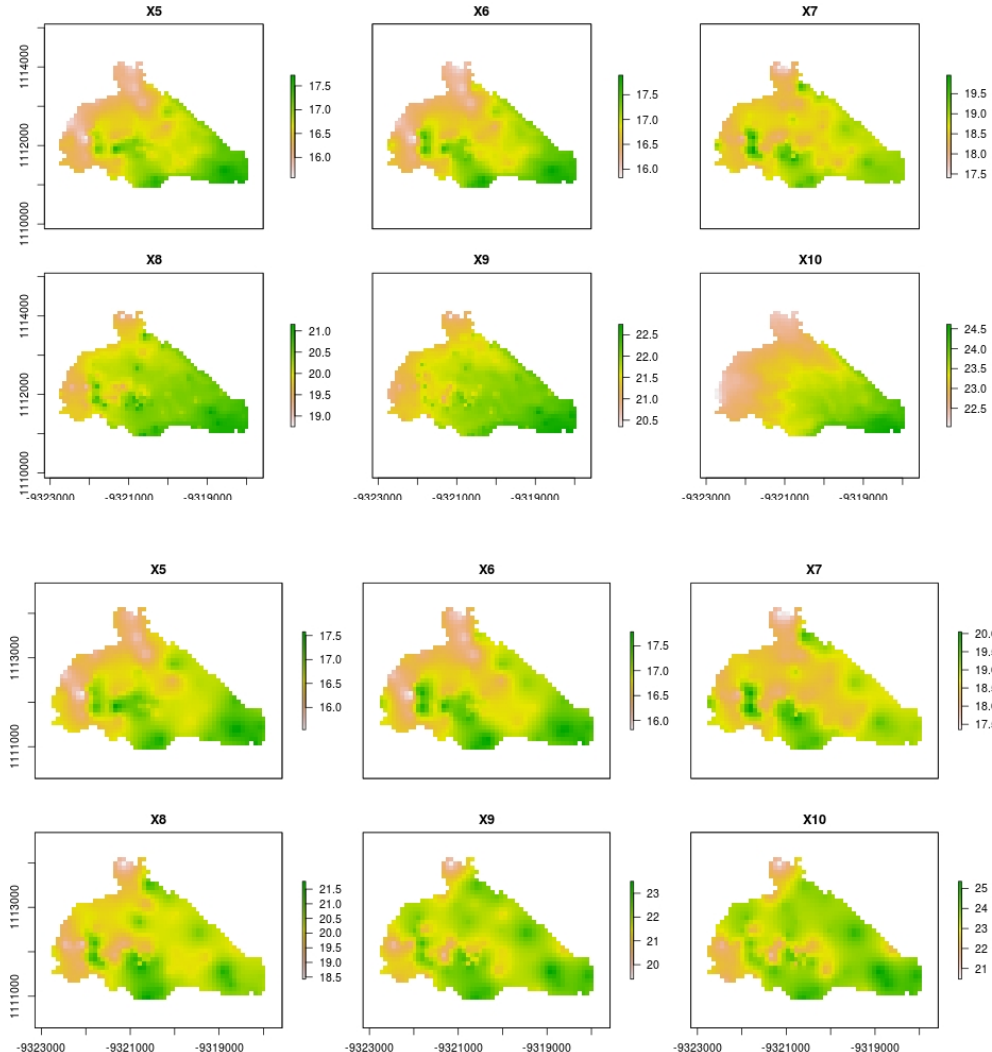


Figure 42: Hourly mean temperature during 5-10AM with Universal Kriging (top) and Co-Kriging (bottom)

5.3.5 Spatio-temporal kriging

Spatio-temporal kriging has been tested with the time dimension only (basic ST-ordinary kriging), with elevation (ST-universal kriging), and with a dynamic set of covariates (ST-dynamic kriging). The RMSE of the approaches is relatively high: the RMSE with 80 sensors (time only) is 0.96, when including elevation this is still 0.96, while addition of radiation, slope and aspect increase the RMSE to 0.99. At 40 sensors, the error remain similar for the three approaches, while with 20 sensors, the errors increase slightly to 0.96 (STOK and STUK) and 1.00 (STDK). The 8-sensor dataset results in a RMSE of 1.07 (STOK), 1.18 (STUK) and 1.20 (STDK). While the errors are larger than for any of the earlier tested approaches, there is a move from the trend that RMSE *temporal* $>$ *spatial*, to a RMSE that is smaller in the temporal domain. The additional interpolation in the time-domain does, however, result in larger errors at the separate hours and also the largest errors of all tested approaches. The inclusion of the time-dimension in ST interpolation is visually attractive when animating the temperature trends, and could provide benefits when reducing the interval of observations, but with the current interval the approach does not perform well. Another limitation of using the temporal interval is that temperature can change quick under different conditions of cast shadows (position of the sun, clouds) and rain/wind. Assuming a strong correlation in time is thus not necessary when being able to sample frequently, as can be seen from the relatively large errors of this approach. A full day of observations using spatio-temporal interpolation is shown in *figure X*.

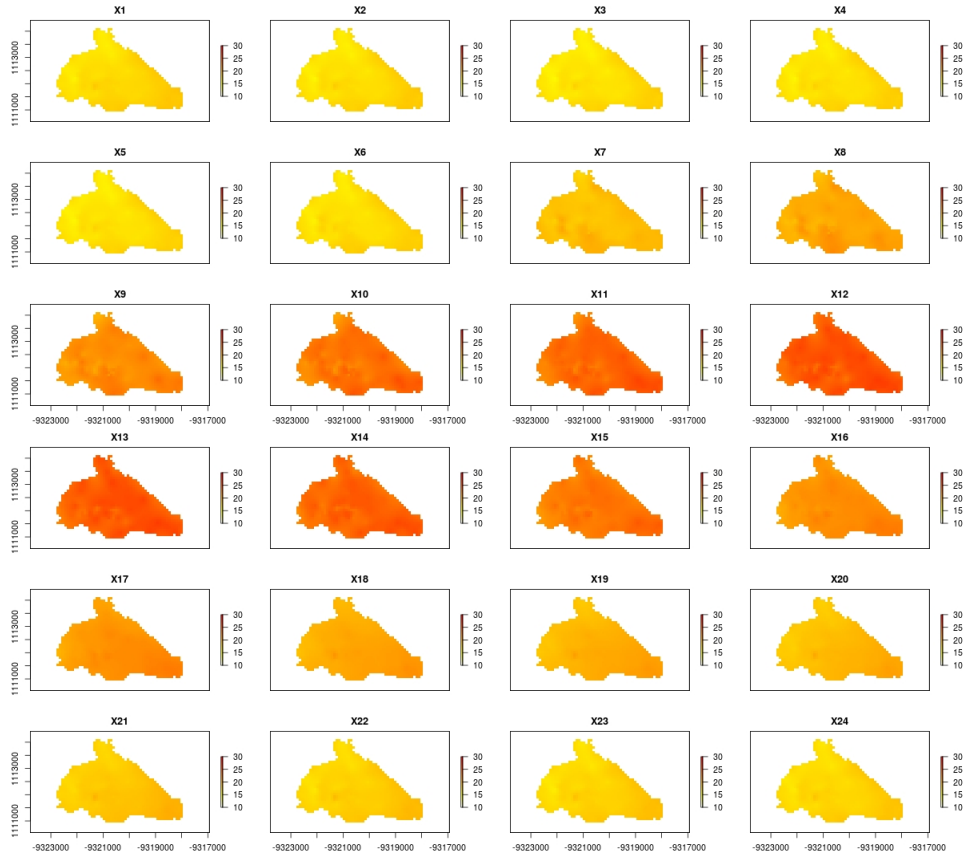


Figure 43: Daily temperature trends in Aquiares, based on ST Ordinary Kriging with 80 sensors

5.4 Discussion

5.5 Recommendations

6 Conclusions & Recommendations

7 References

- ◊ Altieri, M. (2002). *Agroecological Principles for Sustainable Agriculture*. In *Agroecological innovations: increasing food production with participatory development* (pp. 4046).
- ◊ Armstrong, M., & Boufassa, A. (1988). *Comparing the robustness of ordinary kriging and lognormal kriging: Outlier resistance*. Mathematical Geology, 20, 447457. doi:10.1007/BF00892988
- ◊ Ashcroft, M. B., & Gollan, J. R. (2013). *Moisture, thermal inertia, and the spatial distributions of near-surface soil and air temperatures: Understanding factors that promote microrefugia*. Agricultural and Forest Meteorology, 176, 7789. doi:10.1016/j.agrformet.2013.03.008
- ◊ Atkinson, P. M., & Lloyd, C. D. (1998). *Mapping Precipitation in Switzerland with Ordinary and Indicator Kriging*. Journal of Geographic Information and Decision Analysis, 2(2), 6576.
- ◊ Baggio, A. (2005). *Wireless sensor networks in precision agriculture*. Precision Agriculture, 122. doi:10.4018/978-1-60960-027-3
- ◊ Barnett, B. J., & Mahul, O. (2007). *Weather index insurance for agriculture and rural areas in lower-income countries*. American Journal of Agricultural Economics, 89, 12411247. doi:10.1111/j.1467-8276.2007.01091.x
- ◊ Barr, S., & Orgill, M. M. (1989). *Influence of External Meteorology on Nocturnal Valley Drainage Winds*. Journal of Applied Meteorology. doi:10.1175/1520-0450(1989)028
- ◊ Benestad, R. E. (2001). *A comparison between two empirical downscaling strategies*. International Journal of Climatology, 21, 16451668. doi:10.1002/joc.703
- ◊ Bivand, R., & Rundel, C. (2013). *rgeos: Interface to Geometry Engine - Open Source (GEOS)*. R package version 0.3-2. R Package Version 0.1-8.
- ◊ Blair, J. B., Rabine, D. L., & Hofton, M. A. (1999). *The Laser Vegetation Imaging Sensor: A medium-altitude, digitisation-only, airborne laser altimeter for mapping vegetation and topography*. ISPRS Journal of Photogrammetry and Remote Sensing, 54, 115122. doi:10.1016/S0924-2716(99)00002-7
- ◊ Blair, J. B., Rabine, D. L., & Hofton, M. A. (2006). *Processing of NASA LVIS elevation and canopy (LGE, LCE and LGW) data products*, version 1.01. Retrieved from <http://lvis.gsfc.nasa.gov>
- ◊ Blumthaler, M., Ambach, W., & Ellinger, R. (1997). *Increase in solar UV radiation with altitude*. Journal of Photochemistry and Photobiology B: Biology, 39, 130134. doi:10.1016/S1011-1344(96)00018-8
- ◊ Bradter, U., Kunin, W. E., Altringham, J. D., Thom, T. J., & Benton, T. G. (2013). *Identifying appropriate spatial scales of predictors in species distribution models with the random forest algorithm*. Methods in Ecology and Evolution, 4, 167174. doi:10.1111/j.2041-210x.2012.00253.x
- ◊ Bristow, K. L., & Campbell, G. S. (1984). *On the relationship between incoming solar radiation and daily maximum and minimum temperature*. Agricultural and Forest Meteorology. doi:10.1016/0168-1923(84)90017-0
- ◊ Budowski, G. (1980). *The Place of Agro-Forestry in Managing Tropical Forests*.
- ◊ Butler, D. R. (1977). *Coffee Leaf Temperatures in a Tropical Environment*. Koninklijke Nederlandse botanische vereniging.

- ◊ Chakraborty, S., Tiedemann, A. V., & Teng, P. S. (2000). *Climate change: potential impact on plant diseases*. Environmental Pollution, 108, 317-326. doi:10.1016/S0269-7491(99)00210-9
- ◊ Charney, J. G. (1949). *On a physical basis for numerical prediction of large-scale motions in the atmosphere*. Journal of Meteorology. doi:10.1175/1520-0469(1949)
- ◊ Cheng, C. S., Li, G., Li, Q., & Auld, H. (2008). *Statistical downscaling of hourly and daily climate scenarios for various meteorological variables in South-central Canada*. Theoretical and Applied Climatology, 91, 129147. doi:10.1007/s00704-007-0302-8
- ◊ Clark, P. E., Johnson, D. E., Harris, N., & Thomas, D. R. (2006). *Low-Cost Radiation Shielding for Use in Mapping the Thermal Environments of Rangeland Animals*. Rangeland Ecology & Management. doi:10.2111/05-093R2.1
- ◊ Cornell University, I. P.-C. of A. and L. S. (n.d.). *Aquiares Estate: Coffee & Community Since 1890*. Retrieved from <http://ip.cals.cornell.edu/undergrad/docs/study-abroad-prog-Aquiares-Estate.pdf>
- ◊ Daly, C., Halbleib, M., Smith, J. I., Gibson, W. P., Doggett, M. K., Taylor, G., Pasteris, P. P. (2008). *Physiographically sensitive mapping of climatological temperature and precipitation across the conterminous United States*. International Journal of Climatology, 28, 20312064. doi:10.1002/joc.1688
- ◊ Dauzat, J., Rapidel, B., & Berger, A. (2001). *Simulation of leaf transpiration and sap flow in virtual plants: Model description and application to a coffee plantation in Costa Rica*. Agricultural and Forest Meteorology, 109, 143160. doi:10.1016/S0168-1923(01)00236-2
- ◊ DAVIS. (2014a). *Remote Integrated Pest Management Station for Agriculture*. Retrieved October 29, 2014, from <http://www.davisnet.com/weather/uses/agriculture-solutions/remote-ipm-station.asp>
- ◊ DAVIS. (2014b). *WeatherLinkIPTM for Vantage Stations*. Retrieved October 29, 2014, from http://www.davisnet.com/weather/products/weather_product.asp?pnum=06555#price
- ◊ Deardorff, J. W. (1978). *Efficient prediction of ground surface temperature and moisture, with inclusion of a layer of vegetation*. Journal of Geophysical Research. doi:10.1029/JC083iC04p01889
- ◊ Oxford Dictionaries. (2015). *Adiabatic lapse rate*. Retrieved February 15, 2015, from <http://www.oxforddictionaries.com/definition/english/adiabatic-lapse-rate>
- ◊ Dodson, R., & Marks, D. (1997). *Daily air temperature interpolated at high spatial resolution over a large mountainous region*. Climate Research, 8, 120. doi:10.3354/cr008001
- ◊ e-Agriculture. (2014). Retrieved November 04, 2014, from <http://www.e-agriculture.org/> Edwards, P. N. (2010). *A Vast Machine: Computer Models, Climate Data, and the Politics of Global Warming*. Thinking (Vol. 28, p. 518). doi:10.1111/j.1541-1338.2011.005223.x
- ◊ Erickson, C. O. (1964). *Meteorological Satellites*. Science (New York, N.Y.), 143, 612613. doi:10.1126/science.143.3606.612
- ◊ Eskelson, B. N. I., Anderson, P. D., Hagar, J. C., & Temesgen, H. (2011). *Geostatistical modeling of riparian forest microclimate and its implications for sampling*. Canadian Journal of Forest Research. doi:10.1139/x11-015
- ◊ Ewel, J., Benedict, F., Berish, C., Brown, B., Gliessman, S., Amador, M., Price, N. (1982). *Leaf area, light transmission, roots and leaf damage in nine tropical plant communities*. Agro-Ecosystems. doi:10.1016/0304-3746(82)90023-3

- ◊ Ewert, F., & Pleijel, H. (1999). *Phenological development, leaf emergence, tillering and leaf area index, and duration of spring wheat across Europe in response to CO₂ and ozone*. European Journal of Agronomy, 10, 171184. doi:10.1016/S1161-0301(99)00008-8
- ◊ Gaur, R. K., & Sharma, P. (2014). *Approaches to Plant Stress and their Management*. Springer India.
- ◊ Geller, T. (2007). *Envisioning the wind: Meteorology graphics at weather underground*. IEEE Computer Graphics and Applications, 27, 9297. doi:10.1109/MCG.2007.124
- ◊ Goovaerts, P. (2000). *Geostatistical approaches for incorporating elevation into the spatial interpolation of rainfall*. Journal of Hydrology, 228, 113129. doi:10.1016/S0022-1694(00)00144-X
- ◊ Goudriaan, J. (1977). *Crop micrometeorology: a simulation study*. Wageningen. Retrieved from library.wur.nl/WebQuery/wda/104086
- ◊ Grimm, R., Behrens, T., Mrker, M., & Elsenbeer, H. (2008). *Soil organic carbon concentrations and stocks on Barro Colorado Island - Digital soil mapping using Random Forests analysis*. Geoderma, 146, 102113. doi:10.1016/j.geoderma.2008.05.008
- ◊ Groemping, U. (2006). *Relative importance for linear regression in R: the package relaimpo*. Journal Of Statistical Software, 17, 139147. Retrieved from <http://www.jstatsoft.org/v17/a01/paper>
- ◊ Hacienda Aquiares. (2008). Retrieved October 01, 2014, from <http://www.cafeaquiares.com/>
- ◊ Hackett, C. (1991). *PLANTGRO: a software package for coarse prediction of plant growth* (p. 242). CAB Direct.
- ◊ Hardwick, S. R., Toumi, R., Pfeifer, M., Turner, E. C., Nilus, R., & Ewers, R. M. (2015). *The relationship between leaf area index and microclimate in tropical forest and oil palm plantation: Forest disturbance drives changes in microclimate*. Agricultural and Forest Meteorology, 201, 187195. doi:10.1016/j.agrformet.2014.11.010
- ◊ Hellstrom, R. A., & Mark, B. G. (2006). *An Embedded Sensor Network for Measuring Hydrometeorological Variability Within an Alpine Valley*. In 63rd Eastern Snow Conference. Newark. Retrieved from http://www.easternsnow.org/proceedings/2006/hellstrom_and_mark.pdf
- ◊ Hengl, T. (2015). *Global Soil Information Facilities*. Retrieved from <http://cran.r-project.org/web/packages/GSIF/index.html>
- ◊ Hiemstra, P. (2013). *automap: Automatic interpolation package*. Retrieved from <http://cran.r-project.org/web/packages/automap/automap.pdf>
- ◊ Hijmans, R. J., Cameron, S. E., Parra, J. L., Jones, P. G., & Jarvis, A. (2005). *Very high resolution interpolated climate surfaces for global land areas*. International Journal of Climatology, 25, 19651978. doi:10.1002/joc.1276
- ◊ Hijmans, R. J., & Graham, C. H. (2006). *The ability of climate envelope models to predict the effect of climate change on species distributions*. Global Change Biology, 12, 22722281. doi:10.1111/j.1365-2486.2006.01256.x
- ◊ Hijmans, R. J., & van Etten, J. (2010). *raster: Geographic analysis and modeling with raster data*. R Package Version.
- ◊ Holden, Z. A., Abatzoglou, J. T., Luce, C. H., & Baggett, L. S. (2011). *Empirical downscaling of daily minimum air temperature at very fine resolutions in complex terrain*. Agricultural and Forest Meteorology, 151, 10661073. doi:10.1016/j.agrformet.2011.03.011

- ◊ Holden, Z. A., Klene, A. E., F. Keefe, R., & G. Moisen, G. (2013). *Design and evaluation of an inexpensive radiation shield for monitoring surface air temperatures*. Agricultural and Forest Meteorology, 180, 281286. doi:10.1016/j.agrformet.2013.06.011
- ◊ Intergovernmental Panel on Climate Change. (2014). *Climate Change, Adaptation, and Vulnerability*. Organization & Environment, 24, 144. http://ipcc-wg2.gov/AR5/images/uploads/IPCC_WG2AR5_SPM_Approved.pdf
- ◊ Jarvis, C. H., & Stuart, N. (2001). *A Comparison among Strategies for Interpolating Maximum and Minimum Daily Air Temperatures. Part II: The Interaction between Number of Guiding Variables and the Type of Interpolation Method*. Journal of Applied Meteorology. doi:10.1175/1520-0450(2001)040
- ◊ Jedermann, R., Behrens, C., Westphal, D., & Lang, W. (2006). *Applying Autonomous Sensor Systems in Logistics - Combining Sensor Networks , RFIDs and Software Agents*. Sensors and Actuators A: Physical, 132, 370375. doi:10.1016/j.sna.2006.02.008
- ◊ Jones, J. W., Tsuji, G. Y., Hoogenboom, G., Hunt, L. A., Thornton, P. K., Wilkens, P. W., Singh, U. (1998). *Decision support system for agrotechnology transfer: DSSAT v3*. In Understanding Options for Agricultural Production (pp. 157177).
- ◊ Jones, P. G., & Thornton, P. K. (2013). *Generating downscaled weather data from a suite of climate models for agricultural modelling applications*. Agricultural Systems, 114, 15. doi:10.1016/j.agsy.2012.08.002
- ◊ Lane, A., & Jarvis, A. (2007). *Changes in climate will modify the geography of crop suitability: agricultural biodiversity can help with adaptation*. SAT eJournal, 4, 112.
- ◊ Lawrence, M. G. (2005). *The relationship between relative humidity and the dewpoint temperature in moist air: A simple conversion and applications*. Bulletin of the American Meteorological Society, 86, 225233. doi:10.1175/BAMS-86-2-225
- ◊ Letten, A. D., Ashcroft, M. B., Keith, D. A., Gollan, J. R., & Ramp, D. (2013). *The importance of temporal climate variability for spatial patterns in plant diversity*. Ecography, 36, 13411349. doi:10.1111/j.1600-0587.2013.00346.x
- ◊ Liaw, A., & Wiener, M. (2002). *Classification and Regression by randomForest*. R News, 2, 1822. doi:10.1177/154405910408300516
- ◊ Lobell, D. B., Cassman, K. G., & Field, C. B. (2009). *Crop Yield Gaps: Their Importance, Magnitudes, and Causes*. Annual Review of Environment and Resources. doi:10.1146/annurev.environ.041008.093740
- ◊ Mainwaring, A., Culler, D., Polastre, J., Szewczyk, R., & Anderson, J. (2002). *Wireless Sensor Networks for Habitat Monitoring*. In Proceedings of the 1st ACM International Workshop on Wireless Sensor Networks and Applications (pp. 8897). doi:10.1145/570738.570751
- ◊ Martnez-Cob, A. (1996). *Multivariate geostatistical analysis of evapotranspiration and precipitation in mountainous terrain*. Journal of Hydrology. doi:10.1016/0022-1694(95)02755-6
- ◊ Maxim Integrated. (n.d.). *No Title*. Retrieved November 05, 2014, from <http://www.maximintegrated.com/en/products/comms/ibutton.html>
- ◊ McNider, R. T., & Pielke, R. A. (1981). *Diurnal Boundary-Layer Development over Sloping Terrain*. Journal of the Atmospheric Sciences. doi:10.1175/1520-0469(1981)038j2198:DBLDOS;2.0.CO;2

- ◊ McWilliam, A.-L. C., Roberts, J. M., Cabral, O. M. R., Leitao, M. V. B. R., Costa, A. C. L. De, Maitelli, G. T., & Zamparoni, C. A. G. P. (1993). *Leaf Area Index and Above-Ground Biomass of terra firme Rain Forest and Adjacent Clearings in Amazonia*. Functional Ecology, 7, 310–317. doi:10.2307/2390210
- ◊ Mendelsohn, R., Kurukulasuriya, P., Basist, A., Kogan, F., & Williams, C. (2007). *Climate analysis with satellite versus weather station data*. Climatic Change, 81, 7183. doi:10.1007/s10584-006-9139-x
- ◊ Menne, M. J., Williams, C. N., & Palecki, M. A. (2010). *On the reliability of the U.S. surface temperature record*. Journal of Geophysical Research: Atmospheres, 115. doi:10.1029/2009JD013094
- ◊ Menzel, A., Sparks, T. H., Estrella, N., Koch, E., Aasa, A., Ahas, R., Zust, A. (2006). *European phenological response to climate change matches the warming pattern*. Global Change Biology, 12, 19691976. doi:10.1111/j.1365-2486.2006.01193.x
- ◊ Merriam-Webster Dictionary. (2014). *Merriam-Webster Dictionary*. Retrieved from <http://www.merriam-webster.com/dictionary/>
- ◊ Miller-Rushing, A., Primack, R., & Bonney, R. (2012). *The history of public participation in ecological research*. Frontiers in Ecology and the Environment, 10, 285290. doi:Doi 10.1890/110278
- ◊ Mittra, S., Van Etten, J., & Franco, T. (2013). *Collecting Weather Data in the Field with High Spatial and Temporal Resolution Using iButtons* (No. June 2013 Version). Retrieved from http://www.bioversityinternational.org/uploads/tx_news/Technical_Guide_for_collecting_weather_data_in_the_field_using_iButtons_1628__2_.pdf
- ◊ Monsanto. (2014). *FieldScripts*. Retrieved October 29, 2014, from <http://www.monsanto.com/products/pages/fieldscripts.aspx>
- ◊ Monteith, J. L. (1972). *Solar radiation and productivity in tropical ecosystems*. Journal of Applied Ecology, 9, 747766. doi:10.2307/2401901
- ◊ Morales, L., Canessa, F., Mattar, C., & Orrego, R. (2007). *Comparison of stochastic and regression geostatistics interpolation methods for detection of microclimatic areas*. Retrieved from http://www.itc.nl/ISSDQ2007/proceedings/Session2SpatialStatistics/PaperMorales_et_al..pdf
- ◊ Morton, J. F. (2007). *The impact of climate change on smallholder and subsistence agriculture*. Proceedings of the National Academy of Sciences of the United States of America, 104, 1968019685. doi:10.1073/pnas.0701855104
- ◊ Nhemachena, C., & Hassan, R. M. (2007). *Micro-Level Analysis of Farmers Adaptation to Climate Change in Southern Africa*. Food Policy, 2. Retrieved from <http://www.ifpri.org/publication/micro-level-analysis-farmers-adaptation-climate-change-southern-africa-0>
- ◊ International Standards Organisation. (2007). *Meteorology – Air temperature measurements – Test methods for comparing the performance of thermometer shields/screens and defining important characteristics (ISO 17714:2007)*. Retrieved from http://www.iso.org/iso/catalogue_detail.htm?csnumber=31498
- ◊ Parmentier, B., McGill, B., Wilson, A., Regetz, J., Jetz, W., Guralnick, R., Schildhauer, M. (2014). *An Assessment of Methods and Remote-Sensing Derived Covariates for Regional Predictions of 1 km Daily Maximum Air Temperature*. Remote Sensing, 6(9), 86398670. doi:10.3390/rs6098639
- ◊ Pebesma, E. (2012). *spacetime: Spatio-Temporal Data in R*. Journal of Statistical Software, 51.

- ◊ Pebesma, E., & Bivand, R. S. (2005). *S Classes and Methods for Spatial Data: the sp Package*. Economic Geography, 50, 121.
- ◊ Pebesma, E., Rowlingson, B., & Bivand, R. (2012). *Package rgdal*. R-CRAN, 4, 141.
- ◊ Perfecto, I., Rice, R., & Greenberg, R. (1996). *Shade Coffee: A Disappearing Refuge for Biodiversity*. BioScience, 46, 598–608. doi:10.2307/1312989
- ◊ Peters, J., Baets, B. D., Verhoest, N. E. C., Samson, R., Degroeve, S., Becker, P. D., & Huybrechts, W. (2007). *Random forests as a tool for ecohydrological distribution modelling*. Ecological Modelling, 207, 304318. doi:10.1016/j.ecolmodel.2007.05.011
- ◊ Pielke, R. A., & Wilby, R. L. (2012). *Regional climate downscaling: Whats the point?* Eos, 93, 5253. doi:10.1029/2012EO050008
- ◊ Porter, J. R., & Christensen, S. (2013). *Deconstructing crop processes and models via identities*. Plant, Cell and Environment, 36, 1919–1925. doi:10.1111/pce.12107
- ◊ Ramirez-Villegas, J., Jarvis, A., & Laderach, P. (2013). *Empirical approaches for assessing impacts of climate change on agriculture: The EcoCrop model and a case study with grain sorghum*. Agricultural and Forest Meteorology, 170, 6778. doi:10.1016/j.agrformet.2011.09.005
- ◊ Ramirez-Villegas, J., Lau, C., Hooker, J., Jarvis, A., Ann-Kristin, K., Arnell, N., Tom, O. (2011). *Climate Analogues: finding tomorrow's agriculture today*. CGIAR Research Program on Climate Change, Agriculture and Food Security.
- ◊ Rerolle, V. M. C., Floquet, C. F. A., Mowlem, M. C., Connelly, D. P., Achterberg, E. P., & Bellerby, R. R. G. J. (2012). *Seawater-pH measurements for ocean-acidification observations*. TrAC - Trends in Analytical Chemistry. doi:10.1016/j.trac.2012.07.016
- ◊ Resources, ESRI. (2005). *Understanding cokriging*. Retrieved February 15, 2015, from http://webhelp.esri.com/arcgisdesktop/9.1/index.cfm?TopicName=Understanding_cokriging
- ◊ Rosenzweig, C., Iglesias, A., Yang, X., Epstein, P. R., & Chivian, E. (2001). *Climate change and extreme weather events - implications for food production, plant diseases, and pests*. Change Human Health, 2, 90104. doi:10.1097/JOM.0b013e31817d32da
- ◊ Rossiter, D. G. (2007). *Technical Note: Co-kriging with the gstat package of the R environment for statistical computing*. Retrieved from <http://spatial-analyst.net/book/node/294>
- ◊ Ruiz-Garcia, L., Lunadei, L., Barreiro, P., & Robla, J. I. (2009). *A review of wireless sensor technologies and applications in agriculture and food industry: state of the art and current trends*. Sensors (Basel, Switzerland), 9, 472850. doi:10.3390/s90604728
- ◊ Sanchez, B., Rasmussen, A., & Porter, J. R. (2014). *Temperatures and the growth and development of maize and rice: a review*. Global Change Biology, 20(2), 408417. doi:10.1111/gcb.12389
- ◊ Schiermeier, Q. (2010). *The real holes in climate science*. Nature. doi:10.1038/463284a
- ◊ Seguinot, J., Khourlev, C., Rogozina, I., Stroeve, A. P., & Zhang, Q. (2014). *The effect of climate forcing on numerical simulations of the Cordilleran ice sheet at the Last Glacial Maximum*. The Cryosphere, 8, 10871103. doi:10.5194/tc-8-10871103
- ◊ Sellers, P. J. (1985). *Canopy reflectance, photosynthesis and transpiration*. International Journal of Remote Sensing, 6, 13351372. doi:10.1080/01431168508948283

- ◊ Selvaraju, R. (2012). *Climate risk assessment and management in agriculture*. In Building resilience for adaptation to climate change in the agriculture sector: Proceedings of a Joint FAO/OECD Workshop. FAO. Retrieved from <http://www.fao.org/3/a-i3084e>
- ◊ Singh, S. (2012). *E-Agriculture and Rural Development*. E-Agriculture and Rural Development: Global Innovations and Future Prospects (pp. 140168). doi:10.4018/978-1-4666-2655-3
- ◊ Staver, C., Guharay, F., Monterroso, D., & Muschler, R. G. (2001). *Designing pest-suppressive multi-strata perennial crop systems: Shade-grown coffee in central america*. In Agroforestry Systems (Vol. 53, pp. 151170). doi:10.1023/A:1013372403359
- ◊ Tarara, J. M., & Hoheisel, G. A. (2007). *Low-cost shielding to minimize radiation errors of temperature sensors in the field*. HortScience, 42, 13721379.
- ◊ Taugourdeau, S., le Maire, G., Avelino, J., Jones, J. R., Ramirez, L. G., Jara Quesada, M., Roupsard, O. (2014). *Leaf area index as an indicator of ecosystem services and management practices: An application for coffee agroforestry*. Agriculture, Ecosystems and Environment, 192, 1937. doi:10.1016/j.agee.2014.03.042
- ◊ Thomas, C. K., & Smoot, A. R. (2013). *An effective, economic, aspirated radiation shield for air temperature observations and its spatial gradients*. Journal of Atmospheric and Oceanic Technology, 30, 526537. doi:10.1175/JTECH-D-12-00044.1 University, Duke. (n.d.). *Whats the bottom line? How to compare models*. Retrieved February 15, 2015, from <http://people.duke.edu/~rnau/compare.htm>
- ◊ Van Etten, J. (2011). *Crowdsourcing crop improvement in sub-Saharan Africa: A proposal for a scalable and inclusive approach to food security*. IDS Bulletin, 42, 102110. doi:10.1111/j.1759-5436.2011.00240.x
- ◊ Van Marken Lichtenbelt, W. D., Daanen, H. A. M., Wouters, L., Fronczek, R., Raymann, R. J. E. M., Severens, N. M. W., & Van Someren, E. J. W. (2006). *Evaluation of wireless determination of skin temperature using iButtons*. Physiology and Behavior, 88, 489497. doi:10.1016/j.physbeh.2006.04.026
- ◊ Viswanadham, N. (n.d.). *Food Security in India: A Logistics and Supply Chain Challenge*. Bangalore. Retrieved from <http://drona.csa.iisc.ernet.in/~nv/37FoodSecurityinIndia.pdf>
- ◊ Von Arx, G., Dobbertin, M., & Rebetez, M. (2012). *Spatio-temporal effects of forest canopy on understorey microclimate in a long-term experiment in Switzerland*. Agricultural and Forest Meteorology, 166-167, 144155. doi:10.1016/j.agrformet.2012.07.018
- ◊ Walvoort, D., Brus, D., & Gruijter, J. de. (2013). *Package spcosa. R*. Retrieved from <http://cran.r-project.org/web/packages/spcosa/spcosa.pdf>
- ◊ Walvoort, D. J. J., Brus, D. J., & de Gruijter, J. J. (2010). *An R package for spatial coverage sampling and random sampling from compact geographical strata by k-means*. Computers and Geosciences, 36, 12611267. doi:10.1016/j.cageo.2010.04.005
- ◊ Wang, E., Smith, C. J., Bond, W. J., & Verburg, K. (2004). *Estimations of vapour pressure deficit and crop water demand in APSIM and their implications for prediction of crop yield, water use, and deep drainage*. Australian Journal of Agricultural Research, 55(12), 12271240. doi:<http://dx.doi.org/10.1071/AR03216>
- ◊ Watson, D. J. (1947). *Comparative physiological studies on the growth of field crops I. Variation in Net Assimilation Rate and leaf area between species and varieties, and within and between years*. Annals of Botany (London), 11, 4176.

- ◊ Welles, J. M., & Cohen, S. (1996). *Canopy structure measurement by gap fraction analysis using commercial instrumentation*. Journal of Experimental Botany, 47, 13351342. doi:10.1093/jxb/47.9.1335
- ◊ Wiesmeier, M., Barthold, F., Blank, B., & Kgel-Knabner, I. (2011). *Digital mapping of soil organic matter stocks using Random Forest modeling in a semi-arid steppe ecosystem*. Plant and Soil, 340, 724. doi:10.1007/s11104-010-0425-z
- ◊ Wilks, D. S., & Shen, K. W. (1991). *Threshold Relative Humidity Duration Forecasts for Plant Disease Prediction*. Journal of Applied Meteorology. doi:10.1175/1520-0450(1991)030
- ◊ Wilks, D. S., & Wilby, R. L. (1999). *The weather generation game: a review of stochastic weather models*. Progress in Physical Geography. doi:10.1191/030913399666525256
- ◊ Winslow, J. C., Hunt, E. R., & Piper, S. C. (2001). *A globally applicable model of daily solar irradiance estimated from air temperature and precipitation data*. Ecological Modelling, 143, 227243. doi:10.1016/S0304-3800(01)00341-6
- ◊ Wood, S. A., Jina, A. S., Jain, M., Kristjanson, P., & DeFries, R. S. (2014). *Smallholder farmer cropping decisions related to climate variability across multiple regions*. Global Environmental Change. doi:10.1016/j.gloenvcha.2013.12.011
- ◊ World Meteorological Organization. (2008). *Guide of Meteorological Instruments and Methods of Observation*. In WMO (Vol. I & II, pp. I.151 to I.151II.210 to II.211). doi:Guide to meteorological instrument and observing practices
- ◊ Yu, K., Lu, Z., & Stander, J. (2003). *Quantile regression: Applications and current research areas*. Journal of the Royal Statistical Society Series D: The Statistician. doi:10.1111/1467-9884.00363
- ◊ Zeileis, A., & Grothendieck, G. (2005). *zoo: An S3 Class and Methods for Indexed Totally Ordered Observations*. Wirtschaftsuniversitt Wien.

8 Annexes

8.1 Regression models

Hour	R2	Elevation	Slope	Aspect	LAI	Canopy	Radiation
1	0.53	0.77	0.11	0.05	0.02	0.04	-
2	0.54	0.77	0.12	0.06	0.02	0.03	-
3	0.50	0.71	0.14	0.09	0.02	0.03	-
4	0.52	0.72	0.14	0.09	0.02	0.03	-
5	0.50	0.72	0.13	0.10	0.02	0.03	-
6	0.57	0.63	0.06	0.07	0.01	0.02	0.21
7	0.50	0.45	0.06	0.10	0.03	0.04	0.32
8	0.41	0.45	0.06	0.08	0.04	0.07	0.30
9	0.36	0.42	0.04	0.07	0.06	0.10	0.31
10	0.33	0.50	0.05	0.05	0.07	0.18	0.16
11	0.28	0.59	0.10	0.03	0.09	0.14	0.05
12	0.24	0.45	0.14	0.06	0.16	0.09	0.10
13	0.28	0.51	0.10	0.08	0.08	0.06	0.17
14	0.34	0.44	0.10	0.07	0.03	0.06	0.30
15	0.48	0.56	0.08	0.05	0.03	0.06	0.23
16	0.62	0.67	0.05	0.03	0.02	0.05	0.16
17	0.82	0.80	0.06	0.02	0.03	0.05	0.05
18	0.83	0.86	0.05	0.03	0.02	0.04	-
19	0.80	0.86	0.04	0.03	0.02	0.04	-
20	0.77	0.86	0.04	0.04	0.02	0.04	-
21	0.72	0.85	0.04	0.05	0.02	0.04	-
22	0.67	0.83	0.06	0.05	0.02	0.04	-
23	0.62	0.81	0.08	0.06	0.02	0.03	-
24	0.54	0.75	0.12	0.08	0.02	0.03	-
Avg	0.53	0.67	0.08	0.06	0.04	0.06	0.10

Table 11: Hourly strength of regression models and relative importance of the selected covariates

Annex

	Spatial			Temporal		
	RMSE	MAE	MAPE	RMSE	MAE	MAPE
<i>80 sensors</i>	0.69 (0.18-2.21)	0.53 (0.41-0.67)	2.52 (0.59-8.12)	0.83 (0.57-1.12)	0.53 (0.40-0.70)	2.52 (1.97-3.27)
<i>40 sensors</i>	0.77 (0.24-2.17)	0.61 (0.42-0.87)	2.85 (1.01-7.79)	0.87 (0.44-1.35)	0.59 (0.32-0.87)	2.85 (1.60-4.18)
<i>20 sensors</i>	0.73 (0.32-1.57)	0.56 (0.38-0.77)	2.57 (1.19-5.34)	0.82 (0.40-1.65)	0.54 (0.29-0.89)	2.57 (1.50-4.33)
<i>8 sensors</i>	0.95 (0.61-1.37)	0.69 (0.28-1.26)	3.30 (2.54-4.32)	0.88 (0.25-2.07)	0.68 (0.21-1.63)	3.30 (1.03-8.32)

Table 12: Errors with Ordinary Kriging

	Spatial			Temporal		
	RMSE	MAE	MAPE	RMSE	MAE	MAPE
<i>80 sensors</i>	0.64 (0.15-2.23)	0.49 (0.39-0.63)	2.35 (0.52-8.17)	0.79 (0.56-1.07)	0.49 (0.39-0.63)	2.35 (1.88-2.99)
<i>40 sensors</i>	0.70 (0.21-2.19)	0.54 (0.41-0.80)	2.51 (0.73-7.89)	0.81 (0.41-1.33)	0.52 (0.28-0.80)	2.51 (1.34-3.70)
<i>20 sensors</i>	0.70 (0.28-1.60)	0.55 (0.40-0.83)	2.42 (1.09-5.32)	0.78 (0.40-1.61)	0.51 (0.27-0.90)	2.42 (1.22-4.24)
<i>8 sensors</i>	0.82 (0.37-1.41)	0.57 (0.30-0.83)	2.47 (1.54-3.88)	0.78 (0.14-1.97)	0.53 (0.12-1.22)	2.47 (0.59-5.68)

Table 13: Errors with Universal Kriging (Elevation)

	Spatial			Temporal		
	RMSE	MAE	MAPE	RMSE	MAE	MAPE
<i>80 sensors</i>	0.64 (0.14-2.21)	0.49 (0.39-0.63)	2.35 (0.50-8.22)	0.78 (0.56-1.04)	0.49 (0.39-0.63)	2.35 (1.87-3.05)
<i>40 sensors</i>	0.70 (0.22-2.24)	0.55 (0.41-0.81)	2.57 (0.73-8.04)	0.82 (0.44-1.29)	0.53 (0.31-0.81)	2.57 (1.52-3.77)
<i>20 sensors</i>	0.71 (0.29-1.60)	0.57 (0.37-0.83)	2.45 (1.07-5.23)	0.78 (0.38-1.50)	0.51 (0.25-0.88)	2.45 (1.22-4.34)
<i>8 sensors</i>	0.84 (0.37-1.44)	0.57 (0.31-0.83)	2.55 (1.53-4.08)	0.81 (0.16-2.05)	0.55 (0.11-1.32)	2.47 (0.59-5.68)

Table 14: Errors with automatized Universal Kriging (Elevation)

	Spatial			Temporal		
	RMSE	MAE	MAPE	RMSE	MAE	MAPE
<i>80 sensors</i>	0.63 (0.15-2.03)	0.48 (0.37-0.63)	2.31 (0.54-7.37)	0.77 (0.54-0.97)	0.49 (0.37-0.63)	2.31 (1.82-3.01)
<i>40 sensors</i>	0.69 (0.21-2.05)	0.53 (0.40-0.73)	2.48 (0.79-7.18)	0.80 (0.46-1.26)	0.52 (0.33-0.76)	2.48 (1.59-3.73)
<i>20 sensors</i>	0.76 (0.28-1.70)	0.55 (0.35-0.76)	2.54 (1.22-5.68)	0.84 (0.31-1.78)	0.54 (0.24-0.99)	2.54 (1.23-4.32)
<i>8 sensors</i>	1.33 (0.62-2.37)	0.91 (0.57-1.41)	3.53 (2.17-5.90)	1.19 (0.23-5.63)	0.77 (0.15-2.91)	3.52

Table 15: Errors with basic dynamic kriging

	Spatial			Temporal		
	RMSE	MAE	MAPE	RMSE	MAE	MAPE
<i>80 sensors</i>	0.64 (0.14-2.21)	0.49 (0.39-0.63)	2.35 (0.50-8.22)	0.78 (0.56-1.04)	0.49 (0.39-0.63)	2.35 (1.87-3.05)
<i>40 sensors</i>	0.70 (0.22-2.24)	0.55 (0.41-0.82)	2.57 (0.73-8.04)	0.82 (0.44-1.29)	0.53 (0.31-0.81)	2.57 (1.52-3.77)
<i>20 sensors</i>	0.71 (0.29-1.60)	0.57 (0.37-0.83)	2.45 (1.07-5.23)	0.78 (0.38-1.50)	0.51 (0.25-0.88)	2.45 (1.12-4.35)
<i>8 sensors</i>	0.84 (0.37-1.44)	0.57 (0.31-0.83)	2.55 (1.54-4.08)	0.81 (0.16-2.05)	0.55 (0.11-1.32)	2.55 (0.54-6.18)

Table 16: Errors with automatized dynamic kriging

	Spatial			Temporal		
	RMSE	MAE	MAPE	RMSE	MAE	MAPE
<i>80 sensors</i>	0.64 (0.19-2.12)	0.50 (0.42-0.58)	2.37 (0.69-7.86)	0.78 (0.60-1.00)	0.50 (0.41-0.65)	2.39 (2.00-3.04)

Table 17: Errors with random forest kriging

	Spatial			Temporal		
	RMSE	MAE	MAPE	RMSE	MAE	MAPE
<i>80 sensors</i>	0.67 (0.14-2.35)	0.51 (0.37-0.68)	2.42 (0.50-8.17)	0.85 (0.57-1.17)	0.51 (0.37-0.69)	2.42 (1.77-3.21)
<i>40 sensors</i>	0.75 (0.21-2.31)	0.58 (0.45-0.80)	2.66 (0.80-8.15)	0.89 (0.53-1.36)	0.56 (0.33-0.84)	2.66 (1.56-4.16)
<i>20 sensors</i>	0.77 (0.28-1.70)	0.60 (0.42-0.90)	2.59 (1.18-5.51)	0.88 (0.42-1.70)	0.55 (0.31-1.06)	2.59 (1.55-5.19)
<i>8 sensors</i>	1.11 (0.46-2.05)	0.65 (0.34-1.16)	3.02 (1.74-5.16)	1.02 (0.20-3.52)	0.66 (0.16-2.07)	3.02 (0.78-9.59)

Table 18: Errors with co-kriging (elevation only)

	Spatial			Temporal		
	RMSE	MAE	MAPE	RMSE	MAE	MAPE
<i>80 sensors</i>	0.66 (0.14-2.31)	0.50 (0.37-0.71)	2.37 (0.50-7.81)	0.83 (0.54-1.16)	0.50 (0.34-0.71)	2.37 (1.66-3.32)
<i>40 sensors</i>	0.73 (0.21-2.15)	0.56 (0.42-0.79)	2.60 (0.81-7.52)	0.86 (0.46-1.38)	0.55 (0.32-0.81)	2.60 (1.54-3.99)
<i>20 sensors</i>	0.75 (0.27-1.66)	0.59 (0.41-0.87)	2.51 (1.14-5.33)	0.85 (0.30-1.58)	0.54 (0.24-1.03)	2.51 (1.24-5.04)
<i>8 sensors</i>	1.14 (0.46-2.46)	0.61 (0.16-1.39)	2.96 (1.70-5.51)	0.98 (0.11-4.08)	0.63 (0.09-2.28)	2.96 (0.44-10.67)

Table 19: Errors of co-kriging (with elevation and radiation)

	Spatial			Temporal		
	RMSE	MAE	MAPE	RMSE	MAE	MAPE
<i>80 sensors</i>	0.66 (0.14-2.31)	0.49 (0.39-0.68)	2.35 (0.51-7.80)	0.82 (0.54-1.13)	0.50 (0.34-0.68)	2.35 (1.67-3.21)
<i>40 sensors</i>	0.72 (0.21-2.15)	0.54 (0.42-0.74)	2.52 (0.82-7.44)	0.84 (0.46-1.38)	0.53 (0.31-0.80)	2.52 (1.51-3.88)
<i>20 sensors</i>	0.71 (0.24-1.58)	0.54 (0.31-0.76)	2.31 (1.06-4.85)	0.80 (0.35-1.54)	0.50 (0.25-0.92)	2.31 (1.27-4.45)
<i>8 sensors</i>	1.05 (0.41-2.17)	0.54 (0.13-1.23)	2.63 (1.38-4.92)	0.91 (0.16-3.83)	0.58 (0.12-2.01)	2.63 (0.50-9.52)

Table 20: Errors with co-kriging (with elevation, radiation, slope and aspect)

	Spatial			Temporal		
	RMSE	MAE	MPE	RMSE	MAE	MPE
<i>80 sensors</i>	0.91 (0.28-1.61)	0.62 (0.14-2.43)	2.91 (0.83-6.53)	0.78 (0.22-2.92)	0.61 (0.14-2.43)	2.91 (0.76-10.50)
<i>40 sensors</i>	0.89 (0.28-1.61)	0.59 (0.14-1.64)	2.91 (0.83-6.53)	0.79 (0.20-2.82)	0.61 (0.14-2.28)	2.91 (0.75-9.87)
<i>20 sensors</i>	0.91 (0.49-1.61)	0.82 (0.21-1.66)	2.83 (1.38-4.81)	0.76 (0.17-2.90)	0.59 (0.12-2.37)	2.83 (0.62-10.76)
<i>8 sensors</i>	1.05 (0.71-1.44)	0.83 (0.65-0.90)	4.07 (2.49-5.55)	0.99 (0.41-3.01)	0.81 (0.32-2.67)	4.07 (1.47-12.06)

Table 21: Errors with spatio-temporal ordinary kriging

	Spatial			Temporal		
	RMSE	MAE	MPE	RMSE	MAE	MPE
<i>80 sensors</i>	0.90 (0.27-1.61)	0.61 (0.10-2.42)	2.89 (0.82-6.18)	0.77 (0.14-2.93)	0.60 (0.10-2.43)	2.89 (0.56-10.52)
<i>40 sensors</i>	0.90 (0.27-1.61)	0.58 (0.10-1.65)	2.90 (0.82-6.18)	0.78 (0.15-2.84)	0.61 (0.10-2.29)	2.90 (0.54-9.91)
<i>20 sensors</i>	0.91 (0.49-1.61)	0.83 (0.20-1.68)	2.84 (1.40-4.86)	0.76 (0.12-2.92)	0.59 (0.08-2.38)	2.84 (0.47-10.81)
<i>8 sensors</i>	1.14 (0.73-1.71)	0.91 (0.74-0.99)	4.57 (2.36-8.13)	1.11 (0.47-3.05)	0.90 (0.39-2.68)	4.57 (1.84-12.42)

Table 22: Errors with spatio-temporal universal kriging (elevation)

	Spatial			Temporal		
	RMSE	MAE	MPE	RMSE	MAE	MPE
<i>80 sensors</i>	0.95 (0.40-1.59)	0.64 (0.10-2.43)	3.16 (1.47-6.35)	0.82 (0.15-2.94)	0.66 (0.10-2.43)	3.16 (0.57-10.54)
<i>40 sensors</i>	0.95 (0.40-1.59)	0.64 (0.10-1.58)	3.19 (1.47-6.35)	0.83 (0.15-2.85)	0.66 (0.10-2.29)	3.19 (0.54-9.94)
<i>20 sensors</i>	0.97 (0.54-1.59)	0.92 (0.33-1.72)	3.13 (1.67-4.81)	0.81 (0.11-2.99)	0.65 (0.08-2.43)	3.13 (0.47-11.05)
<i>8 sensors</i>	1.16 (0.78-1.65)	0.98 (0.74-1.11)	4.68 (2.71-7.70)	1.13 (0.59-3.05)	0.93 (0.46-2.69)	4.68 (2.14-12.37)

Table 23: Errors with spatio-temporal dynamic kriging (elevation, radiation, slope and aspect)